NASA TECHNICAL MEMORANDUM NASA TM-75339

FLOW-FIELD IN A VORTEX WITH BREAKDOWN ABOVE SHARP EDGED DELTA WINGS

Yoshio Hayashi and Teruomi Nakaya

Translation of "Breakdown o Tomonau Sankaku-Yoku Zen-En Hakuri Uzu no Nagareba," National Aerospace Laboratory, Tokyo (Japan), Report NAL-TR-423, Aug. 1975, 46 pages

NATIONAL AERONAUTICS AND APACE ADMINISTRATION
WASHINGTON, D.C. 20564 NOVEMBER 1978

STANDARD TITLE PAGE

1. Report No. NASA TM-75339	2. Government Accession No.	3. Recipient's Catalog No.
4. Title and Subtitle FLOW-FIELD IN A VORTEX WITH BREAK-DOWN ABOVE SHARP EDGED DELTA WINGS		5. Report Date November 1978 6. Performing Organization Code
7. Author(s) Yoshio Hayashi and Teruomi Nakaya Second Division of Aerodynamics, the Japanese National Aerospace Laboratory		8. Performing Organization Report No. 10. Work Unit No.
9. Performing Organization Name and Address Leo Kanner Associates Redwood City, California 94063		11. Contract or Grant No. NASW-3199 13. Type of Report and Period Covered Translation
12. Sponsoring Agency Name and Address National Aeronautics & Space Administration Washington, D. C. 20546		14. Sponsoring Agency Code

15. Supplementary Notes

Translation of "Breakdown o tomonau sankaku-yoku zen-en hakuri uzu no nagareba," National Aerospace Laboratory, Tokyo (Japan), Report NAL-TR-423, Aug. 1975, 46 pages (N76-31157)

16. Abstract

The abstract is given in the text.

17. Key Words (Selected by Author(s))	18. Distribution Statement
	Unclassified - Unlimited

19. Security Classif. (of this report)	20. Security Classif. (of this page)	21. No. of Pages	22. Price
Unclassified	Unclassified		

TABLE OF CONTENTS

FLOW-FIELD IN A VORTEX WITH BREAKDOWN ABOVE SHARP EDGED DELTA WINGS[1]

Yoshio Hayashi and Teruomi Nakaya
Second Division of Aerodynamics, the
Japanese National Aerospace Laboratory

/1

ABSTRACT

This paper describes the behavior of vortex-flow, accompanied with breakdown, formed above sharp-edged delta wings, which has been investigated experimentally as well as theoretically at NAL. Emphasis is placed particularly on the criterion for the breakdown at sufficiently large Reynolds numbers.

First shown are the mean velocity components U_x, U_y, U_r, and the total head H_c along the vortex axis measured in the vortex-flow field over three flat-plate delta wing models with apex angles of 40°, 50° and 60°. Experimental data are conveniently non-dimensionalized in terms of the maximum velocity U_o and the distance L, at which the velocity along the vortex axis becomes half of U_o. These results show that the pronounced effect of the vortex breakdown presents itself on the mean axial-velocity distribution across the vortex and the total head change along the vortex central axis. The breakdown point can therefore be determined from the criterion $dH_c/dX=0$ or $(\partial^2 U_x/\partial R^2)_{R=0}=0$. The spiral form of the vortex and the velocity fluctuation in the vortex breakdown flow field are illustrated as results of the precession of the vortex core section, analogous to the preces-

---

[1]The manuscript was received on May 8, 1975.

*Numbers in the margin indicate pagination in the foreign text.

sion of the vortex core section, analogous to the precession of a solid body with a fixed point. The frequency of the velocity fluctuation is demonstrated experimentally and theoretically to be proportional to U_o/L.

Secondly, a modification, accounting for turbulence, of Hall's method of numerical calculation is described. The concept of eddy viscosity is introduced, and the fundamental system of the theory consists of a set of quasi-two dimensional equations which are to be solved numerically. Calculation is actually carried out in the case of a flat-plate delta wing model with an apex angle of 50^o and an attack angle of 17^o, with initial and boundary conditions specified in accordance with the measured values. Comparison is made between the numerical and experimental results, showing good agreement between them, when chosen value of eddy viscosity is 4 to 5 times larger than the kinematic viscosity.

1. Introduction

Owing to the recent progresses in researches and technologies concerning high-speed aircraft, supersonic passenger aircraft have been realized for practical use. Inspired by the development of the SST's, energetic studies have been made on wings which are economically efficient as well as able to ensure high standard of safety.[1], [2], [12], [18] These studies have mostly been converged to the conclusion that sharp-edged delta wings are most advantageous for supersonic passenger aircraft for the following reasons: The flow in the wings' neighborhood is stable, sufficient structural strength may be provided and their low resistance makes them economically feasible.

The flow-field around these wings, however, tends to be extremely sensitive to three-dimensional influences since their aspect ratio is small and their front edges are very sharp. The /2

most characteristic phenomenon may be described as follows: When the angle of attack becomes larger than a certain limit, the flow cannot make a sharp turn at the leading edge of such a wing and separates from the wing, thus generating a three-dimensional flow. Generally, a wing with a large aspect ratio is designed so as to prevent such a separation on the wing surface as much as possible and to obtain as ideal lift as possible.

On the contrary, a delta wing utilizes this separation rather in a positive way. The flow separated at the leading edge of the wing concentrates on the wing surface and induces strong vorteces. Since the leading edge is sharp, the separation point is fixed and the generated vorteces are very stable. Thus, the flow separated at the leading edge forms a stable three-dimensional separated flow, including a pair of concentrated vorteces, each of which is located above each tail side of the wing. Such a vortex above the wing is accompanied by very low static pressure and, hence, the lift of the wing portion above which the vortex exists is higher than the lift obtained according to the potential theory.[3] The lift increases nonlinearly as the angle of attack increases. Thus, the aerodynamic characteristics of a sharp edged delta wing are highly dependent on the behavior of the vortices which are separated at the leading edge.

Concerning the aerodynamic characteristics of a delta wing generating vortices, many results have been already reported, such as: a theory by Brown and Michael[4] in which a separated vortex is treated as a linear vortex applying fine-body theory; a theory by Mangler and Smith[5] in which a separated vortex is analyzed after it is decomposed into a linear vortex and a vortex layer; a theory by Smith[6] in which the vortex layer is approximated by a piecewise linear function; a theory by Levinsky and Wei[7] in which Smith's theory is expanded with the fuselage being taken into account; a theory[8], [9] by Polhamus in which a separated vortex is assumed to act similarly to the suction force

generated by a sharp edged wing; a numerical method by Ohmura and Takaoka [11] in which the vortex lattice method [10] as a conventional three-dimensional wing surface theory is extended for application to a delta wing with separated vortices. Thus, aerodynamic characteristics of delta wings with flow separation have been theoretically established.

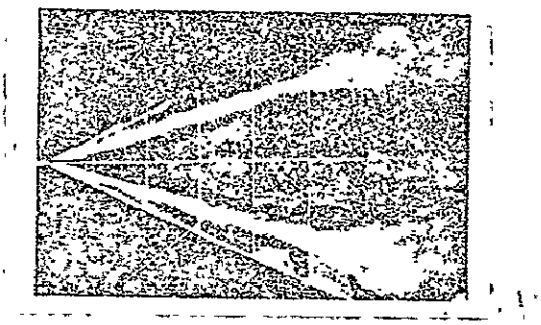

Fig. 1. Vorteces Separated at Front Edge of a Delta Wing and Breakdown.

Concerning overall aerodynamics of a delta wing, it suffices to convert each separated vortex into a linear vortex and a vortex layer and to calculate a field induced by the vortices. The vortex separated at the front edge, however, induces a phenomenon which is called "breakdown" or "burst" at a location down the rear edges of the wing, as shown in Fig. 1, as the angle of attack increases. As the angle of attack is increased further, this phenomenon begins to take place above the wing surface. When this phenomenon appears above the wing surface, the velocity fluctuation becomes furious as well as pressure fluctuation on the wing surface, and the aircraft is consequently shaken badly. When the breakdown is generated above the wing surface, no lift increase can be expected by the contribution of the vortices and the head-up moment of the aircraft is increased, thereby deteriorating the lateral static stability. The vortex separated at the front is sensitive to cross winds. Namely, even when the angle of attack is small, if the aircraft is at an angle to the wind, one vortex on the windward side breaks down. [13], [17]

deteriorating the traverse static stability.[1] Furthermore, the relative location of the vortex separated at the leading edge changes with respect to the wing according to the angle of attack and to the deviation angle. The location changes in response to these angles with a certain phase delay, thus influencing also the dynamic stability.[14], [15], [16] In summary, the phenomenon of the vortex separation at the leading edge and of the breakdown has a significant influence over both static and dynamic characteristics of an aircraft, and, therefore, in order to establish a complete flight safety, thorough studies must be made on the properties of the vortices separated at the leading edge. In addition, the phenomenon of the breakdown can not be rationally explained by a wing theory in which the vortices separated at the leading edge are collections of linear vorteces and vortex layers. This indicates that a study must be done for exploring the properties of the vortex itself.

At the early stage, there were only a few experimental researches for studying the structure of the vortex itself. They were mainly qualitative studies in which smoke or dye is fed into the center of a vortex in a wind tunnel or a water pool and visualized generation and development of the vortex are photographed. Although such photographs provide valuable information on the vortex location, the vortex development and the location of the breakdown, they are not enough for studying the structure inside the vortex. Werlé[19] put various shapes of objects, including simple delta wings, in a water pool and photographed behaviors of vortices at low speeds using several kinds of dyes fed into the water pool. Elle[20] photographed vortex generation at a high subsonic speed by the schlieren method. In such a case, although the vortex is interferred with the shock and shows a complicated formation, it was clearly shown that the vortex is actually generated at a high speed as well as a low speed and dominates the flow-field around the wing. Lambourne and Bryer[21] put delta wings in a water pool and studied the

development and the breakdown phenomenon of the vortices. They concluded from their experiments that the breakdown phenomena can be classified into two types: (1) axisymmetric type and (2) spiral type, and that the axisymmetric type of vortex is unstable and is gradually transformed to the spiral type. The central velocity of an axisymmetric type vortex decreases until the vortex center does not move and a tapered region of counter-flow is generated. On the other hand, the central axis of a spiral type vortex makes a turn at a certain point and is transformed into a turbulent flow behind that point forming several spirals. It should be noted that the rotation direction of the spiral of a spiral vortex is reversed to the original direction of the vortex core rotation in the process of the vortex transformation.

The movement of the dye photographed by a cinematograph /3
camera for measuring the movements of fluid portions indicates that the axial speed of the vortex center is more than twice as high as that of a uniform flow before the breakdown occurs but becomes less than the uniform-flow speed once the breakdown occurs. Furthermore, it was experimentally clarified [22] that, at the breakdown of a spiral type vortex, the fluid in the vortex core portion does not move along the spiral but moves downstream along generatrices of a cone including the spiral surface and that, when the spiral is viewed as a whole, the fluid of the vortex core portion appears as if it were moving along the spiral. Hummel [13] measured the total pressure distribution of the flow-field generated by a vortex and its velocity vector and showed that the total pressure of the vortex center is lower than that of the peripheral portion while the circumferential velocity is significantly high. However, in his experiment, the velocity distribution within the vortex core was not measured. Therefore, his observation is not sufficient for clarifying the structure of the vortex. It was Earnshaw [23] who measured the velocity distribution within the vortex core as well as the pressure

distribution. He used a five-hole Pitot tube for measuring the flow-field generated by the vortex, and showed that the spiral is concentrated in an extremely narrow space along the center and that the axial velocity reaches 2 to 3 times as high as that of a uniform flow while the maximum circumferential velocity is almost the same as that of a uniform flow.

In addition, besides the vortices on the delta wing surface, many researchers [53] have studied swirl flow in a cylindrical tube which shows a phenomenon similar to the vortex breakdown. Harvey [24] showed that an egg-shaped counter-flow region is generated in the central portion of the spiral-flow vortex core in a cylindrical tube and that a flow-field with an abruptly changing tail is formed on the downstream. He further concluded that the breakdown phenomenon is generated by such stagnation in the vortex core center. Lambourne [22] succeeded, by increasing the spiral flow in a cylindrical tube, in photographing the transient states in which an initially generated axisymmetric types of breakdown is transformed into a spiral type of breakdown. He also measured the fluctuations of velocity and pressure due to the spiral type of breakdown. Cassidy and Falvey [25] reported their experimental discovery of the fact that a precession with a constant period, such as that of a gyroscope, appears in a vortex after a spiral form of breakdown. According to a recent experimental result by Sarpkaya, the breakdown can be classified into (1) axisymmetric form, (2) spiral form, and (3) double-helix form. It was reported as a quantitative experimental result that which form of breakdown appears depends on Reynolds number, size of the circulation and pressure gradient, and the breakdown location changes also in response to those parameters. The report also dealt with transient states of the breakdown. According to Sarpkaya, the spiral rotation of a spiral vortex has the same direction as that of the vortex initially generated, but the spiral transformation appearing in the downstream of an axisymmetric form breakdown has reversed direction, coinciding with the

conclusion by Lambourne about the spiral transformation. As seen from the above description, besides spiral flow in cylindrical tubes, there have been no available quantitative experimental results concerning the structure of vortices separated at the leading edge of delta wings, except for Earnshaw's experiment in which the flow-field before breakdown was studied. According to the authors' knowledge, there have been reported no quantitative experimental result describing an entire process in which a vortex is generated and is followed by a breakdown.

Based on the above recognition of the current research stage of the vortex separated at the leading edge of delta wings, the authors planned a quantitative experiment for studying the flow-field of the vortex separated at the leading edge of delta wings. Three kinds of flat-plate delta-wing models with different apex angles were built and the total pressure in the center of the vorteces generated by those models were measured, together with the distribution of average velocity vector of the vortex-generating flow-field ahead of and behind the breakdown. The results obtained by this experiment showed the same velocity distribution of the vortices before the breakdown as those reported by Earnshow. However, the distribution of the axial velocity in the vortex after the breakdown has occurred is completely different from the velocity distribution before the breakdown. The distribution after the breakdown has the minimum at the vortex center and the maximum at a location remote from the center. At the same time, it was discovered that the total pressure of the vortex center has its minimal value at the location of the breakdown. Furthermore, the authors reached a conclusion that the location of the breakdown can be determined by the condition in which the 2nd-order derivatives of the axial velocity along the radial direction is zero at the center, $(\partial^2 U_x/\partial R^2)_{R=0}=0$, or in another expression, the derivative of the total pressure in the vortex center along the direction of the vortex axis is zero, $dH_c/dx=0$. Thus, one of the main objectives of this paper is to

describe such conditions for determining the vortex breakdown.

In Chapter 2, experimental results of the flow-field generated by vortices with breakdown on delta wings are described in connection with the above-mentioned experimental results. The first half of Chapter 3 is used for analyzing the current stage of theoretical researches and, exploiting our experimental results, for demonstrating the fact that if the Reynolds number is relatively high the location of the breakdown may be determined by numerically solving the Navia-Stokes equation by a different method under the quasi two-dimension assumption similar to the boundary layer approximation. Our numerical method is based on that proposed by Hall [29], [30]. However, he made a calculation in the case of a laminar flow vortex. Considering the fact that the vortex in our study is in turbulent flow, we will state a calculation method using a vortex-viscosity model in order to take that effect into account in the process of the numerical analysis. In the rest of Chapter 3, using the experimental results obtained from a 65°- apex angle and 17°-attack angle model and a numerical calculation with given initial and boundary conditions, it is shown that calculated distribution of average velocity vector and calculated breakdown location coincide well with the experimental results if the vortex viscosity coefficient is set to be 4 to 5 times as much as the dynamic viscosity coefficient. In the last chapter, Chapter 4, the experimental results are compared with calculated theoretical results, and it is concluded that a turbulence model, including the /4
turbulence structure of the flow-field, instead of a simple viscosity model, is necessary for further advanced studies of the numerical computation with improved accuracy.

2. Experiment

2.1 Measurement Method

Delta Wing Models

The delta wing models employed in the present study are flat-plate wing models with three different apex angles, 60°, 65° and 70°, as shown in Fig. 2. In order to fix the separation point, the leading and tail edges of the models are tapered. The models with 65° and 70° apex angles have a center chord length of 400 mm while that of 60°-apex angle models is reduced to 350 mm in order for the wing width at the tail not to be too large. Each model has a width of 3 mm and is made of duralumin. In the experiments, each model was vertically supported by a 10-mm diameter cylinder at the location of 2/3 chord length from the wing tip within a wind tunnel. If a model has a small size, the vortex core of leading edge vortex is small, making the flow-field measurement difficult. Therefore, the model size had to be selected to be large enough compared with the measurement cross-section of the wind tunnel. Thus, the effect of the wind-tunnel walls was not taken into account at all.

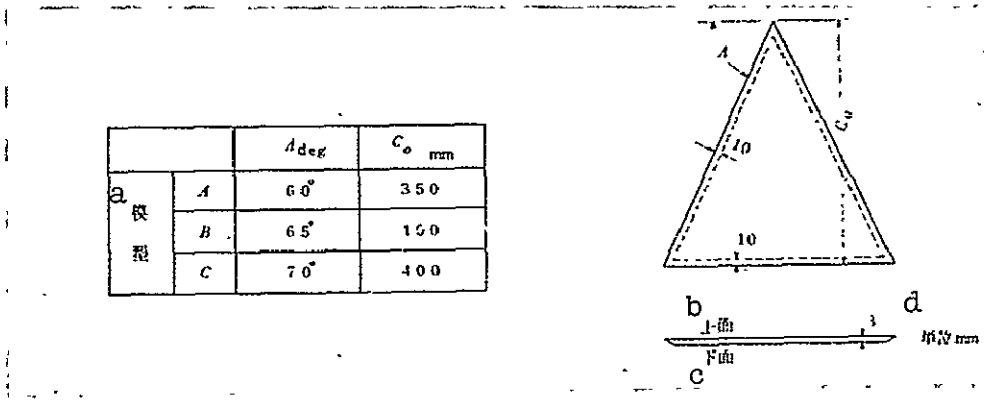

Fig. 2. Shape of Models.

Key: a: Models
b: Upper Surface
c: Lower Surface
d: Unit = mm

Wind Tunnel and Traverse Means

The wind tunnel used in the present experiment is a slender circulation-type low-speed wind tunnel with a cross section of 650 x 550 mm, as shown in Fig. 3. The wind tunnel is capable of creating a wind speed up to about 40 m/s. Due to the strength of the models and the model supporting means, the wind speed in the measurement was limited to low speeds: 15 m/s and 6 m/s. The Reynolds number standardized by the center chord length of 400 mm is 4×10^4 when the uniform-flow wind speed is 15 m/s and is 1.6×10^5 at 6 m/s. The turbulence of the flow at the measurement point was about 0.3% when the wind speed was 15 m/s.

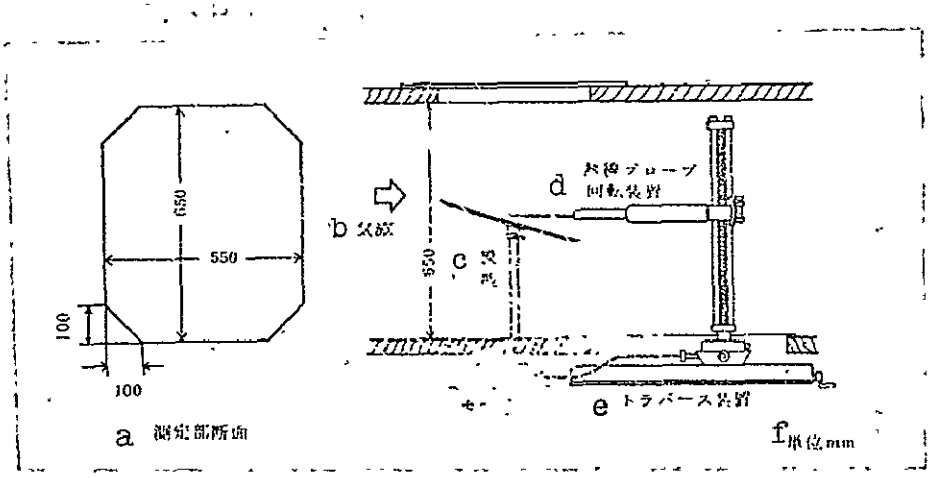

Fig. 3. Wind Tunnel and Traverse Means.

Key: a: Cross Section of Measurement Point.
b: Air Flow
c: Model
d: Hot-Wire Probe Rotating Means
e: Traverse Means
f: Unit = mm

In order to measure the velocity-field and the pressure-field of the vortices created above the delta wing upper surface, the measurement probe must be 3-dimensionally moved, i.e., laterally, traversely and vertically. For this purpose, a traverse means (See Fig. 3) is located on the downstream of the measurement

point. By this traverse means, the models are moved manually in the horizontal direction and electrically in the vertical direction. The resolution of the position reading is 0.1 mm. /5

Measurement of Average Velocity Vector and Total Pressure

The flow-field of the vortices created at the leading edge of a delta wing is 3-dimensional. Therefore, if the flow-field is measured by a usual method in which a static-pressure tube is used with a fixed direction, a large difference between the flow direction and the tube direction results in inaccurate readings of the static pressure. It is for this reason that only the relatively easy total-pressure and average-velocity vector measurement was performed in the present experiment.

The total pressure in the center of vortices was measured by a keel tube (see Fig.5) which has a double-pipe construction and an outer diameter of 1.2 mm. The tube is designed so as to have a high sensitivity in the flow direction. The directional characteristics of this keel tube are shown in Fig.5. It is seen in Fig.5 that the accurate total pressure may be measured by this keel tube if the angle between the keel tube axis and the flow direction is within the range of about $\pm 30^{\circ}$. When considering the case where the angle between the flow direction and the central axis of the vortex is extremely large, e.g., in the flow-field within a vortex, it is easy to see that a measurement limit of 30° is not sufficient for measuring the total pressure if the keel tube direction is fixed. Therefore, when measuring the total pressure in the center of a vortex, the positions at which the keel tube pressure reading is minimal are measured beforehand by a trial-and-error method; the trace of the vortex center is obtained by connecting these points, and finally, the total pressure is measured with the axis of the keel tube being approximately aligned to the vortex central axis thus obtained.

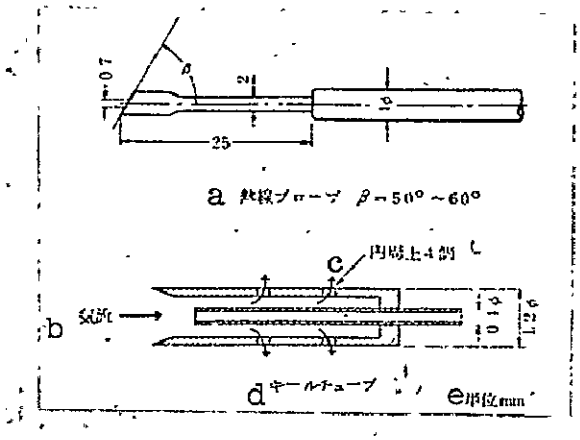

Fig. 4. Measuring Probe

Key: a: Hot Wire Probe
b: Air Flow
c: 4 Holes on the Circumference
d: Keel Tube
e: unit = mm

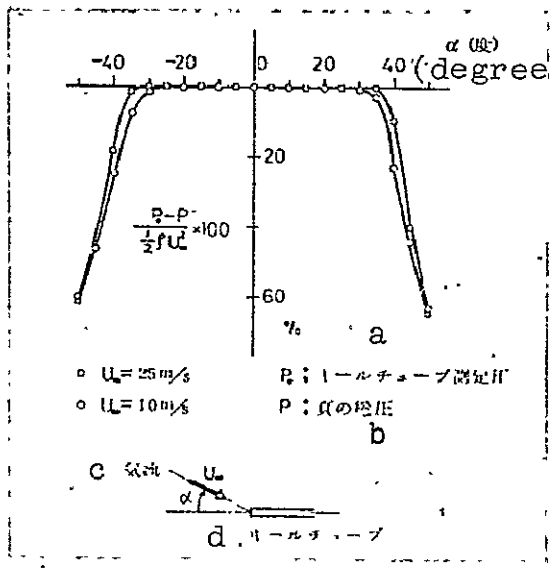

Fig. 5. Directional Characteristics of Keel Tube

Key: a: Pressure Measured by Keel Tube
b: True Total Pressure
c: Air Flow
d: Keel Tube

Average velocity vector is measured usually by a yaw meter with a tube or a Pitot tube [50]. However, when the velocity gradient is extremely large and the direction of the velocity vector varies largely depending on the location, such as in case of the leading edge vorteces created by a delta wing, it becomes very difficult to measure the vector by a yaw meter or the like. In the present experiment, the average vector was measured by a method in which one hot wire is rotated along the axis of its probe [51]. According to this method, while the hot wire is rotated one turn along the axis of its probe, the rotation angle is stopped several times for measuring the angle of the hot-wire probe and the output signal from the hot wire, and then, the three components of the average velocity vector are obtained by solving a 3-variable simultaneous quadratic equation using a computer. Furthermore, according to this method, if the fluctuation signal is measured by an RMS meter when the hot wire is operated for the average-velocity vector measurement, the Reynolds stress can also be measured. In the present experiment, however, the average velocity vector was measured but the Reynolds stress was not measured. As shown in Fig.4, a tungsten wire with a diameter of about 5 micron was used as a hot wire and both ends of the wire were copper-plated and soldered to two needles with an angle. The space between the needles is about 3 mm, and the tungsten wires functioning as hot wires which are not copper-plated are about 0.7 mm long. In measuring the velocity vector, as shown in Fig. 6, the hot wire probe is attached to a hot-wire probe rotating means which is fixed to the traverse means. A total-pressure tube for measuring the vortex-center position is located at a position adjacent to the hot-wire probe. The velocity in the vortex center is measured after the hot-wire probe is moved to the vortex center which is determined by the total-pressure measuring tube. The velocity vector in the cross section perpendicular to the vortex central axis is obtained by manipulating the traverse means laterally, traversely and vertically to the vortex central axis which is determined by the

total-pressure measuring tube fixed on the side of the hot-wire probe. A view of a measurement procedure in the wind tunnel is shown in Fig. 7.

/6

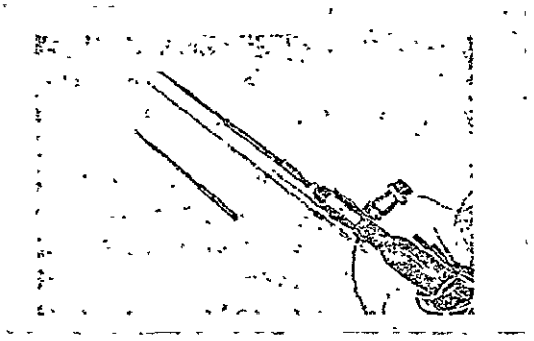

Fig. 6. Hot-Wire Probe Rotating Means and Total-Pressure Measuring Tube.

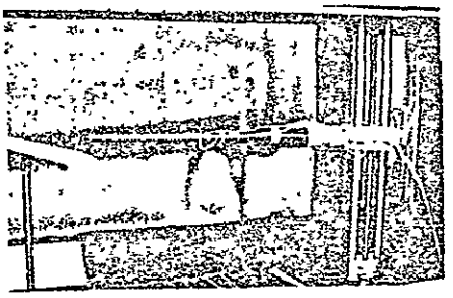

Fig. 7. View of Measurement System.

2.2. Characteristics of Vortex Center

2.2.1. Location of Vorteces

Figs. 8 to 10 show time-average locations at which vorteces are generated on the delta wing surface. The abscissae of these figures designate a variable which represents the distance X along the wind tunnel axis from the origin, the wing tip, and is normalized by the center chord length of the wing.

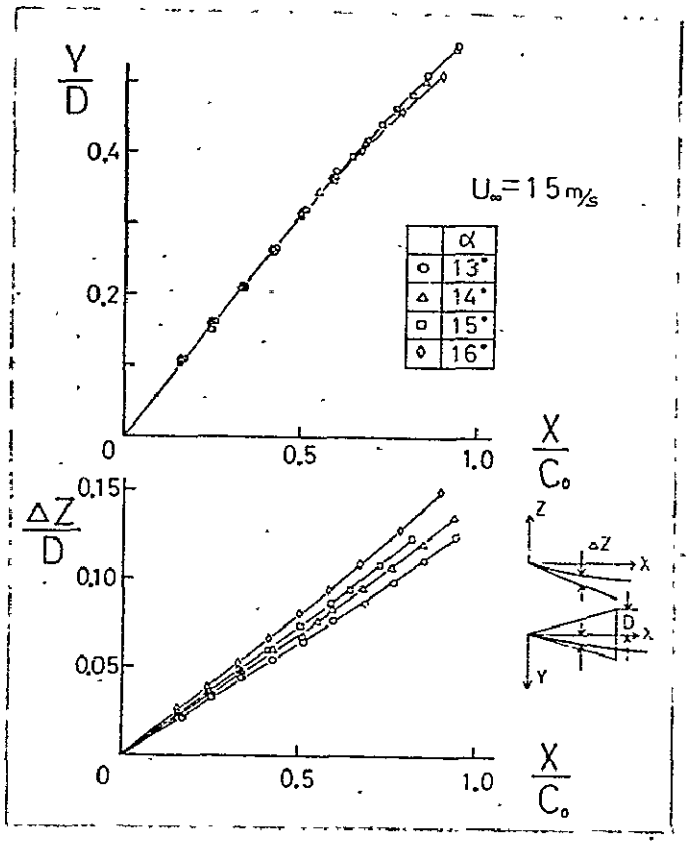

Fig. 8. Vortex Location ($\Lambda = 60^{\circ}$)

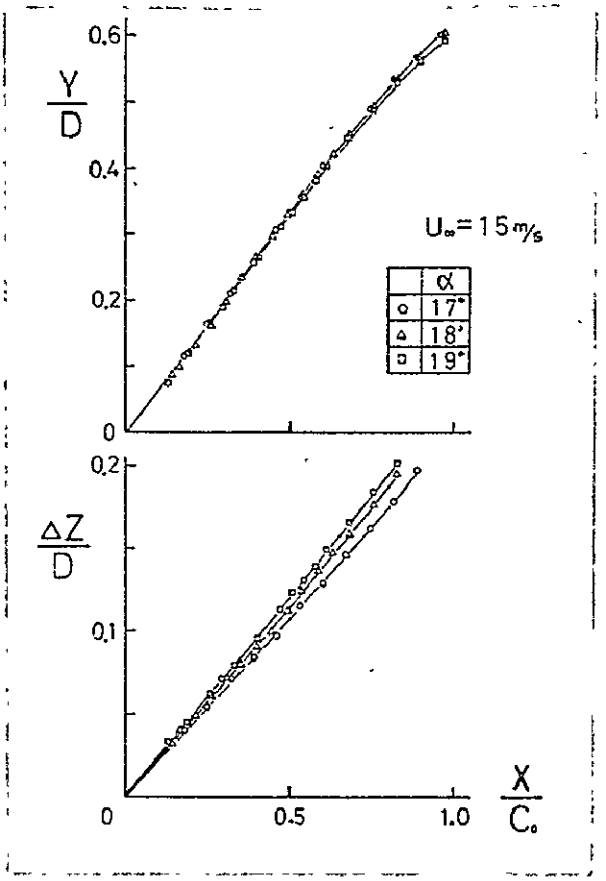

ORIGINAL PAGE IS
OE POOR QUALITY

Fig. 9. Vortex Location (Λ = 65°)

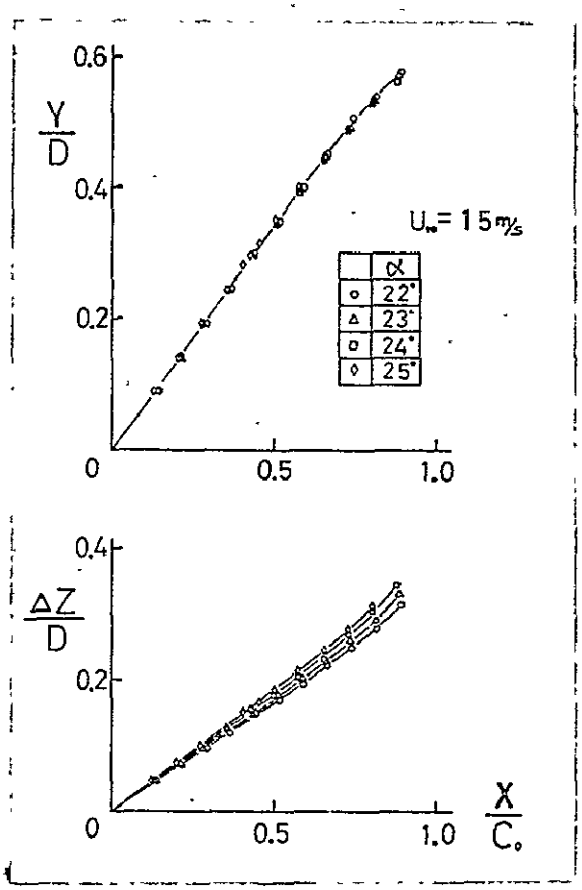

Fig. 10. Vortex Location ($\Lambda = 70^{\circ}$)

/8

Z denotes the distance along the vertical axis of the wind tunnel. ΔZ in the ordinates designates the distance from the wing surface to the vortex center along the Z-axis. Y designates the distance from the wing center line to the vortex center along the horizontal direction. These variables, Y and ΔZ, are normalized to be dimensionless by D, one-half of the wing width at the tail edge.

As seen from these figures, although the location of the vortex center is almost along a straight line on the upstream side in both horizontal and vertical directions; as the location becomes more downstream, it begins to curve toward the uniform flow. In each kind of model, the location at which the curve begins to be formed is more upstream with larger angle of attack. Furthermore, as the angle of attack becomes larger, the location

of the vortex center separates from the wing surface and moves upward while it moves toward the wing central axis horizontally. The data shown in these figures were obtained in steady-state conditions. However, it was reported [56] that there is a hysteresis in the location change of the vortex in non-steady states and that hysteresis has a significant effect on the damping of the pitching movement. In any case, the center of a vortex separated at the leading edge of a delta wing is located approximately along a straight line in steady-state conditions. Therefore, it is conceivable that linear vortex approximation is reasonable in such conditions when being treated theoretically.

2.2.2. Velocity in the Vortex Center.

Fig. 11 shows the average velocity in the vortex center when the apex angle is 60° and the angle of attack is varied from 13° to 16°. The abscissa designates the distance (measured by mm) from the wing tip along the central axis of the vortex, while the ordinate designates the central axis velocity U_c non-dimensionalized by the uniform-flow velocity U_∞.

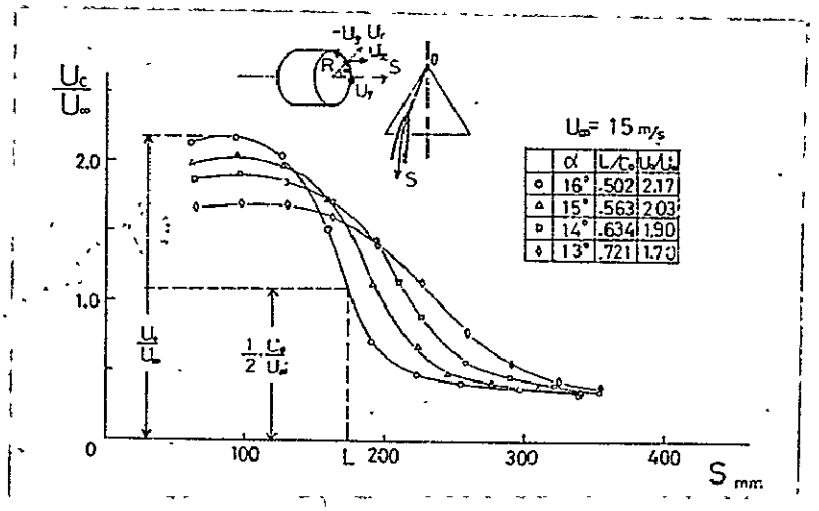

Fig. 11. Velocity in Vortex Center ($\Lambda = 60^{\circ}$)

Due to the positioning limitation of the traverse means, the /9
measurement was made from the wing tip. When the attack angle is constant, the vortex core is formed at the wing tip and grows rapidly. Therefore, the velocity on the central axis is larger than uniform-flow velocity U_∞. However, downstream beyond that point, the speed of the flow is rapidly decreased and finally falls beneath the level of the uniform flow. When the attack angle is large, the maximum velocity U_o on the central axis is larger and the reducing rate of the speed greater than when the attack angle is small. Using a 60°-apex angle model, measurements with an attack angle of 12° were done, but a rapid speed reduction such as one observed in the measurement with an attack angle of 13° or more was not observed and the velocity is held almost constant in the downstream region. In this case, the fluctuation of the hot-wire output signal is almost the same as the signal fluctuation on the upstream and any rapid change in the velocity is not observed, unlike the region in which the central axis velocity is reduced. This indicates that the breakdown does not occur on the wing when the attack angle is 12° or less. On the other hand, a rapid reduction of the velocity on the central axis suggests the occurence of the breakdown. As seen in Fig. 11, even when the velocity is reduced rapidly, it is not conceivable that stagnation is formed within the flow and the counter-flow region is spread toward the downstream side. By using a hot-wire, the direction, head or fair, cannot be differentiated. Therefore, it cannot be concluded that there is no counter-flow region, on the basis of the fact that the velocity in Fig. 11 does not become negative. In order to certify the /10
existence of the counter-flow region, the hot-wire probe was dismounted from its rotating means and an object with a shape similar to the probe and with a piece of woolen yarn attached to its tip is placed for observing the flow direction. According to this observation, there was no proof of the existence of the counter flow. Thus, it was concluded that the average velocity had been appropriately measured in the experiments.

It is very convenient if these velocity characteristics may be non-dimensionalized by an appropriate parameter and may be represented by a single curve. In this paper, the maximum velocity U_o on the central axis is used as a reference for the velocity, and the distance L between the wing tip and the location at which the velocity on the central axis becomes $U_o/2$ is used as a reference of the distance. The value L does not indicate the position of the breakdown, but has a certain relationship with the breakdown position. Figs. 12 to 14 show the changes of the velocity on the central axis with variables being non-dimensionalized by U_o and L. In each model, as the attack angle α gets larger, the value of L becomes smaller. In addition, the velocity changes are dependent on the apex angle Λ, i.e., the velocity reduction is more rapid when the apex angle of the model is larger. The data shown in these figures indicate that the average velocity on the central axis can be represented by a single curve using dimensionless variables U_c/U_o and S/L independent of the attack angle.

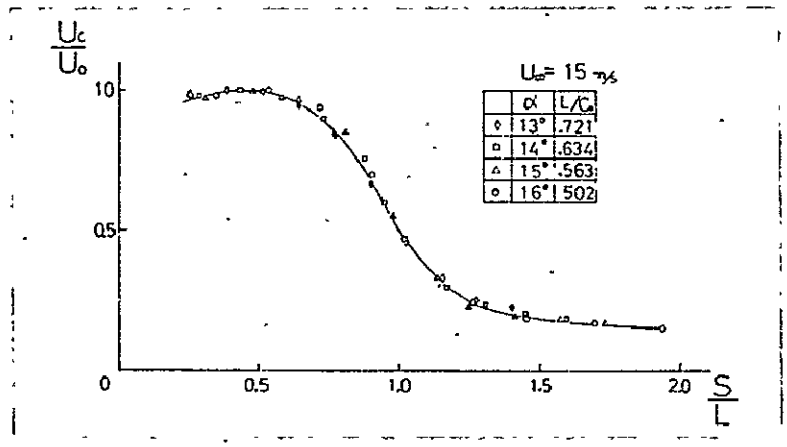

Fig. 12. Velocity in Vortex Center ($\Lambda = 60^o$)

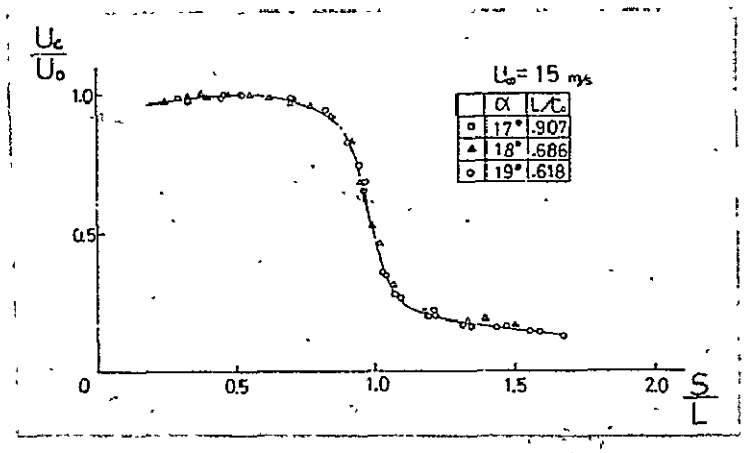

Fig. 13. Velocity in Vortex Center (Λ = 65°)

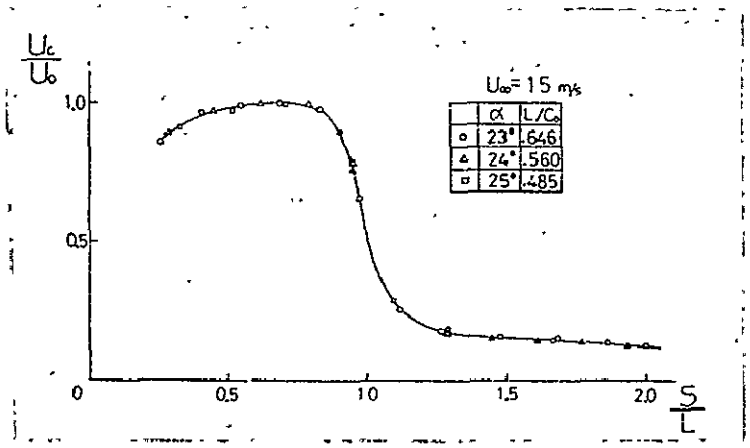

Fig. 14. Velocity in Vortex Center (Λ = 70°)

2.2.3. Total Pressure (Total Head) of Vortex Center

The position of the vortex center was obtained from the measurement results of the total pressure using the device attached parallel to the hot-wire probe, as seen in Fig. 6. However, since the hot-wire probe rotating means has a diameter which is larger than the vortex core diameter, the breakdown position judged from the total pressure measurement by this device is more downstream than the breakdown position determined by the central axis velocity measurement by the hot-wire. This fact[1] can be explained as follows: When the velocity on the central axis is measured by the hot-wire, a blockage, i.e., the hot-wire probe rotating means, is located at the vortex center. Consequently, the reverse pressure divergence on the vortex central axis gets greater and the breakdown is pushed forward. On the other hand, when the vortex center is measured by the total-pressure tube, the hot-wire probe rotating means is separated from the vortex center and the reverse pressure divergence does not get acute as before. Namely, when the total pressure is measured by the total-pressure measuring tube attached to a side of the hot-wire probe rotating means, the total-pressure measuring tube is measuring the total pressure in a flow-field which is different from that when being measured by the hot wire. Hence, the total pressure and the velocity on the vortex central axis measured by one of these methods is not consistent with those measured by the other.

For this reason, in a course of the experiment with the 17°-apex angle model, the hot-wire probe was dismounted and replaced

---

[1] According to the experimental results in [54], the breakdown position predicted from Fig. 5 in [54] is different from the discontinuous point of the total pressure shown in Fig. 6 in [54]. This is due to the fact that the total pressure was not measured by a keel tube but by a total-pressure measuring tube attached to a side of the hot-wire probe.

by a probe with the same shape and with a keel tube (shown in Fig. 4) at its tip, for measuring the total pressure. As a result, it is confirmed that the breakdown position judged from this arrangement is substantially well consistent with that determined by the velocity distribution. However, it should be noted that, since the diameter of the used keel tube is too large compared with the vortex core diameter, the data measured on the upstream where the absolute value of the total pressure is small as well as the vortex core diameter are not necessarily reliable. It should be further noted that, since instantaneous flow directions changed very rapidly behind the breakdown, the measured data may include large error terms. As mentioned above, the flow-field we measured is the vortex flow-field in the condition under which the reverse pressure gradient gets large due to a blockage of the hot-wire probe rotating means so that the breakdown is pushed forward and is located on the wing surface. This situation is similar to that in which Hummel put an obstacle in the downstream of a flow-field so that the breakdown position is pushed forward and examined for its effects.

Fig. 15 shows the measurement results of the total pressure on the vortex central axis, with a keel tube being used for a 65°-apex angle model at 17°-apex angle. In the ordinate, P_o designates the static pressure at the location where the velocity on the central axis reaches its maximum U_o, and Q_o designates the dynamic pressure $\rho U_o^2/2$ at the same position. The value of P_o was determined by the difference between the total pressure and the dynamic pressure obtained by the velocity. As seen from Fig. 15, the total pressure decreases toward the downstream, attains its minimal at the S/L value of about 0.9 and increases rapidly beyond that point. In the region where the total pressure increases, the fluctuation both in the total pressure and the velocity becomes very large, in particular, the hot-wire output signal for measuring the velocity fluctuates so furiously that it is difficult to read the average value. This fact indicates

that the flow-field after the breakdown occurs is in the region where the total pressure is very high. It should be pointed out in Fig. 15 that the total pressure on the vortex central axis changes discontinuously. On the upstream of the breakdown, since the time-average central axis of the vortex coincides with the instantaneous vortex center, the exact average of the total pressure can be measured if the vortex diameter is large enough compared with the keel tube diameter when the keel tube is aligned with the time-average central axis of the vortex. However, as mentioned in Section 2.4.1, on the downstream of the breakdown, the vortex is subject to the spiral transformation showing a precession movement, and, therefore, the time-average central axis of the vortex does not coincide with the instantaneous /11
vortex center. Thus, even if the keel tube is aligned to the time-average central axis of the vortex, the instantaneous flow direction may be greatly different from the direction of the probe, and the time-average of the total pressure cannot be measured accurately. However, at the location further downstream, the spiral transformation begins to disappear and to be replaced by a mild turbulent flow, and the time-average total pressure may be measured accurately. The discontinuous change in the total pressure, as seen in Fig. 15, may probably well be explained by the above description.

It should also be pointed out that, as a consequence of the above arguments, the accurate time-average of the total pressure was not obtained in the range where S/L is greater than about 0.9 or is less than about 0.5, in Fig. 15. Regardless of the explanation, it can be clearly pointed out that the total pressure decreases before the breakdown while increasing beyond the breakdown, as a matter of fact. Even when the measurement is done using the total-pressure measuring tube attached to a side of the hot-wire probe, not using a keel tube, the shape of the resulting data is similar to that shown in Fig. 15. However, in such a case, the discontinuity point of the total pressure is moved

toward the direction in which S/L increases, i.e., the downstream direction. Besides this fact, the overall pattern of the change in the total pressure and the relative values are almost identical to those shown in Fig. 15.

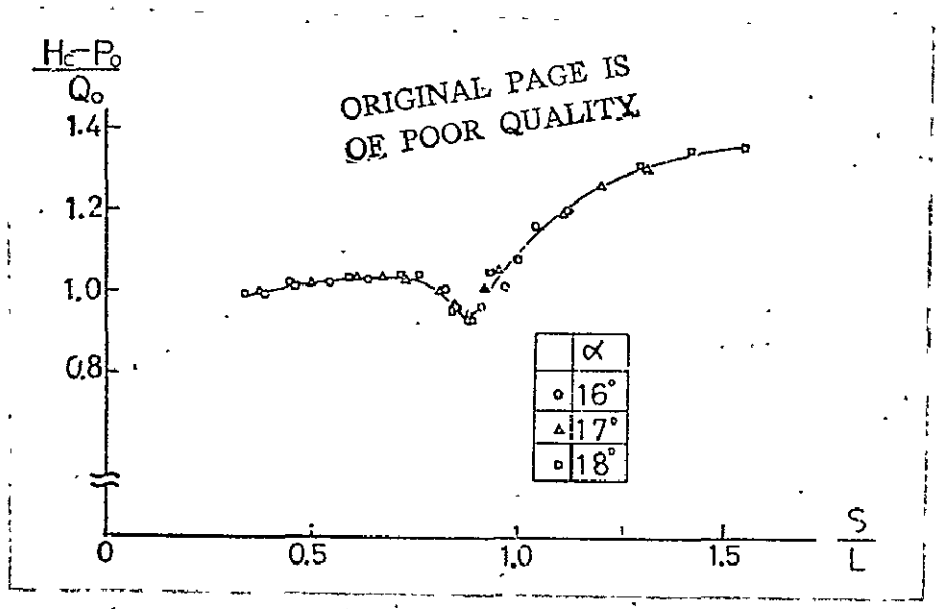

Fig. 15. Total Pressure at Vortex Center (Λ = 65°)

As seen from Fig. 15, as in the case of the velocity at the vortex center, the variation of the total pressure on the vortex central axis is independent of the attack angle and can be represented by a single curve using the dimensionless variables, S/L and $(H_c-P_o)/Q_o$ if the apex angle is constant.

2.2.4. Effects of Reynolds Number

Reynolds' number has a significant effect on the separation phenomenon in which the boundary layer is separated from the object surface, and in particular, the separation point and the phenomena caused by the separation are highly dependent on the Reynolds number. However, it is said that the effect of the Reynolds number is relatively little on the breakdown of the vortices created on the surface of a delta wing with an acute

leading edge which fixes the separation point at the leading edge. It is shown by the experiments by Lambourne et al, [21] in which the Reynolds number is between 0.01×10^6 and 4.6×10^6 and the delta wings have very sharp leading edges, that the breakdown position does not greatly change in response to the change in the Reynolds number. On the other hand, with regard to experiments [26] of swirl flow within a cylinder, it was reported that the breakdown position of the vortex changes according to the Reynolds number and moves forward toward the upstream side when the Reynolds number becomes greater, and that [27] the breakdown position is also influenced by the boundary layer which developes along the wall of the cylinder. In the experiments by Lambourne et al, the water or the air was used as a fluid medium and dye or smoke was injected for determining the breakdown position, but this has the following disadvantages: Namely, according to their method, the breakdown position cannot be obtained with a quantitative accuracy and a systematic procedure of experiments is impossible since different Reynolds numbers require different measurement methods. Therefore, it is not appropriate to conclude that the experimental results by Lambourne et al. imply the independence of the breakdown position from the Reynolds number.

In order to investigate such effects of the Reynolds number, we measured the velocity change on the central axis of the vortex and the value of L with a 65°-apex angle model fixed at an 18°-attack angle and with the uniform flow of wind speeds changed from about 5 m/s to 15 m/s. The result of that experiment is shown in Fig. 16. Due to the model which is lacking in strength, the speed of the uniform flow cannot be changed over a wide range. Accordingly, the change in the Reynolds number was /12 relatively small; i.e., the Reynolds numbers $U_\infty C_o/\nu$ normalized by the central chord length of the wing and by the uniform flow were 1.6×10^3 and 4×10^3. In this range of the Reynolds number, the results of our experiments, $L/C_o=0.603$ and 0.605, did not

indicate any significant change due to the change in Reynolds number and it is conceivable that the obtained change is within the range of the measurement error.[2] This fact seems to indicate that the value of L is not determined by a viscous flow but by a non-viscous flow created by the model fixed at an attack angle.

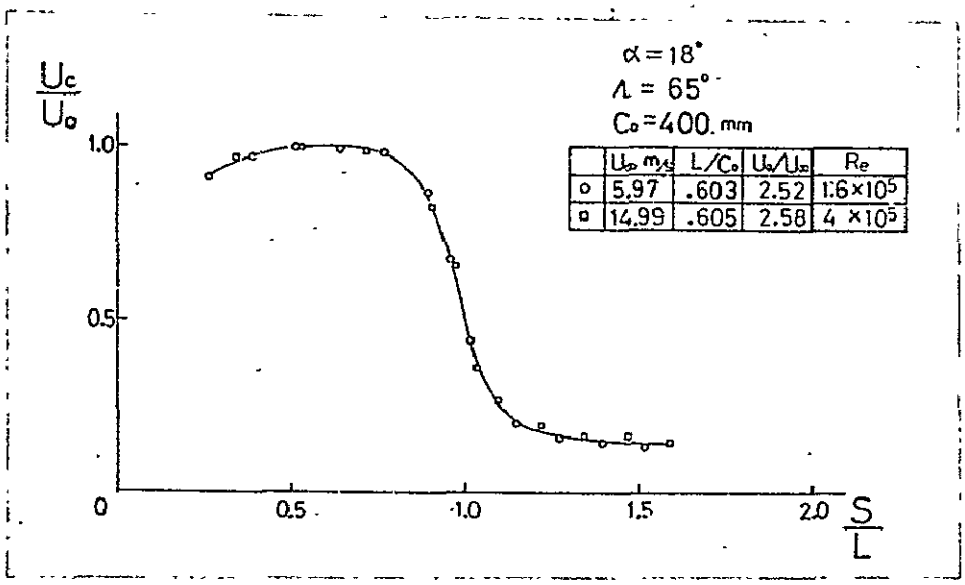

Fig. 16. Effect of Reynolds Number.

Although the value of L is related to the breakdown position, it cannot be concluded only by the result of this experiment that the breakdown position is independent of the Reynolds number since the value of L is not a quantity which directly indicates the position of the breakdown. In order to obtain more accurate conclusions with respect to this matter, a number of additional experiments are necessary, in which the breakdown positions are directly measured with many different Reynolds numbers.

---

[2] The central chord length C_O of the model is 400 mm. The difference of L/C_O values, 0.605 and 0.603, corresponds to a very small difference, 0.8 mm, when it has been converted to the actual size. Since the position of L is determined on the graph by seeking the point where $U_O/2$ is obtained, the difference, 0.8 mm, is included entirely within the range of errors.

2.3. Characteristics of Vortex Cross Section

2.3.1. Axial Symmetry of Vortex

If the structure of the vortex is axially symmetric, theoretical analysis becomes relatively easy. Figs. 17 and 18 show the distribution of the average axial velocity component U_x and that of the circumferential velocity U_φ component, which were measured by a hot-wire probe moved horizontally and vertically within a cross-section perpendicular to the central axis of the left vortex created on the surface of the wing having a 65°-apex angle and fixed at a 17°-attack angle. Since the radial component of the velocity is relatively very small compared with the other variables, the axial velocity component and the circumferential velocity component and, hence, the figure showing the radial velocity component are omitted. Fig. 17 shows the measurement results on the upstream of the breakdown position while Fig. 18 shows the measurement results at the locations which are far downstream of the breakdown point. As seen from these two figures, the time-average velocity distribution exhibits a substantial axial symmetry despite the existence of the breakdown. The results of the measurements in which the device is traversed horizontally indicate an aspect which is considerably different from that when traversing vertically. This difference is due to the vortex layer which is involved from the leading edge on the left side, i.e., in the neighborhood of the leading edge. However, when considering a narrow portion near the vortex center, e.g., the vortex core, it will be relatively reasonable that the axial symmetry may be assumed. Since this experiment thus insures the axial symmetry of the vortex to some extent, the velocity distribution measurements described from now on were done only for the horizontal direction which is the easiest direction for the measurements.

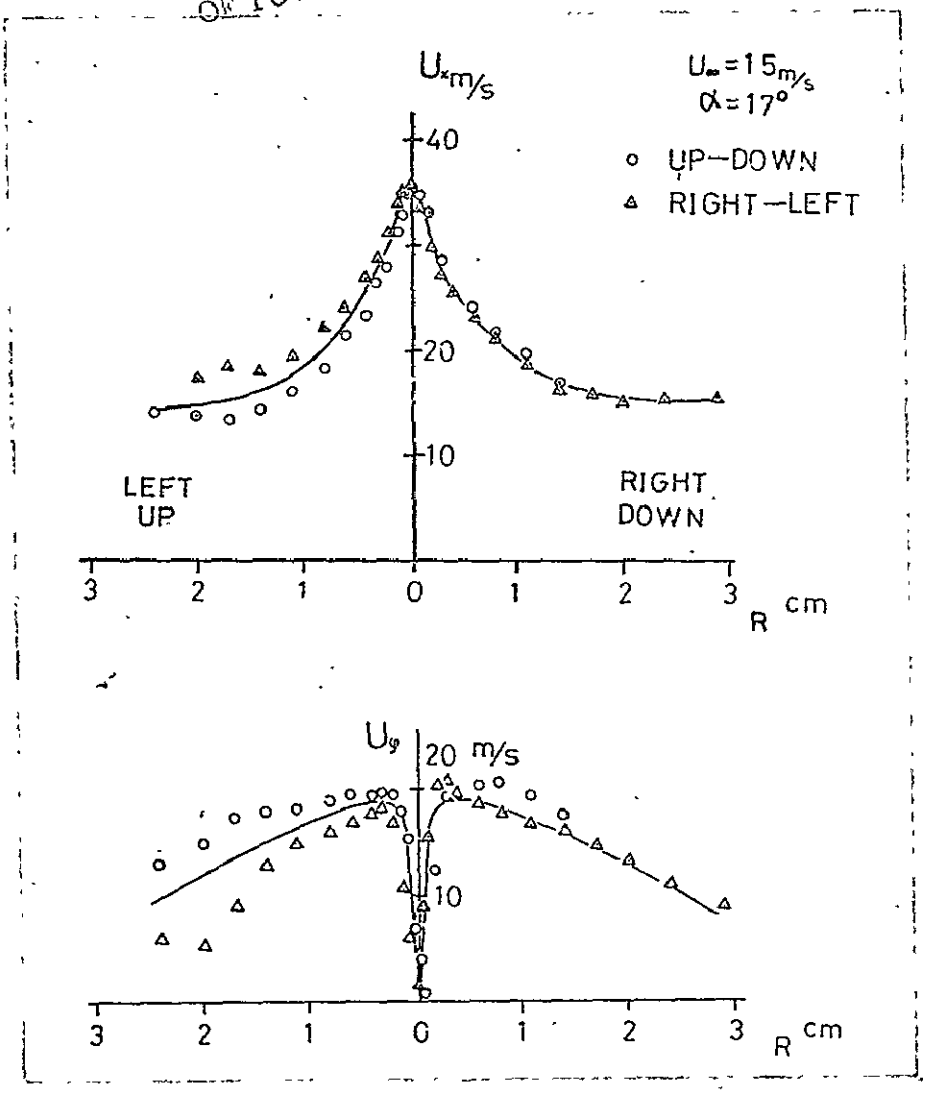

Fig. 17. Axial Symmetry of Vortex
(Before Breakdown)

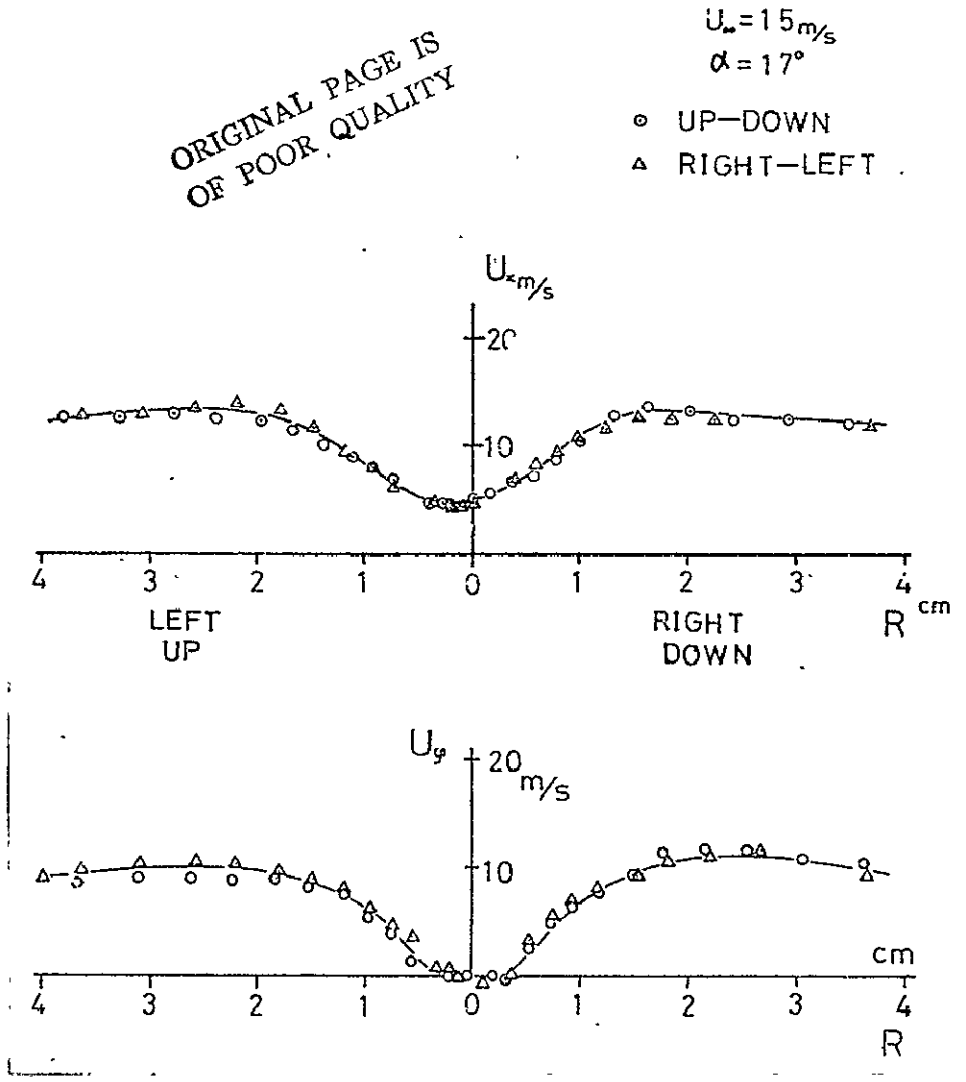

Fig. 18. Axial Symmetry of Vortex (After Breakdown)

Fig. 19 shows the characteristics of the velocity distribution before and after the breakdown. The experiment was done with respect to the right vortex on the model having a 65°-apex angle and fixed at an 18°-attack angle, while traversing horizontally. In the figure, the ordinate y designates the horizontal distance from the origin at the central axis toward the right direction perpendicular to the central axis, U_x, the velocity component in the direction of the vortex central axis,

the absolute value of U_z, the circumferential velocity, and U_y, the radial velocity. The location where S/L = 0.766 is on the upstream of the breakdown while the location where S/L = 1.01 or 1.22 is on the downstream of the breakdown. This figure indicates three characteristic features of the development and the breakdown of the vortex. First, the distribution of the axial velocity component has completely different shapes after and before the breakdown. Second, there is no substantial change in the distribution of the circumferential velocity. Third, the radial velocity component is relatively small compared with the other two velocity components, despite the breakdown, and the velocity vector is directed away from the center. In the measurement in which a hot-wire is rotated, the measurement accuracy is about 2% of the full scale and the measurement error is about 1 m/s. When considering this fact, it seems to be reasonable to use an approximate quasi 2-dimensional model for theoretical analysis, assuming that the radial velocity component is small enough to be ignored compared with the other two velocity components. /13

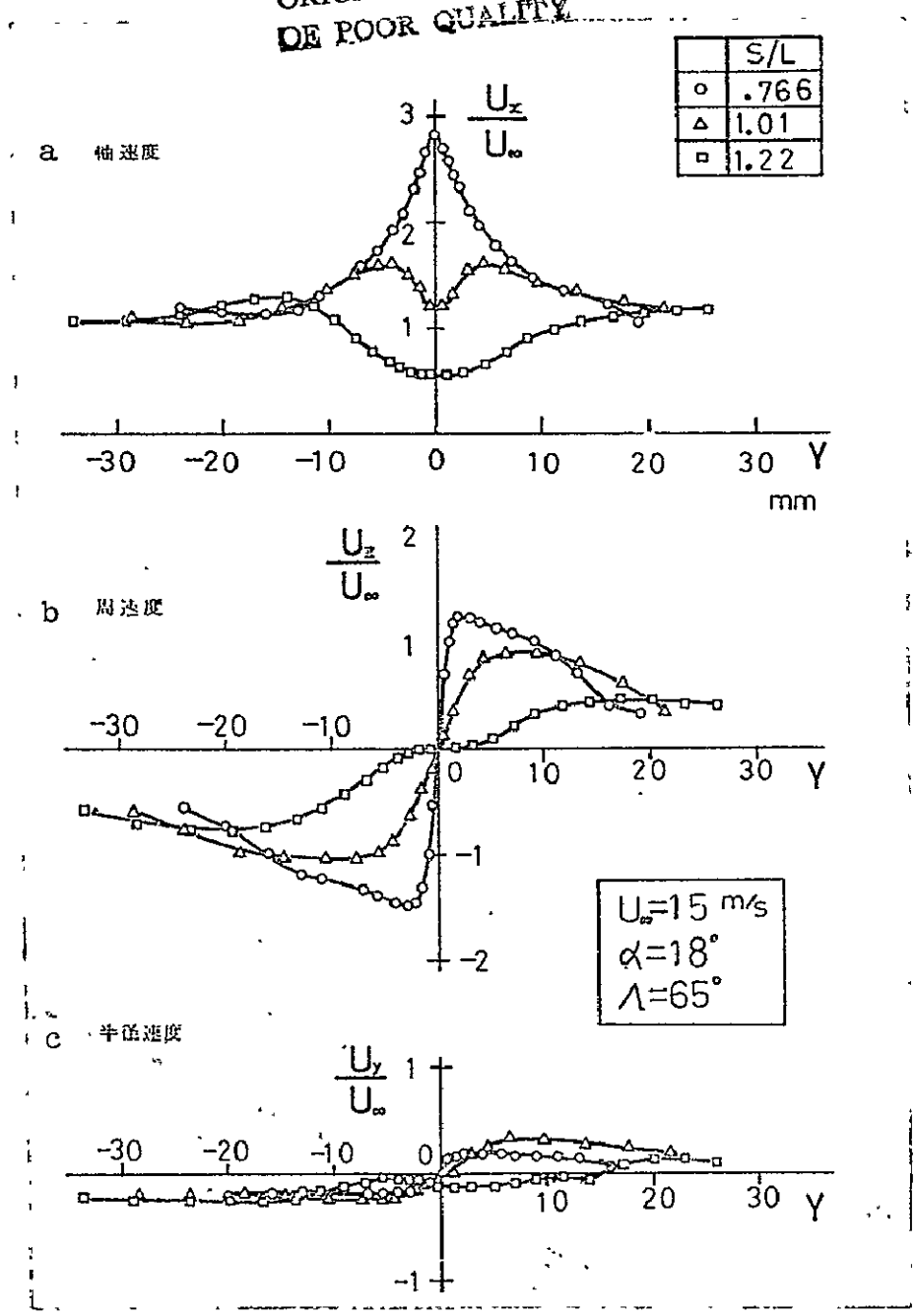

Fig. 19. Characteristics of Velocity Distribution

Key: a: Axial Velocity
b: Circumferential Velocity
c: Radial Velocity

2.3.2. Distribution of Velocity

Figs. 20 and 21 show the results of the average velocity distribution which was measured with respect to the left vortex created on a 65°-apex angle model while varying the angle of attack from 17° to 18° and traversing horizontally. In this experiment, the maximum axial velocity U_o and the L were as follows:

	U_o/U_∞	L/C_o
18°	.2.73	0.607
17°	2.48	0.716

/14

In these figures, the abscissae are represented by the parameter R/L which is non-dimensionalized from the radial distance R in terms of the reference length L, and the parameters, U_x/U_o and U_φ/U_o in the ordinates are non-dimensionalized from the axial velocity U_x and the circumferential velocity U_φ in terms of the maximum axial velocity U_o.

Distribution of Axial Velocity

On the upstream side where the value of S/L is small, the average axial velocity attains its maximum value in the vortex center and decreases rapidly in response to the increase of the radial distance. Although the maximum values vary depending on the attack angle, they reach 2 to 3 times as great as those of the uniform flow. Thus, the axial velocity distribution on the upstream side where S/L is small may be characterized by the fact that the velocity is very high in a narrow region, including the vortex center and by the distribution's shape which is convex upwardly in the neighborhood of the central axis of the vortex. On the downstream where the value of S/L is larger, the value on the vortex central axis decreases rapidly and the region of high

axial velocity extends outwardly, indicating the increase of the vortex core diameter. When S/L reaches 0.963, the shape of the distribution is completely different from that on the upstream and the value on the vortex central axis becomes less than that on the peripheries. Namely, in this distribution, the value in- /15
creases from a low value in the center as moving radially away from the center and attains a maximum value, decreasing slowly after it attains its maximum. This distribution has the minimal point on the vortex central axis and the maximal points outside the central axis. Such a tendency, i.e., a rapid decrease of the velocity on the vortex central axis, becomes stronger as it moves toward the downstream, and the axial velocity on the vortex central axis goes down to values which are less than the level of the uniform flow. Such distribution on the downstream where S/L is large is characterized by the distribution's shape which is convex downward in the neighborhood of the vortex central axis. When the distribution with such a shape was observed, the readings of the velocity and the total pressure fluctuated to a large extent and it became difficult to read average values of the output signals from the hot wire and the pressure probe, indicating the non-stationarity of the flow-field and the existence of the breakdown. Thus, the shape of the distribution changes entirely from "upward convex" to "downward convex," at the point of the breakdown when moving downstream. Fig. 20 shows that the breakdown occurs at the position where S/L is approximately 0.9 under the experimental conditions with an apex angle of 65° and an attack angle of 17° to 18°.

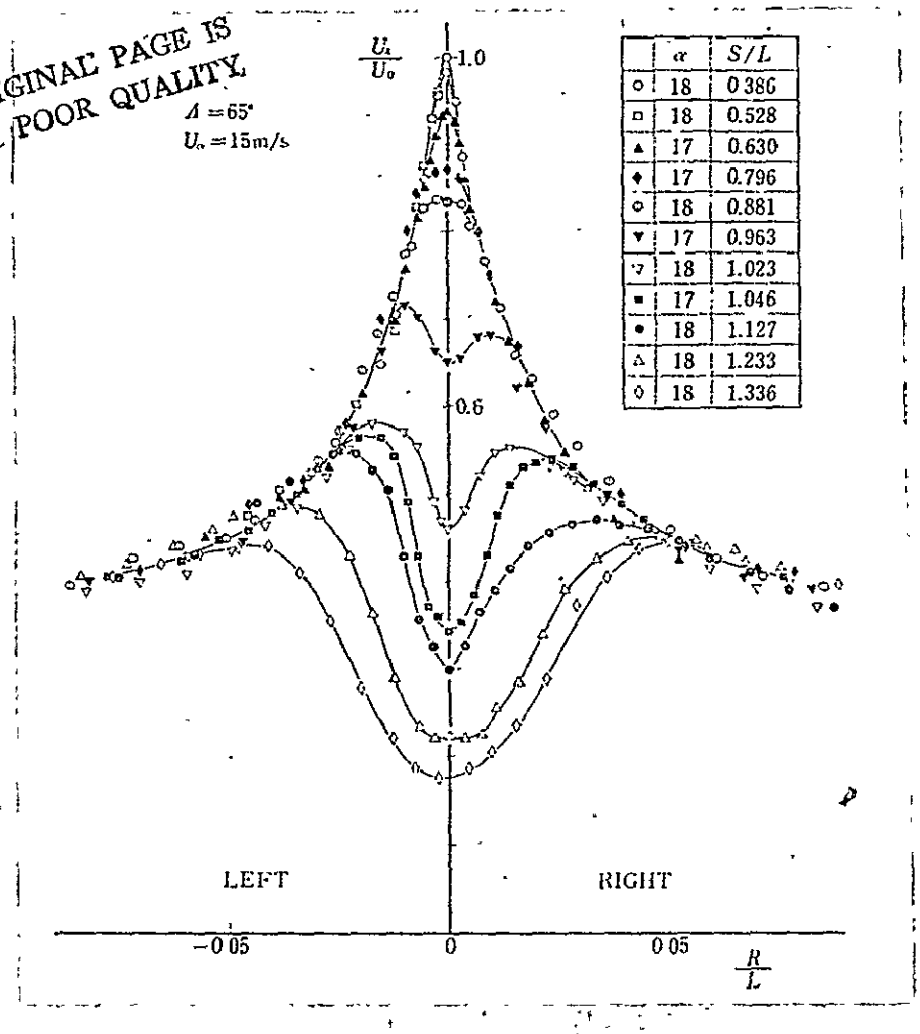

Fig. 20. Distribution of Axial Velocity.

Distribution of Circumferential Velocity

On the upstream side where the value of S/L is small, the velocity gradient is large within a narrow region in a neighborhood of the central axis and becomes linear as it moves radially. After attaining a maximum point, the velocity distribution has an approximately hyperbolic shape like the distribution without vortex. Thus, it may be concluded that, on the upstream side, there exists a vortex core where the fluid is rotating at a constant angular velocity as if it were a solid body and the vortex core has a very small diameter. As S/L becomes larger, i.e., moving downstream, the angular velocity of

the vortex core rotation decreases as well as the maximum value of the circumferential velocity. However, the diameter of the vortex core increases on the contrary. When the value of S/L reaches 0.963 on the further downstream side, the distribution no longer has a portion which resembles a hyperbole in the neighborhood of the vortex core and is dissipated outward. When S/L is 1.213, there appears a region in the neighborhood of the vortex central axis where the gradient of the circumferential velocity is zero, i.e., the angular velocity of the rotation is zero. This region where the circumferential velocity is zero is radially expanded as it moves further downstream.

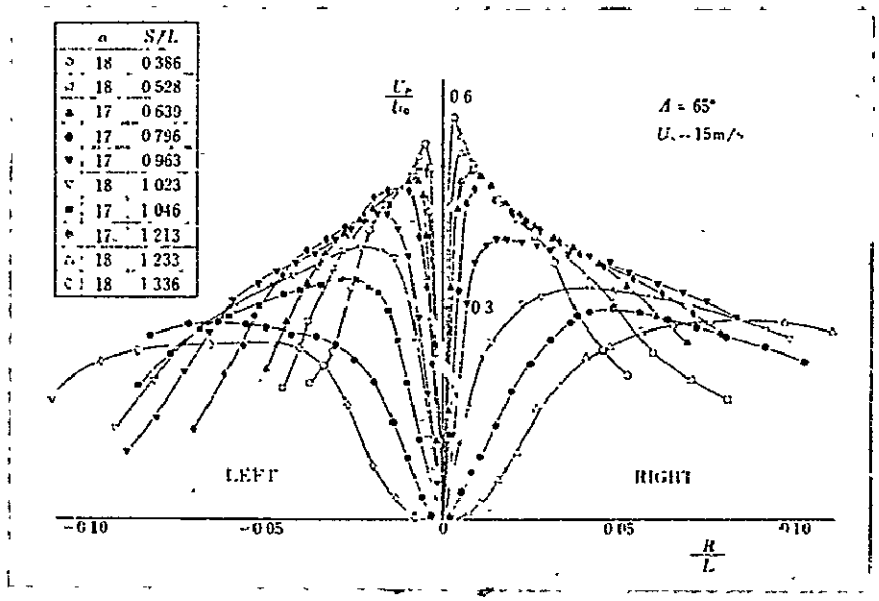

Fig. 21. Distribution of Circumferential Velocity.

The change of the circumferential velocity distribution can be characterized by the fact that the angular velocity of the vortex rotation decreases as it moves downstream and becomes zero at last. As mentioned previously, the distribution of the average axial velocity changes its shape completely at the position of the breakdown. Contrasting this fact, the distribution of the circumferential velocity does not change its shape

drastically at the point of the breakdown. It is only observed that the angular velocity of the vortex core rotation changes at the breakdown point.

Thus, it may be concluded that, in a case of a vortex with a high axial velocity in its vortex core with a very small diameter, such as the vortex separated at the leading edge of a delta wing, the most outstanding change in the average velocity components due to the breakdown is that of the shape of the axial velocity-component distribution. Hence, it is quite understandable that our experimental results show the possibility of determining the breakdown position by observing the point at which the axial velocity distribution in the neighborhood of the central axis changes its shape from "upwardly convex" to "downwardly convex".

2.3.3. Distribution of Swirl

For investigating the structure of the time-average flow-field created by a vortex separated at the leading edge of a delta wing, it is convenient to analyze the swirl distribution. The components of the swirl vector in a time-average flow-field can be calcualted from the average velocity vector using the cylindrical coordinate representation according to the following equation.

$$\omega_x = \frac{1}{r}\frac{\partial(r\,u_\varphi)}{\partial r},$$

$$\omega_\varphi = \frac{\partial u_r}{\partial x} - \frac{\partial u_x}{\partial r} \fallingdotseq -\frac{\partial u_x}{\partial r} \qquad (1)$$

and

$$\omega_r = -\frac{\partial u_\varphi}{\partial x}.$$

In (1), ω_r designates the radial component of the swirl vector and is ignored in this section since the rotational direction of the vortex line is only a matter of concern in this section. In calculating the circumferential component ω_φ, the term $\partial U_r / \partial x$ is much less than the other term $\partial U_x / \partial r$ and is therefore ignored. The swirl distribution was obtained by numerically differentiating the measurement results of the flow-field created by a model having a 65°-apex angle and being fixed at a 17°-attack angle. Since the measured average velocity distribution is not completely axisymmetric about the vortex central axis, the average values of both sides were used.

Fig. 22 shows the distribution of the axial component of the swirl vector which was calculated according to the equation (1). On the upstream side where S/L is small, the swirl is concentrated in a very narrow region, including the vortex center and forms a so-called vortex core. As it moves toward the downstream side where S/L is larger, however, the swirl vector becomes smaller in size and the diameter of the vortex core is extended instead. As it moves further downstream, the swirl in the center becomes smaller than that in the periphery and the swirl axial component ω_x exhibits its maximum point at a location apart from the center. This fact indicates that the breakdown phenomenon does not simply mean a relative dissipation of the swirl distribution but corresponds to a drastic transformation of the flow-field where the swirl distribution changes its shape completely.

ORIGINAL PAGE IS
OF POOR

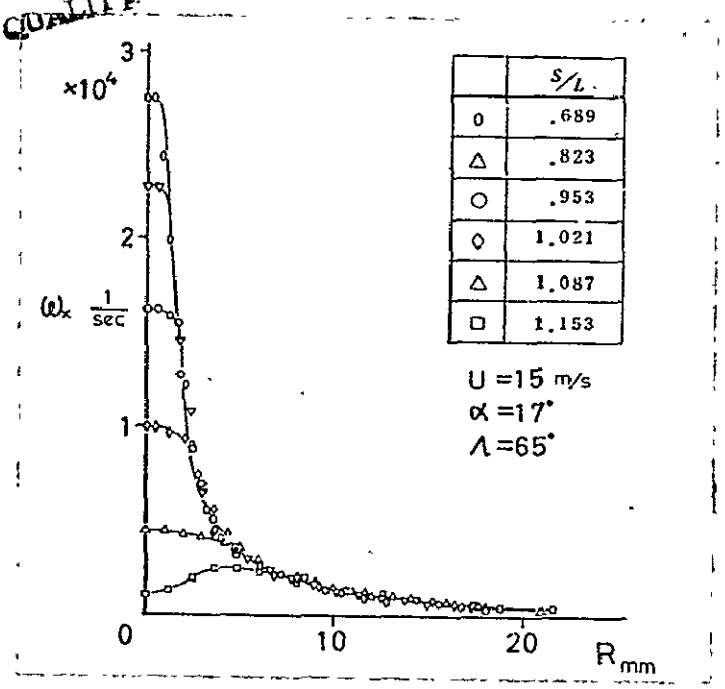

Fig. 22. Distribution of Swirl (ω_x-Component)

Fig. 23 shows the distribution of the circumferential component of the swirl vector. The circumferential component ω_φ is one-order smaller in size than the axial component ω_x. However, it is one important element which determines the rotational direction of the swirl vector. On the upstream side where S/L is small, the value of ω_φ increases rapidly from zero to the maximum value in the radial direction and decreases gradually afterwards approaching the zero level again. The maximum point moves outward as the location moves to the downstream. On the further downstream where the value of S/L reaches 0.953, the value of ω_φ decreases rapidly from zero to a negative minimum value, increases gradually beyond this point, attains a positive maximum value, and then decreases again approaching the zero level, as the point moves outward. The location at which this negative minimum value is attained moves outward as S/L increases, and its absolute value increases initially and decreases afterwards. The fact that the value of ω_φ is negative means

/18

/19

that the axial velocity U_x is low in the center and high around it, showing a distribution curve which is convex downward. It also characterizes the condition after the breakdown occurs.

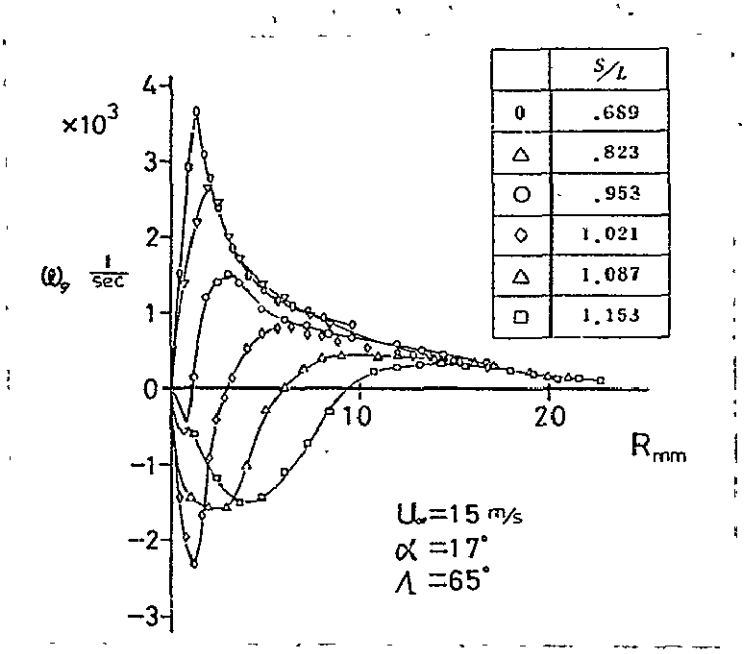

Fig. 23. Distribution of Swirl
(ω_φ -Component)

Fig. 24 shows the direction of the swirl which is calculated based upon the following equation:

$$\theta = \tan^{-1}\left(\frac{\omega_\varphi}{\omega_x}\right) \qquad (2)$$

When S/L is less than 0.823 (upstream), θ is positive independent of the radial distance. However, as it moves downstream and S/L reaches 0.953 where the flow-field enters the region after the breakdown, a region where θ is negative appears in the neighborhood of the center. The region where θ is negative is widened as S/L increases and the absolute value of the negative minimum value of θ is similarly increased. Fig. 24 shows the condition in which the direction of the swirl vector is

reversed due to the breakdown, and the reversed region extends outward from the center.

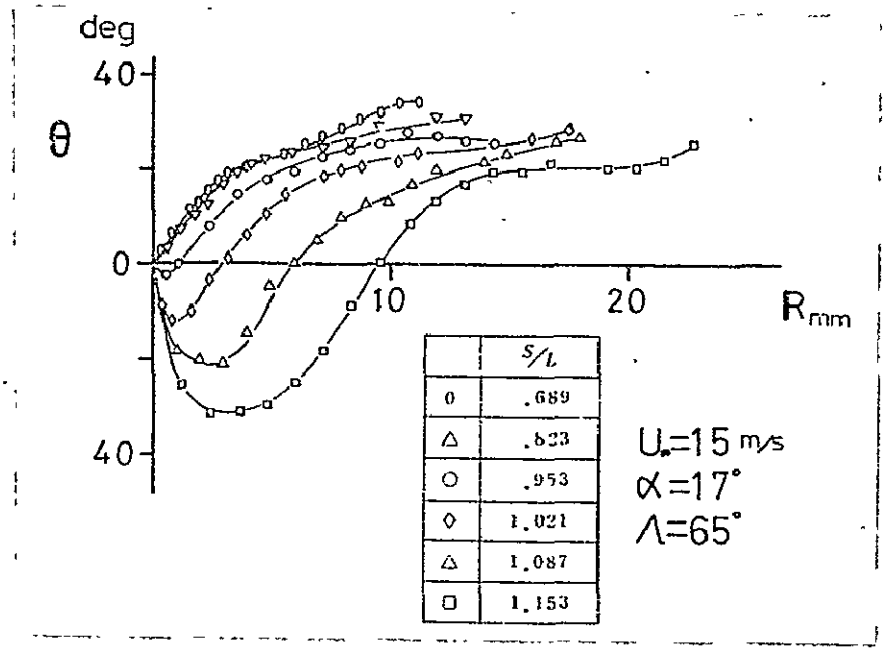

Fig. 24. Direction of Swirl Vector

Fig. 25 shows a model of the right vortex separated at the leading edge of a delta wing. The model is depicted based on the deformation of the swirl vector (Figs. 22 to 24) which has been described above. In the figure, two swirl tubes are drawn, one close to the central axis and the other away from it. Each direction of the swirl vector existing on the surface of each swirl tube is represented by solid and broken lines. The swirl vector initially rotates spirally around the central axis with the same rotational direction as that of the vortex core. As moving downstream, the value of θ becomes less, and the number of turns of the spiral per unit length in the direction of the central axis becomes less. Moving further downstream, θ becomes zero at last, and the swirl vector has the same direction as the central axis and stops rotating around the central axis. Further downstream, the swirl vector has a rotation direction which is opposite to the initial rotation

direction and rotates again spirally around the central axis. Then, both the value of θ and the number of turns per unit length increase moving downstream. It is an important fact to observe that the region where the swirl vector rotates in the opposite direction expands outwardly as it moves toward the downstream, as shown by the broken line in Fig. 25.

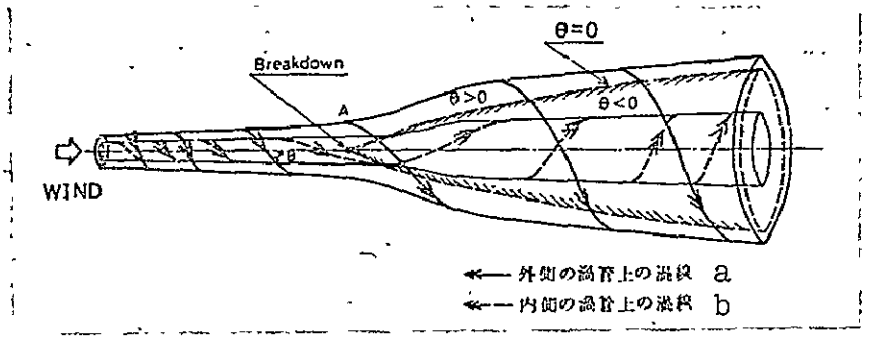

Fig. 25. Transformation of Vortex Lines

Key: a. Vortex Line on an Outer Vortex Tube.
b. Vortex Line on an Inner Vortex Tube.

Das [56] gave the following explanation of the breakdown phenomenon and made a simple calculation: "Vortex string is separated from the leading edge of a delta wing, concentrates on the wing surface and forms a vortex core. The other end of the vortex string is either washed away downstream from the tail edge, or separated from the wing surface at a separation point if such a separation occurs on the wing surface. Such vortex string which is washed away is involved into a vortex core on the downstream. However, the rotational direction of the vortex separated at the leading edge is different from that of the vortex which is washed away from the tail edge or separated on the wing surface, and, moving downstream, the vortex with negative rotational direction becomes stronger, thus inducing the velocity directed from the downstream to the upstream in the neighborhood of the central axis and creating the breakdown." /20

However, according to this explanation, the region where the vortex string rotates in a reverse direction must expand from the outside of the vortex axis toward the central axis. Therefore, the explanation is not consistent with our experiment which indicates that the reverse rotation region expands outwardly, as shown in Fig. 25. On the contrary, the result shown in Fig. 25 is one of the experimental proofs for the observational results by Lambourne et al.[21] which say that the center of the vortex core is subject to a reverse-rotation spiral transformation and will lead to a breakdown. In Fig. 25, however, the structure of the time-average flow-field created by the vortex is explained by the transformation of the vortex lines, but the instantaneous direction of the swirl vector is not shown. Therefore, it should be noted that the condition depicted in Fig. 25 is different from the instantaneous condition of the vortex observed by Lambourne et al. The relationship between instantaneous and time-average flow-fields will be described later in Section 2.4.1.

2.3.4. Distribution of Turbulence

Fig. 26 shows the turublence distribution which was measured with respect to the right vortex generated by a 65°-apex angle model fixed at an 18°-attack angle while the hot wire was fixed horizontally and traversed in the right and left directions. In the measurement, a linearizer was used, and the dc and ac components of the hot-wire output were read by a dc voltmeter and an RMS-meter, respectively. The turbulence is represented by the ratio of the ac components to the dc component by percentage. It should be noted that the hot wire was fixed at a fixed angle in the wind tunnel and was not necessarily perpendicular to the average velocity vector.

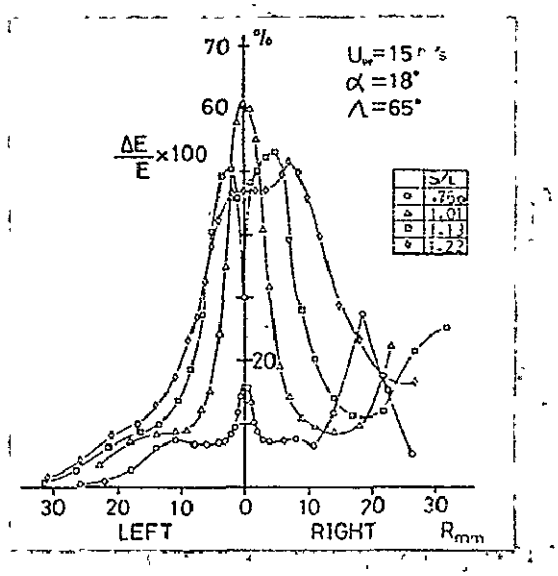

Fig. 26. Distribution of Turbulence.

On the upstream where S/L is 0.766, the turbulence has the maximum value, 16%, on the vortex central axis and decreases in radial directions. It is thought that the turbulence is greater on the right side since the existence of the leading edge causes vortex layers to be wound up.

When S/L is 1.01, although the distribution has the same shape, the maximum value reaches 61%. On the further downstream where S/L is 1.13, the distribution has a completely different shape which is convex downwardly, in the neighborhood of the center. Further downstream, where S/L is 1.22, the value on the central axis is increased and the distribution has a shape similar to that on the upstream. As seen in Section 2.4.1, the phenomenon in which the turbulence becomes large and the distribution comes to have a downward convex shape can be explained by the fact that the instantaneous vortex center moves outward due to the spiral transformation according to the breakdown and that the precession motion of the vortex causes the velocity fluctuation. In the region downstream of the region where the spiral transformation can be clearly observed, the spiral

transformation is not clearly formed with less swirl concentration, and the velocity fluctuation is averaged by the resulting turbulence flow, thereby making the distribution have the same shape as that at the position ahead of the breakdown, where the shape is upwardly convex in the neighborhood of the central axis. However, although the shape is the same, the maximum value of the distribution is much greater than that ahead of the breakdown and the region of the turbulence grows outwardly as the vortex diameter increases.

The frequencies of the velocity are around several Hz and the high frequencies are dominant when S/L is 0.766. At that /21
point, the low frequency components are hardly observable. When S/L becomes 1.01, however, the frequencies are around fifteen Hz and the low frequency components prevail. The appearance of those low frequency components is related to the spiral transformation of the vortex, as described later in Section 2.4.1. Further downstream, where S/L reaches 1.22, the low frequency components begin to decrease. This corresponds to the fact that the spiral transformation of the vortex decays and becomes a mild turbulent flow.

Fig. 27 shows a vidi-corder record of the output waveform of the hot wire which is placed on the central axis at the location where S/L is 0.567, when the apex angle is 65° and the attack angle is 18°. Since this location is ahead of the breakdown position, low frequency fluctuation with a large amplitude is not observed. Instead, high frequency components are observed in a random waveform and are likely to be due to the rotational angular velocity of the vortex core. Fig. 28 shows a waveform of the hot-wire output at the location immediately after the breakdown, where S/L is 0.935. As seen from this figure, the hot-wire output voltage fluctuates largely from OV (zero wind speed) to 1V (which corresponds to the wind speed of about 50 m/s if the air stream is assumed as flowing along the

probe axis of the hot wire). The measurement point was not exactly on the central axis. Instead, the hot wire was located at the position where the vortex after the breakdown should exhibit the spiral transformation and the vortex center should pass through. As seen from the waveform, unlike that observed on the upstream of the breakdown, low frequency components around fifteen Hz are observable. Fig. 29 shows a result obtained at the location which is a little further downstream, where S/L is 1.13. Also, in this case, the hot wire was set aside from the central axis and the output was filtered by a 500-Hz low pass filter so as to reject the high frequency components which are supposed to be generated by the rotational angular velocity of the vortex core. Fig. 30 shows the result of the hot-wire output signal after being filtered by a 10-Hz low pass filter. This was done for the purpose of investigating the low frequency components which appear after the breakdown, and was performed after having observed the prevailing low frequency components by an oscilloscope so as to determine the necessary low pass filter. According to this figure, the existence of a low frequency of about 13 Hz is observed.

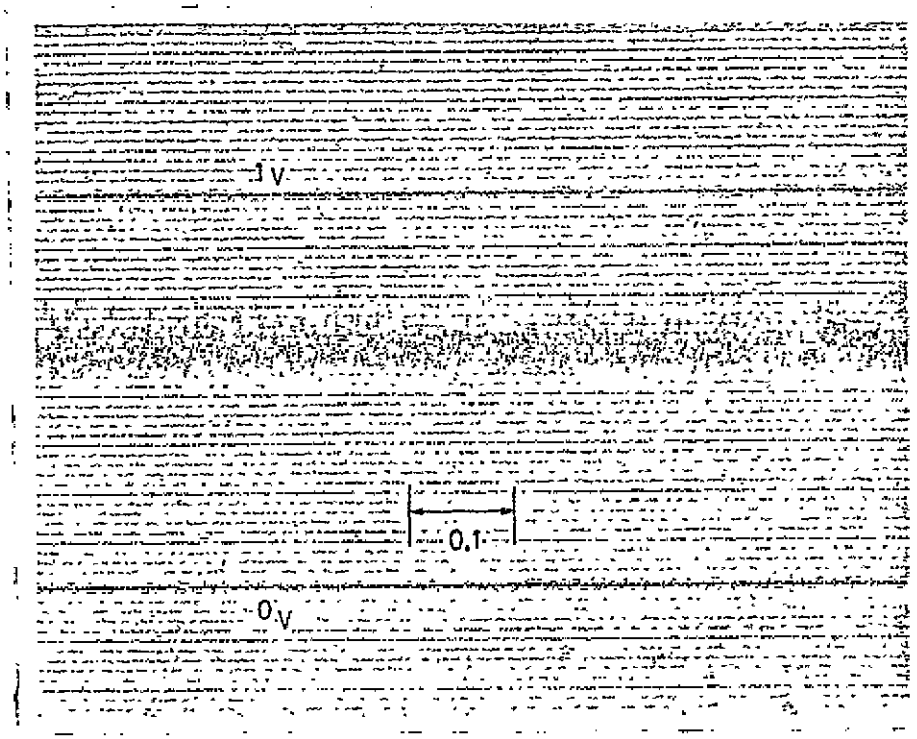

Fig. 27. Hot Wire Output Signal
(Ahead of Breakdown, S/L = 0.567)

/22

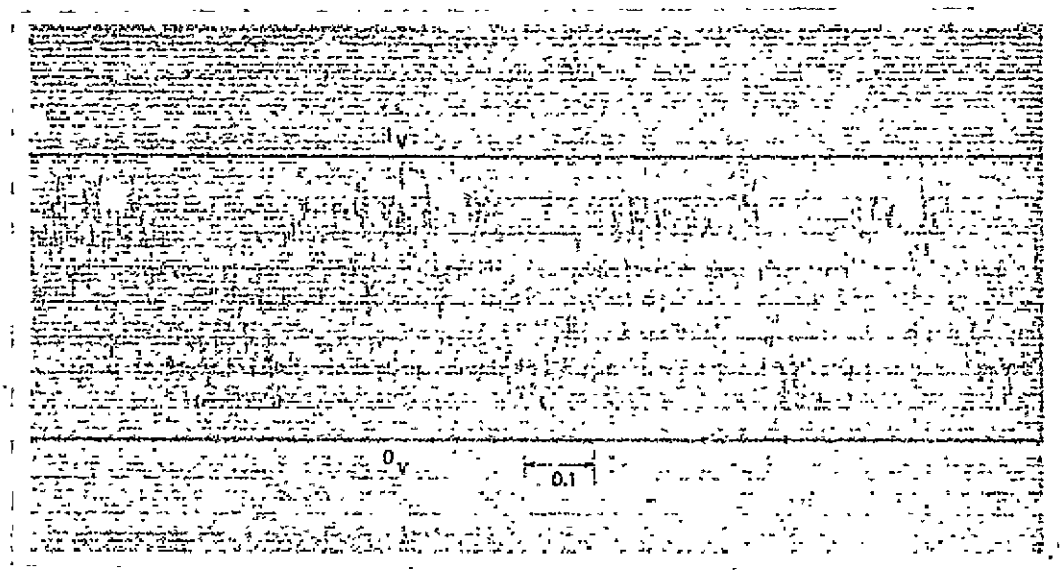

Fig. 28. Hot Wire Output Signal
(After Breakdown, S/L = 0.935)

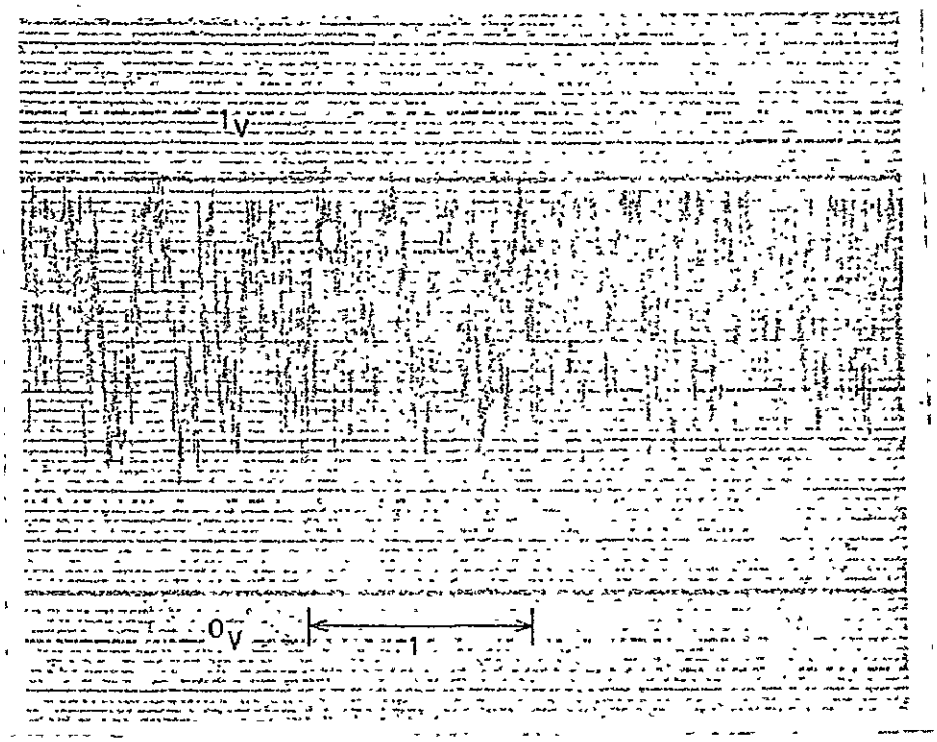

Fig. 29. Hot Wire Output Signal
(After Breakdown, S/L = 1.13,
500-Hz Low Pass Filter Used)

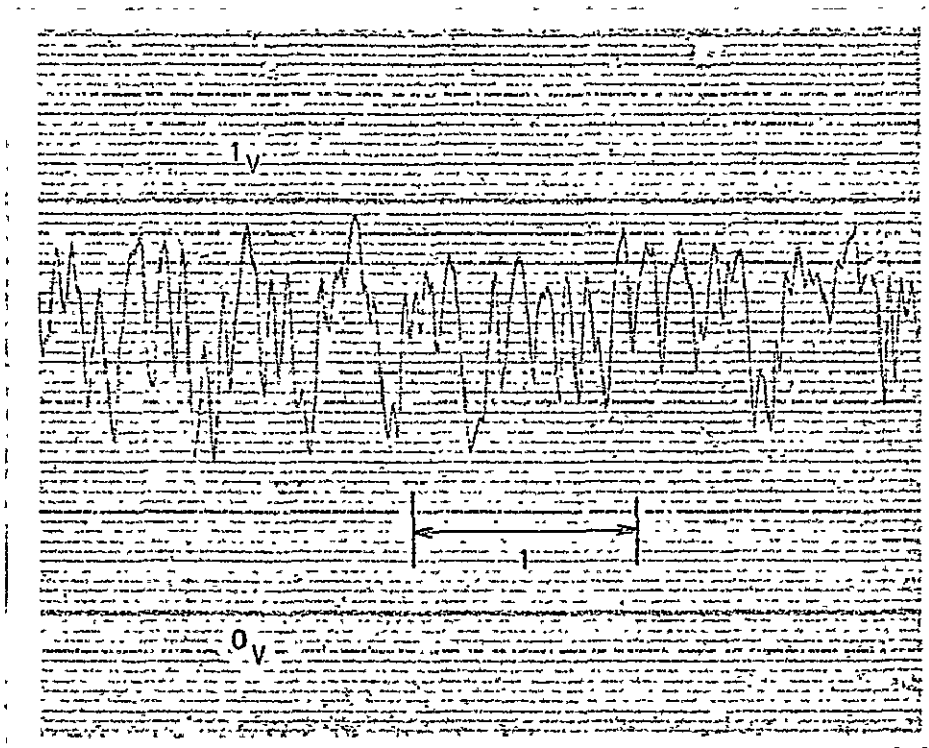

Fig. 30. Hot Wire Output Signal
(After Breakdown, S/L = 1.13,
10-Hz Low Pass Filter Used)

/23

2.4. Vortex Breakdown

2.4.1. Precession Motion and Spiral Transformation of the Vortex

Since the vortex separated at the leading edge of a delta wing is approximately axisymmetric, the total sum of the swirl penetrating a circle with a radius of R can be expressed as the circulation $\Gamma = 2\pi u_\varphi R$. When the vortex is located in a potential flow, a flow portion encircling a vortex tube always encircles the same one, and hence, the circulation along this closed loop does not change temporally and the vortex tube encircling the circulation Γ coincides with the flow tube. Therefore, even in viscous regions, in order to examine the expansion of the swirl, it is convenient to assume approximately that the circulation Γ is constant while the radius R of the vortex tube changes along the direction of the flow.

Fig. 31 shows the change (along the flow direction) of the non-dimensionalized radius R/L at which the non-dimensionalized circulation Γ^* becomes constant, where Γ^* is the non-dimensionalization of the circulation $\Gamma = 2\pi u_\varphi R$ by the standard value $2\pi u_o L$. The results shown in this figure were obtained from the measurement results of the velocity distribution where the models have the apex angle of 65° and are fixed at the attack angles of 17°, 18° and 19°. The figure suggests that the expansion of the swirl does not depend greatly on the attack angle, at least within the range of the experiment. In the neighborhood of the central axis, in moving downstream, the swirl is gradually diffused radially, and it begins to diffuse abruptly. On the other hand, at the location away from the central axis, the swirl initially decreases slightly as S/L increases, but it increases gradually afterwards and rapidly after the location where S/L is about 0.9, indicating that the diffusion is outstanding. This may be explained as follows: In case of a delta wing, the vortex layer separated at the leading edge is concentrated along the central axis and forms an intense

vortex core, thus being able, to some extent, to confine the swirl within a narrow region in the neighborhood of the central axis. However, in moving downstream, the confinement becomes impossible due to the reverse pressure gradient, and finally, breakdown takes place at the location where S/L is about 0.9. Then the vortex core which has been firmly concentrated disappears and diffuses rapidly in radial directions.

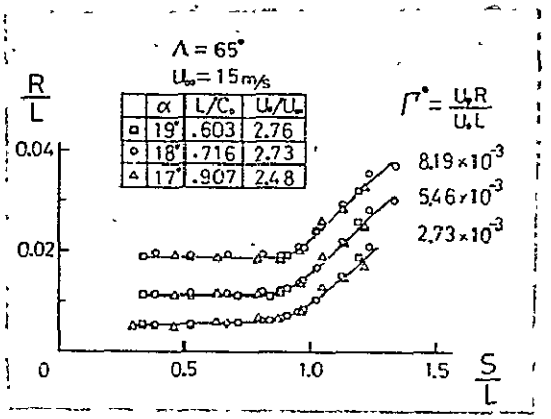

Fig. 31. Diffusion of Swirl.

Sarpkaya [26] concluded, based on his observation of a swirl flow, that the spiral transformation appearing after an axisymmetric breakdown is caused by the gyration of the vortex ring confined in an approximately axisymmetric bubble. On the other hand, Lambourne [21] concluded, based on his observation of the vortex separated at the leading edge of a delta wing, that the center of the vortex core is curved and the spiral transformation takes place after the breakdown, as shown in Fig. 32, but fluid portions do not move along the spiral. According to his observation by cinecamera, the fluid portion arriving at the O point at a certain time moves along the direction $\vec{OA}$ and, immediately afterwards, along the direction $\vec{AA'}$. In case of a swirl flow, the swirl is not concentrated around the central axis so intensely as in the case of the vortex separated at the leading edge of a delta wing. The vortex core is thus somewhat loose, suggesting the appearance of a large bubble at breakdown.

In case of the vortex separated at the leading edge, however, almost all the swirls are concentrated within the region where the radius is less than 1.5 mm (approximately) and the vortex core is intense. Therefore, the generated bubble is probably very small and may not be observed as a bubble. Thus, in case of a spiral-form breakdown (by which, in this paper, is denoted the spiral transformation appearing after an axisymmetric breakdown, if said with regard to a swirl flow), we may conclude that the spiral transformation is caused by the vortex precession of the vortex core cross-section at the location of the breakdown, whether it is a swirl flow or a vortex separated at the leading edge of a delta wing. (In the case of a swirl flow, the vortex cross-section at the breakdown has a greater radius and a bubble is formed.)

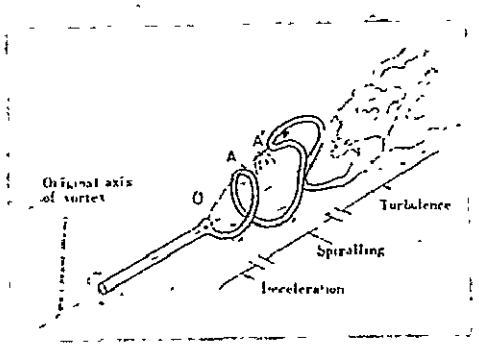

Fig. 32. Vortex Spiral Transformation.
(Cited from Ref. [21].)

In the rest of this section, an attempt will be made to explain the relationship between the spiral transformation after the breakdown and the period of the velocity fluctuation, based on an analogy to the phenomenon in which a rigid body exhibits a precession motion. Consider a vortex core portion with a small radius of ΔR and a length of Δx, as shown in Fig. 33. Take into account only the force caused by the pressure gradient along the direction of the flow and ignore all other influences to the vortex core portion. Under these assumptions, when the vortex core portion is placed in a reverse pressure gradient at

a small angle θ to the direction $\vec{OB}$ of the pressure gradient a moment around the fixed point O appears so as to turn down the vortex core portion. Let the moment of inertia around the axis OA be C . Then, when the vortex core portion rotates around the axis OB being at an angle θ , the rotational angular velocity Ω is the same as the angular velocity of the rigid body exhibiting a precession motion and is expressed as,

$$\Omega = \frac{T}{C\omega} \tag{3}$$

where

$$T = \frac{1}{2} \cdot \frac{dp}{dx} \cdot \pi \Delta R^2 \Delta x^2 \quad , \text{ and}$$

$$C = \frac{1}{2} \cdot \rho \pi \Delta R^4 \Delta x .$$

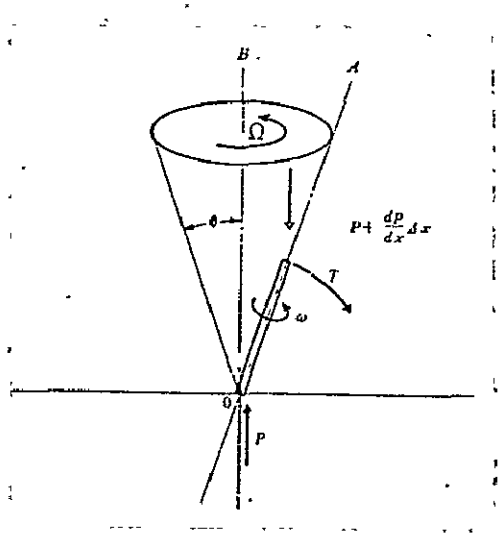

Fig. 33. Vortex Precession -- An Analogy from Rigid Body Movement.

(Δx: Vortex Core Length,
ΔR: Vortex Core Radius)

On the other hand, assuming the one-dimensional non-viscosity and incompressibility, the following equation holds true:

$$\frac{1}{2} \frac{du^2}{dx} = - \frac{1}{\rho} \frac{dp}{dx} \tag{4}$$

Letting the angular frequency of the precession motion be and substituting equ. (4) into equ. (3), the following equation is obtained. /25

$$f = \frac{\Omega}{2\pi} = - \frac{I}{4\pi} \cdot \left(\frac{\Delta X}{\Delta R^2} \right) \cdot \frac{1}{\omega} \cdot \frac{du^2}{dx} \qquad (5)$$

Non-dimensionalize the velocity and the distance in terms of U_o and L, as follows:

$$U^* = u/U_o, \quad x^* = x/L, \quad \Delta R^* = \Delta R/L,$$

$$v_e^* = v_e/U_o \text{ and } \quad \Gamma^* = \Delta R^* \, v_e^*.$$

Rewriting equ. (5) by the above dimensionless variable, the following equation is obtained.

$$f = - \frac{\Delta x^*}{4\pi} \cdot \frac{1}{\Gamma^*} \cdot \frac{du^{2*}}{dx^*} \cdot \left(\frac{U_o}{I} \Omega \right) \qquad (6)$$

As shown in Fig. 13, if the apex angle is constant, the axial component of the velocity on the central axis remains the same, being independent of the attack angle. Also, as shown in Fig. 31, the dimensionless variable Γ^* may be considered to be constant, independent of the attack angle. Δx^* designated the length of the rigid body which is supposed to model the vortex core portion under consideration. If the dimensionless variable Δx^* is held constant, independent of the change in the attack angle, the equation (6) may be rewritten as follows, using a constant K:

$$f = K \left(\frac{U_o}{L} \right) \qquad (7)$$

This equation indicates that the low frequency f, appearing after the breakdown, is proportional to the value of U_o/L. Namely, the frequency is higher when the velocity of the uniform flow increases or when L decreases due to the increase of the attack angle. For the next step, a deduction will be made in order to explain the vortex transformation when the vortex core cross-section begins the precession motion described above.

When a vortex core portion exhibits a precession motion when pivoted at the breakdown position, the fluid portion around the vortex core portion is forced away in directions which are perpendicular to the vortex cross-section. As shown in Fig. 34, when the vortex core cross-section confined in the position O of the breakdown, rotates with the angular velocity Ω in the same direction as that of the angular velocity ω of the vortex core which is at an angle θ to the axis OO', the fluid portion discharged from the point O moves along generatrices of a cone surface, i.e., O $\rightarrow$ A, O $\rightarrow$ B, O $\rightarrow$ C and so on. Therefore, the curve plotting the core centers at time t is the curve passing through A, B, C, D,..... and O, exhibiting a spiral with a rotational direction which is opposite to that of ω. After time Δt has passed, the fluid portions discharged from the point O move along generatrices of the cone surface, i.e., A $\rightarrow$ A', B $\rightarrow$ B', C $\rightarrow$ C' and so forth. Now, the curve plotting the vortex centers is a curve A', B', C',....., O which is perturbed in the direction of OO'. Thus, the fluid portions of the vortex core do not move along the spiral passing through the vortex centers, such as O $\rightarrow$ .... $\rightarrow$ D $\rightarrow$ C $\rightarrow$ B $\rightarrow$ A, but move along generatrices of the cone surface as O $\rightarrow$ A, O $\rightarrow$ B, O $\rightarrow$ C and so forth, while the vortex centers at any moment exhibit a spiral form in a reverse direction. This observation, shown in Fig. 3.4, is quite consistent with the observational results obtained by Lambourne.

According to the above explanation, the low frequency of the velocity fluctuation which is observed by a hot wire located in the flow field after the breakdown must be the same as the frequency determined by the time period of a spiral passing the observation point, and hence, is identical with the frequency of the precession motion of the vortex core cross-section confined at the breakdown position. Fig. 35 shows the low frequency components of the velocity fluctuation when a 65°-apex angle model was used with varying the attack angle and the magnitude

of the uniform flow. The low frequency components were obtained from the oscilloscope observation of the output-signal frequency of the hot wire which is located in the flow field after the breakdown. The waveform of the hot-wire output is very random, as shown in Fig. 28, and hence, the separation of the low frequence components is very difficult. Therefore, the obtained frequencies have a great variation and every result must be shown with a certain interval. Two different wind speeds, 6 m/s and 15 m/s, and three different attack angles were used in the experiment. Although the experiment does not cover a wide range, it may be concluded that the equation (7), i.e., the fact that the frequency f is proportional to U_o/L, is proved experimentally, at least for the range in which the experiment was done.

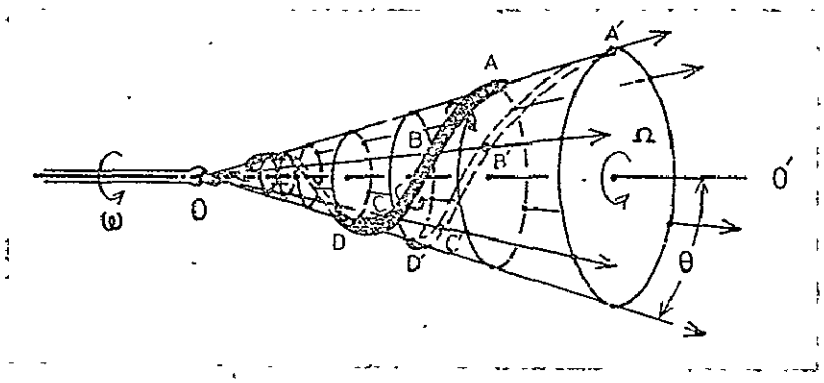

Fig. 34. Spiral Transformation Caused by Precession Motion of Vortex Core Cross-Section.

ORIGINAL PAGE IS
OF POOR QUALITY

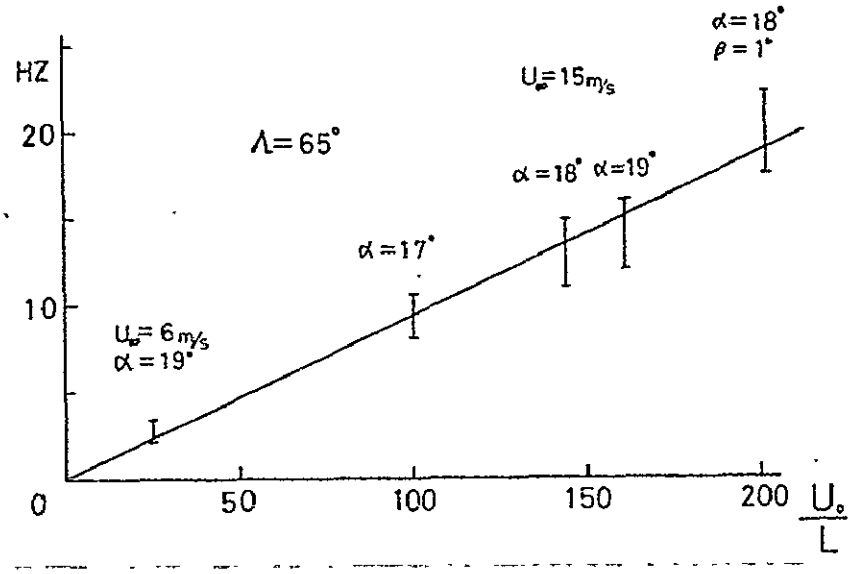

Fig. 35. Frequency of Velocity Fluctuation After Breakdown.

By calculating the constant K from Fig. 35, the value of /26
9.3×10^{-2} was obtained. From this result, the length of the vortex core portion when it is supposed to be a rigid body was calculated as $\Delta X/\Delta R \approx 0.1$. This small value of ΔX indicates that the vortex core portion confined at the breakdown position is not long and that only a thin vortex core cross-section exhibits the precession motion. This means that a bubble can be hardly recognized. It may be concluded from the above discussions that the breakdown may be explained as a vortex spiral transformation which is caused by the precession motion of the vortex cross-section.

Fig. 36 shows the radius designating the maximum of the axial velocity distribution. That maximum value can be thought to be the spiral radius after the breakdown. The figure indicates that the spiral transformation begins at the location where S/L is approximately 0.9, being independent of the attack angle, and that the surface where the spiral passes is a cone.

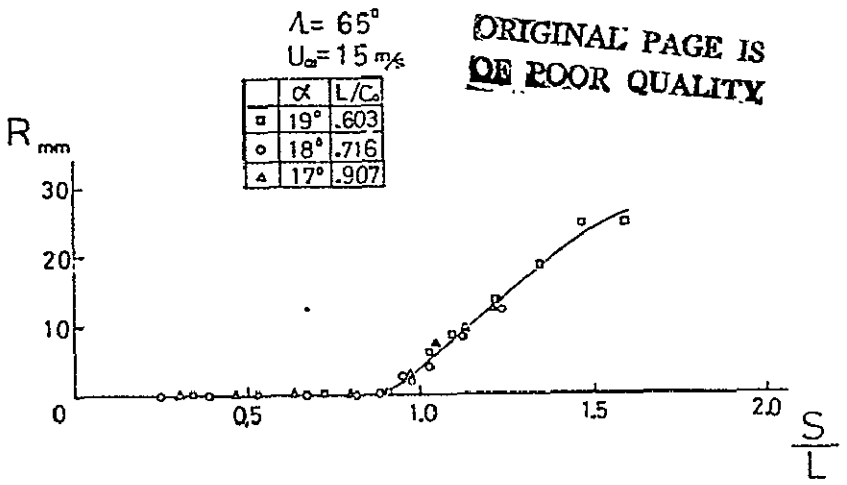

Fig. 36. Spiral Radius After Breakdown.

2.4.2. Position of Breakdown

In the previous section, the breakdown and the spiral transformation thereafter have been clearly depicted. In this section, discussion is focused on the following questions: /27
When such a spiral transformation occurs, what kinds of changes will appear in the velocity along the central axis, the velocity within the cross-section perpendicular to the central axis, the total pressure (head) and the turbulence?

When the breakdown occurs and the vortex is subject to the spiral transformation, the spiral rotates in a direction which is different from the initial rotational direction of the vortex core. On the other hand, even when the spiral transformation occurs, the vortex core rotates around the spiral curve as a central axis with the same direction as the initial rotational direction before the breakdown. Consequently, when the spiral transformation occurs, such rotational movements of the vortex core induce a flow which is directed from the outside of the spiral toward the central axis OO'. As indicated by the experimental results by Earnshaw [23] and the numerical results by others, the total pressure is lower in the vortex center than in the periphery before the breakdown occurs. When the spiral

transformation takes place and the peripheral fluid flows into the neighborhood of the central axis with high energy, the total pressure on the central axis is increased after the breakdown. As mentioned in Sec. 2.2.3, the model discussed previously can explain the mechanism whereby the total pressure on the central axis is increased rapidly according to the outbreak of the breakdown. In addition, this mechanism suggests that the numerical analysis be done after the structure of the turbulence is made clear.

Other characteristics of the flow field generated by the spiral direction opposite the vortex core rotational direction may be clearly seen in the distribution of the average axial velocity. As seen in Sec. 2.3.2, the distribution exhibits its maximum on the central axis and decreases radially, at the location ahead of the breakdown. When the breakdown occurs and the vortex is subject to the reverse spiral transformation, a flow from downstream to upstream is induced inside the spiral, as indicated by Biot-Savart's law. On the contrary, a flow from upstream to downstream is induced outside the spiral. Such induction in the flow field varies with the period of the precession motion of the vortex core cross-section. However, when it is time-averaged, the axial velocity inside the spiral is decreased while the axial velocity outside the spiral is increased. Thus, the distribution exhibits an overall shape which is convex downward in the neighborhood of the central axis. The location at which the axial velocity distribution reaches a maximum corresponds to the location through which the spiral passes.

As stated in Section 2.3.4, the location where the velocity fluctuation is the greatest is located at a position away from the central axis, immediately after the breakdown. Moving away from the breakdown point downstream, the fluctuation decreases and the maximum distribution is attained on the central axis. This fact can also be explained by the spiral transformation

after the breakdown. The velocity in the vortex core is very high as it is before the breakdown. Therefore, when the location of the vortex core changes temporally, the fluctuation at the time-average position of the vortex core becomes intensive. After the breakdown occurs and the spiral transformation takes place, the vortex core exhibits a spiral curve, and, hence, the fluctuation at the location through which the spiral curve passes is the maximum. Thus, the maximum point of the turbulence distribution is away from the central axis, after the breakdown. Moving further towards the downstream side where the spiral transformation becomes unclear and the vortex core becomes less intensively concentrated, the flow becomes a mild turbulence and the characteristics seen in the spiral transformation region become invisible, so that the fluctuation is spacially averaged.

In accordance with the above discussion, it can be concluded that the breakdown of the vortex separated at the leading edge of a delta wing is the spiral-form breakdown as defined by Lambourne, when the Reynolds number is high. In addition, the following fact was experimentally proved: the position of the breakdown is identical with the position where the axial velocity distribution changes its shape, or the position where the total pressure on the central axis increases. Based on these results, the criteria for determining the breakdown position from numerical calculations will be sought in the following paragraphs.

Assume an axisymmetric and laminar flow-field. Define the Reynolds number by $R_e = U_o L/\nu$, with respect to a standard length L and a standard velocity U_o. As seen in the experimental results, the radial velocity u_r is very small compared with the axial velocity component. Therefore, it may be non-dimensionalized by multiplying $\sqrt{R_e}$ by the radius r and in terms of L. Other velocity components, u_x and u_φ, are non-dimensionalized by U_o, and the axial distance by L. The pressure is non-dimensionalized by ρU_o^2. These variables which have been non-

dimensionalized are denoted by U_x, U_r, P, R and X. The equation of motion in the x-direction, using the cylindrical coordination system, can be written as follows using the Reynolds number R_e:

$$U_x \frac{\partial U_x}{\partial X} + U_r \frac{\partial U_x}{\partial R} = - \frac{\partial P}{\partial X} + \frac{\partial^2 U_x}{\partial R^2} + \frac{1}{R} \frac{\partial U_x}{\partial R} + \frac{1}{R_e} \frac{\partial^2 U_x}{\partial X^2} \tag{8}$$

As an approximation for the case when the Reynolds R_e is high, the last term in equ. (8) is omitted. When the relationship on the central axis is taken into account, since the vortex is assumed to be axisymmetric,

$$(\partial U_x / \partial R)_{R=0} = 0 \quad \text{and} \quad (U_r)_{R=0} = 0$$

are obtained on the central axis. Using a subscript C indicating the central axis and letting the non-dimensionalized total pressure be H, the equation (8) can be approximated by,

$$\frac{d}{dx} \left(\frac{1}{2} U_C^2 + P_C \right) = \frac{dH_C}{dx} = \left(\frac{\partial^2 U_x}{\partial R^2} \right)_{R=0} \tag{9}$$

The equation (9) is the one which indicates that the change in the total pressure on the central axis in the direction of the

flow is equal to the second derivative of the axial velocity distribution. In the region where the total pressure decreases, i.e., $dH_c/dx < 0$, the second derivative of the axial velocity $(\partial^2 U_x/\partial R^2)_{R=0}$ is negative, indicating that the axial velocity distribution has a shape which is convex upward in the neighborhood of the central axis. On the contrary, in the region where the total pressure increases, i.e., $dH_c/dx > 0$, the second derivative $(\partial^2 U_x/\partial R^2)_{R=0}$ of the axial velocity is positive, indicating that the axial velocity distribution has a shape which is convex downward in the neighborhood of the central axis.

The experimental results described in Sections 2.2.3 and 2.3.2 indicate that, when the Reynolds number is high, the breakdown position of the vortex separated at the leading edge of a delta wing is identical to the position where the total pressure on the central axis is minimum, or equivalently, identical to the position where the axial velocity distribution changes its shape from "upward convex" to "downward convex". In this section, it has been demonstrated that a conclusion equivalent to the above statement is also theoretically obtained from the equation of the motion. /28

Therefore, the breakdown position may be theoretically determined as the position where the following condition (10) is satisfied. Although a laminar flow has been assumed in the above discussion, even in the case of a turbulent flow, if a vortex-viscosity model can be applied with (Reynolds stress) $-\overline{u_r u_x} = \varepsilon \frac{\partial u_x}{\partial R}$ and if the vortex viscosity coefficient is used instead of the dynamic viscosity coefficient, the equations (8) and (9) still hold true. Thus, in each case, a criterion for determining the breakdown position may be given as follows:

$$\frac{dH_c}{dx} = 0 \qquad \text{or} \qquad (\partial^2 U_x/\partial R^2)_{R=0} = 0 \tag{10}$$

3. Theory

3.1. Theoretical Methodologies

Among the monographs theoretically treating the flow-field generated by the vortex separated at the leading edge of a delta wing, one can first cite the analytic solution by Hall [58] and Brown's theory [32] which was developed based on Hall's theory where compressibility is taken into account. According to Hall, the vortex is separated into two portions: the central portion where the viscosity effect prevails and the outside portion which may be treated by the non-viscosity theory. A conical flow-field is assumed for the outside portion so that the conical flow calculation is possible. This calculation is then connected with the solution for the inside involving viscosity, thereby giving an overall flow-field of the vortex. However, according to this method, the connection between the inside-region and outside-region solutions may not be smoothly made. In order to alleviate this disadvantage, Stewartson and Hall [31] proposed another expanded method, in which the solutions are given in terms of series and the overall flow-field is given in a more integrated way. They compared their computational results with the experimental results by Earnshaw. Except for the fact that the theory gives too large a velocity in the vortex center and too low a static pressure in the vortex center, both results can be said to be relatively consistent. Judging from this observation, at least in the present stage, it can be said that there is only a slight problem in analytically solving the flow-field of the vortex on the upstream of the breakdown.

As for the theoretical study on solving the development of the vortex, Hall [29] proposed a method in which the flow-field is treated as a quasi 2-dimensional field and the solution may be obtained by a step-by-step way downstream, using a different method, with given initial and boundary conditions. In the example which he studied, a downward convex shape of the axial

velocity distribution was observed at a certain position downstream, manifesting consistency with our experimental results. However, Hall concluded that there is no stagnation in the flow and he did not treat the breakdown. In another monograph [33], Hall insists that the breakdown position be determined as a point where the quasi 2-dimensional assumption cannot be valid any more. Although it is true that the axial velocity changes rapidly and the quasi 2-dimensional approximation becomes worse at a location near the breakdown, the discussion by Hall is highly dependent on his experimental result, which shows that he failed to obtain the velocity distribution of the flow-field after the breakdown. However, our experimental results indicate that a breakdown occurs without stagnation. Based on this observation, we may conclude that the quasi 2-dimensional difference method for numerical calculation, proposed by Hall, is still an efficient method for solving the development of the vortex separated at the leading edge of a delta wing and the phenomenon of the breakdown.

Bossel [34] proposed a numerical method for solving a circular flow in a cylinder, although it is not for a vortex generated by a delta wing. He separated the flow field into the following four regions: (1) the outermost region where the quasi 2-dimensional assumption is valid and a hyperbolic equation is satisfied, (2) the breakdown region where a non-viscosity elliptic equation is valid, (3) the non-viscosity region around the vortex center where the elliptic equation is valid, and (4) the region around the stagnation point where bubble created by he breakdown exists. After having defined the above four regions, he gave a solution under an appropriate boundary condition. He showed that an egg-shaped bubble, including a counterflow, appears in the neighborhood of the vortex center. The same result can be seen in the experimental result by Harvey. However, the bubble is closed and the direction of the circumferential velocity inside the bubble is reversed, according to his result.

As for the breakdown, the existing theories are as follows: Ludweig's theory [35], [36], [37], the conjugate vortex flow theory [38], [39], [40] advocated by Benjamin, Fraenkel, Sheer and others, the weakly nonlinear wave theory [41], [42], [43], [44] advocated by Leibovich, Randal and others, Lambourne's theory [22] and Mager's theory.

Ludwieg analyzed the stability of the circular flow in a narrow region between two coaxial cylinders and gave the stable region by considering spiral small perturbation and by solving a non-viscosity axisymmetric equation. He further expanded his result to concentrated vortices. However, his theory originated for solving the field of a narrow region between two coaxial cylinders and cannot be applied to a general concentrated vortex. Nevertheless, when our experimental results are plotted on the stability region obtained by Ludwieg, we see that the plotted data representing the region after the breakdown fall into the instability region. [48] The experiment by Petersohn [47] shows a similar consistency with the result by Ludwieg. However, in order to predict the breakdown based on Ludwieg's theory, the distributions of the circumferential and axial velocities must be known for each stage of the vortex development. Hence, it is impractical to use Ludwieg's theory for predicting the breakdown.

Benjamin assumed a quasi 2-dimensional non-viscous axisymmetric flow and derived an equation which the flow function must satisfy, based on the equation of motion. Assuming a uniform axial velocity and a combined forced-and-free vortex, he showed that there is a plurality of flow functions which satisfy the boundary condition and that the breakdown is a finite transition between supercritical and subcritical flows which are conjugate to each other. He also concluded that the critical condition can be represented by $V/U = 1.2$, where V/U is the ratio of the circumferential and axial velocities at the end of the vortex core. This conclusion is consistent with a result of a special /29

case when Lambourne's theory is applied.

Like Benjamin, Lambourne assumed a combined forced-and-free vortex. He considered the change in the axial velocity outside the vortex core, i.e., the pressure gradient. After giving a relationship between the parameter K representing the radius of the vortex core and the ratio V/U_1 of the axial velocity at the end of the vortex core on the upstream of the breakdown, he showed that there exists a critical condition for the relation of V/U_1 to the ratio of axial velocities at the ends of the vortex on upstream and downstream of the breakdown, and that there exists no solution under such critical condition. He also showed that the axial velocity in the vortex center decreases and a counter-flow region appears in the neighborhood of the vortex, under such a condition. However, the following points in this theory are questionable: According to the theory, the condition under which a stagnation point appears and a counter-flow region is generated is different from the condition under which there is no solution. However, the theory cannot state clearly what kind of phenomenon in the flow-field corresponds to these conditions. Furthermore, it should be pointed out that the direction of the circumferential velocity is reversed in the counter-flow region. Nevertheless, unlike Ludwieg's theory, Lambourne's theory can provide a critical condition based on the reverse pressure gradient, and hence, it may give a practical prediction of the breakdown to some extent.

By applying the non-linear wave theory by Leibovich and Randall, a swirl flow in a cylinder was calculated. This theory can be characterized as follows:

1) Like Benjamin's theory, this theory tells that there exists a supercritical flow on the upstream of the breakdown and a subcritical flow on the downstream of the breakdown, and that nonlinear waves propagate in the subcritical flow but they do not exist in the supercritical flow.

2) Stationary waves are generated only when the tubes are expanded in the direction of the flow, i.e., when there exists a reverse pressure gradient.

3) The flow lines determining the boundary of the trapped waves form a bubble which was observed in the experiments by Harvey, Sarpkaya and others.

4) The changes of the wall pressure in the axial direction are very similar to those shown by the experimental results provided by Sarpkaya or Kirkpatrick. [49]

5) The response of the breakdown position to the change in the Reynolds number is almost identical to that observed in the experiment by Sarpkaya.

6) The nonlinear transient movement is consistent with the observation by Sarpkaya.

Thus, as a whole, the theory provides the results which are consistent with the results which Sarpkaya obtained in his experiments in a cylinder. Therefore, it provides a very effective method for analyzing the transient mechanism of the bubble generation. However, the theory does provide some unreasonable consequences, such as, the reverse direction of the circumferential velocity in the solitary waves or the implication that the critical condition appears only in the swirl flow with a constant circulation.

Mager used a representation in which the axial velocity distribution is a 4-th order algebraic function while the circumferential velocity distribution is a cubic algebraic function. Using these representations, and under the quasi 2-dimensional assumption, he derived an integral equation relating the momentum, the circulation and others, and showed that there exists a continuous solution under a certain condition when the vortex core diameter increases moving downstream, but that, beyond a certain boundary, there is no continuous solution and a finite transition appears in the flow-field, exactly the way Benjamin described. He further concluded that such conditions are the conditions

which may determine the breakdown position. Sarpkaya made a numerical calculation according to Mager's method based on his own experimental results, and showed that the breakdown position, obtained with the Reynolds number and the circulation as parameters, is very consistent with the experimental results.

The assumption which Mager made about the form of the axial velocity distribution does not allow a shape which has the maxima at the locations away from the vortex center, which is the case of the results which our experiments show in the after-breakdown flow-field of the vortex separated at the leading edge of a delta wing. Therefore, it is still questionable if there exists a continuous solution or not when such a shape of the distribution is allowed, despite Mager's conclusion that there is no continuous solution under his assumptions. Thus, Mager has left an open problem.

The present status of the theoretical studies on the vortex structure and the breakdown phenomenon has been surveyed up to this point. It is natural to require any theory to give a sufficient explanation for all the experimental results described in Chapter 2, in order for that theory to be capable of determining the development of the leading-edge vortex of a delta wing and its breakdown position. When the Reynolds number is high, the breakdown of the vortex generated on a delta wing is not of the axisymmetric type in which the flow is stopped on the vortex central axis but of the spiral type in which the vortex center is bent at a certain location. Therefore, Ludwieg's theory on the circular flow in a cylinder, the conjugate vortex flow theory by Benjamin et al., or the weakly nonlinear wave theory by Leibovich, Randall et al. cannot be applied to our case. Furthermore, Mager's theory is also inapplicable since it cannot represent the velocity distribution after the breakdown adequately.

The experimental results in Chapter 2 reveal that, when the Reynolds number is high, the vortex generated on a delta wing model may be characterized as follows:

(1) The time-average central axis of the vortex is almost a straight line and, hence, can be used as one of the coordinates in a theoretical calculation.

(2) The diameter of the vortex core which moves as if it were a rigid body is very small. The time-average flow-field is almost axially symmetric despite the breakdown, except for the winding-up portion of the vortex layer near the leading edge and the close neighborhood of the wing surface. Hence, the axial symmetry may be assumed in a numerical calculation. /30

(3) The radial velocity component U_r is very small compared with the axial velocity component U_x or the circumferential velocity component U_φ.

(4) The radial change of the flow-field is greater than the change along the vortex axis, and, hence, the quasi 2-dimensional treatment is possible, as it is for a boundary layer.

(5) The turbulence is concentrated in a narrow region around the vortex core center on the upstream of the breakdown. As seen from the analytic solution by Hall and our experimental results, the viscosity effect is very small at a location which is far enough from the vortex core and, hence, a potential flow may be assumed in the region outside the vortex.

(6) Even though the vortex is a turbulent flow, its vortex core rotates as if it were a rigid body and there is only a little momentum transportation or dissipation due to the turbulence. The vortex growth, the vortex development and the breakdown are mostly subject to the potential, i.e., the pressure gradient.

(7) The velocity fluctuation of the flow-field on the downstream of the breakdown is large, creating a significant turbulence effect. In order to determine the breakdown position, a discussion using an equation describing the time-average flow-field is enough.

The above observations suggest that, when the Reynolds number is high enough, the development of the leading-edge vortex of a delta wing and the breakdown position may be determined by Hall's method [29], in which an axisymmetric Navier-Stokes equation describing the average flow-field under the assumption of quasi 2-dimensionality is solved by a difference equation with a certain boundary condition. Since the actual flow is a turbulent flow, in order to solve its development, the dynamic viscosity coefficient ν in Hall's calculation of the laminar flow should be replaced by the vortex viscosity coefficient ε, with the turbulence effect taken into account. Then, the breakdown position can be determined by numerical calculation using the criterion represented by equ. (10), since the validity of this criterion has been experimentally proved. In the following section, a numerical method based on Hall's method and the corresponding computational results will be described.

3.2. Numerical Computation

3.2.1. Nomenclature

x, r	Cylindrical coordinate system, axial and radial directions.
X, R	Cylindrical coordination system (non-dimensionalized).
u_x; u_φ, u_r	Axial, circumferential and radial velocity.
U, V, W	Axial, circumferential and radial velocity (non-dimensionalized). $U = u_x/U_o$, $V = u_\varphi/U_o$ and $W = \sqrt{R_e}\, u_r/U_o$.
p, P	Statis pressure, its non-dimensionalization.
U_o	Maximum axial velocity (see Fig. 11).
L	Reference distance (see Fig. 11).
ε	Vortex viscosity coefficient.
ν	Dynamic viscosity coefficient.

R_e	Reynolds number, $R_e = U_o L/\varepsilon$ or $R_e = U_o L/\nu$.
ζ	Radius, $\zeta = R/\lambda$.
k	Circulation, $k = \lambda \cdot \zeta \cdot V$.
h	Radial velocity, $h = W/\lambda$
$\Delta x, \Delta\zeta$	Difference division in the x- and ζ-directions.
a,b,c,d	Coefficients in the equation of k.
a*,b*,c*,d*	Coefficients in the equation of u.
λ	Parameter representing the vortex radius, $\lambda = r_e(x)/r_e(x_i)$
Q_o	Dynamic pressure, $Q_o = \frac{1}{2} \cdot \rho \cdot U_o^2$.
α	Attack angle.
Λ	Apex angle.
Γ	Circulation quantity.

Subscripts

i	Initial conditions for the cross-section.
C	Vortex central axis.
e	Vortex outside boundary.
m	Lattice position, the x-direction.
n	Lattice position, the ζ-direction.

3.2.2. Basic Equations

In order to describe the equation of motion in terms of dimensionless quantities, the L defined in Section 2.2.2 is used for the reference of the distance, and the maximum velocity U_o on the vortex central axis is used as the reference of the velocity.

In order to make a matching among the scales of the variables, a common practice in the boundary layer approximation, the radial distance r and the radial velocity u_r are expanded by the factor $\sqrt{R_e}$. The Reynolds number R_e used here is not that of the laminar flow, used by Hall with the dynamic viscosity coefficient, but it is defined by using the vortex viscosity coefficient ε, i.e., $R_e = U_o L/\varepsilon$. The non-dimensionalization of the coordinates and the velocity components is determined as follows:

$$X = \frac{x}{L} \quad , \quad R = \sqrt{R_e}\,\frac{r}{L} \quad ,$$

$$U = \frac{u_x}{U_o} \quad , \quad V = \frac{u_\varphi}{U_o} \quad , \quad \text{and} \quad W = \sqrt{R_e}\,\frac{u_r}{U_o} \tag{11}$$

where

$$R_e = \frac{U_0 L}{\varepsilon} \quad \text{and} \quad P = \frac{p-P_0}{\rho U^2} \quad .$$

Taking into account the fact that the flow-field is a turbulence, a simplest viscosity model is assumed and a scalor vortex coefficiency of Boussinesq [57] is used instead of the dynamic viscosity coefficient. Under the assumption of the quasi 2-dimensionality and with the above non-dimensionalization, the axisymmetric Navier-Stokes equation of motion and the equation of continuity may be written in terms of the dimensionless quantities as follows:

$$U\frac{\partial(RV)}{\partial X} + W\frac{\partial(RV)}{\partial R} = \frac{\partial^2(RV)}{\partial R^2} - \frac{1}{R}\frac{\partial(RV)}{\partial R} + \frac{1}{R_e}\frac{\partial^2(RV)}{\partial X^2} ,$$

$$U\frac{\partial U}{\partial X} + W\frac{\partial U}{\partial R} = -\frac{\partial P}{\partial X} + \frac{\partial^2 U}{\partial R^2} + \frac{1}{R}\frac{\partial U}{\partial R} + \frac{1}{R_e}\frac{\partial^2 U}{\partial X^2} ,$$

$$\frac{U}{R_e}\frac{\partial W}{\partial X} + \frac{W}{R_e}\frac{\partial W}{\partial R} - \frac{V^2}{R} = -\frac{\partial P}{\partial R} + \frac{1}{R_e}\left(\frac{\partial^2 W}{\partial R^2} + \frac{1}{R}\frac{\partial W}{\partial R} - \frac{W}{R^2} + \frac{1}{R_e}\frac{\partial^2 W}{\partial X^2}\right) , \quad \text{and} \tag{12}$$

$$\frac{\partial U}{\partial X} + \frac{\partial W}{\partial R} + \frac{W}{R} = 0$$

In the equation (12), each term including $1/R_e$ can be omitted under the assumption that the Reynolds number is high enough. Under that assumption, the basic equations can be simplified as,

$$U\frac{\partial(RV)}{\partial X} + W\frac{\partial(RV)}{\partial R} = \frac{\partial^2(RV)}{\partial R^2} - \frac{1}{R}\frac{\partial(RV)}{\partial R}$$

$$U\frac{\partial U}{\partial X} + W\frac{\partial U}{\partial R} = -\frac{\partial P}{\partial X} + \frac{\partial^2 U}{\partial R^2} + \frac{1}{R}\frac{\partial U}{\partial R} \qquad (13)$$

$$\frac{V^2}{R} = \frac{\partial P}{\partial R} \quad , \text{ and}$$

$$\frac{\partial U}{\partial X} + \frac{\partial W}{\partial R} + \frac{W}{R} = 0$$

The equations (13) have been derived under the quasi 2-dimensional assumptions: The flow-field is axisymmetric and the Reynolds number is high enough. So that the change in the R-direction is much greater than that in the X-direction. Therefore, the equations (13) cannot be applied to the case where stagnation exists in the flow or where there exists a counter-flow region. However, as mentioned in Chapter 2, if there is no stagnation in

the flow and the change in the X-direction is greater than that in the R-direction, but only to some extent near the breakdown or on its upstream, the flow-field including the breakdown may probably be solved by equation (13).

The equations (13) have complicated terms involving the velocity components U, V, W and the pressure P and cannot be separated easily. However, if the axial velocity component U is assumed, the radial velocity W can be determined by the equation of continuity. Then, the circumferential component V can be obtained from the first equation and the pressure P can be determined by substituting V in the third equation. Finally, by substituting W and P in the second equation, U is obtained. The value of U thus obtained can be used for correcting the initially assumed value of U. By repeating this procedure until a convergence is obtained for each variable, the variables on the next cross-section may be obtained with a given initial condition. Thus, the equations (13) constitute a hyperbolic equation which can be solved in a step-by-step method.

The boundary condition treatment is the next problem: The boundary outside the vortex changes its form according to the development of the vortex. Therefore, the problem would be very complicated if the boundary condition is given on the deformed surface. In order to make the boundary condition assignment easy, a parameter representing the expansion of the vortex, $\lambda = r_e(x) / r_e(x_i)$ is introduced so that the computational region may be rectangular. The subscript e designates the end of the vortex and signifies the external boundary. x_i is the first cross-section in the vortex computation and corresponds to the initial condition. If the variables R, V and W are converted to ζ, k and h in terms of λ, i.e.,

$$\zeta = R/\lambda , \quad k = \lambda\zeta V, \text{ and } \quad h = W/\lambda . \tag{14}$$

and if the axial velocity component U is denoted by the lower case u and the axial distance X by the lower case x, the basic equations become,

$$
\begin{aligned}
u\frac{\partial k}{\partial x} - \frac{1}{\lambda^2}\frac{\partial^2 k}{\partial \zeta^2} + \left(h - \frac{\lambda'}{\lambda}\zeta u + \frac{1}{\lambda^2\zeta}\right)\frac{\partial k}{\partial \zeta} &= 0 \\
u\frac{\partial u}{\partial x} - \frac{1}{\lambda^2}\frac{\partial^2 u}{\partial \zeta^2} + \left(h - \frac{\lambda'}{\lambda}\zeta u - \frac{1}{\lambda^2\zeta}\right)\frac{\partial u}{\partial \zeta} &= \\
&= \frac{\lambda'}{\lambda^3}\frac{k^2}{\zeta^2} - \frac{\partial P}{\partial x} \\
\frac{\partial P}{\partial \zeta} &= \frac{k^2}{\lambda^2\zeta^3} \\
\frac{\partial}{\partial \zeta}(\zeta h) &= -\zeta\frac{\partial u}{\partial x} + \frac{\lambda'}{\lambda}\zeta^2\frac{\partial u}{\partial \zeta}
\end{aligned}
\qquad (15)
$$

In equation (15), λ' denotes $d\lambda/dx$. The physical region, $o \leqq r \leqq r_e$ and $x_i \leqq x$, is transformed to the computational region, $o \leqq \zeta \leqq \zeta_e = \sqrt{R_e} \cdot r_i / L = R_i$ and $x_i \leqq x$, which is a rectangular region with one open end, by using the coordinate transformation (14).

The initial condition consists of the axial velocity distribution u_i at the cross-section $x = x_i$ and of the circulation distribution k_i, i.e.,

$$u = u_i(\zeta) \text{ and } k = k_i(\zeta) \text{ at } x = x_i. \tag{16}$$

The boundary condition on the central axis is determined by the condition that the circulation k and the radial velocity h are both zero and by the condition that the axial velocity u is axially symmetric, and hence, it is given as,

$$k = o,\ h = o \text{ and } \frac{\partial u}{\partial \zeta} = o \text{ at } \zeta = o. \tag{17}$$

For the external boundary condition, we have,

$$k = k_e(x),\ u = u_e(x) \text{ and } P = P_e(x) \text{ at } \zeta = \zeta_e \tag{18}$$

If several assumptions are added to the external boundary condition, the expression (18) may be further simplified.

In the external boundary is a flow tube, the relationship between the geometrical expansion of the flow tube and the velocity vector may be written as,

$$h_e/u_e = \zeta_e(\lambda'/\lambda) \quad . \tag{19}$$

and hence the assignment of all the conditions in equation (18) is impossible. Furthermore, if the external boundary of the vortex is assumed to be non-viscous and there is no swirl dissipation through the boundary, the first equation in (15) implies $dk_e/dx=o$ and we have, /32

$$k_e(x) = k_e(x_i) = \text{constant} \tag{20}$$

and the second equation in (15) implies,

$$u_e \frac{du_e}{dx} = \frac{\lambda'}{\lambda^3} \frac{k_e^2}{\zeta_e^2} - \frac{dP_e}{dx} \tag{21}$$

When such assumptions can be made, all the conditions in (18) cannot be assigned at one time as the external boundary condition; only one -- P_e, u_e or λ -- is allowed to be assigned while the rest of the conditions are substituted by equations (19), (20) and (21). In the case of the delta-wing leading-edge vortex where the Reynolds number is sufficiently high, the assumptions (19), (20) and (21) can be made approximately, as mentioned in Section 3.1, and hence, it suffices to assign one among P_e, u_e and λ as the external boundary condition.

Our experimental data are the axial velocity and circumferential velocity distributions in the cross-sections at the breakdown and on its upstream and downstream, and the velocity on the central axis. Therefore, it is meaningless to assign P_e as the external boundary condition. The measurement cross-section is too small for u_e or λ to be assigned as the external boundary condition. Since the change of the velocity on the central axis has been most accurately measured in detailed experiments, its data are most suitable for use in numerical computation. Thus, the change of the velocity u_c on the central axis is used as the boundary condition. At first, assuming the pressure P_e on the external boundary, the flow-field is solved and the velocity u_c on the central axis is computed. Then, the value of P_e is corrected so that the computed value of u_c may be equal to that initially given. By repeating the procedure until the value of u_c converges, the computation of a cross-section is finished and the next cross-section is computed in a similar way.

3.2.3. Difference Approximation

In order to numerically solve the partial differential equations (defined in the previous section) with a given boundary condition, they are approximated by a set of difference equations. A lattice with M points in the x-direction and N points in the ζ - direction was used. The subscript m denotes the lattice position in the x-direction and the subscript n denotes the lattice position in the ζ -direction. In order to obtain the values of the functions at (m+1, n), the evaluations are made at (m+½, n), (m+½, n), (m+1, n+½) and (m+½, n-½). The difference form is a 1st-order central difference using the central point. The partial differential equations involve the 1st-order derivative with respect to x and up to the 2nd-order derivative with respect to ζ. For example, the difference form for k is given by,

$$k_{m+1/2,n} = (1/2)\,(k_{m+1,n} + k_{m,n}),$$

$$\left(\frac{\partial k}{\partial x}\right)_{m+1/2,n} = \frac{1}{\Delta x}\,(k_{m+1,n} - k_{m,n}), \tag{22}$$

$$\left(\frac{\partial k}{\partial \zeta}\right)_{m+1/2,n} = \frac{1}{4\Delta\zeta}\,(k_{m+1,n+1} - k_{m+1,n-1} + k_{m,n+1} - k_{m,n-1}),$$

$$\left(\frac{\partial^2 k}{\partial \zeta^2}\right)_{m+1/2,n} = \frac{1}{2\Delta\zeta^2}(k_{m+1,n+1} - 2k_{m+1,n} + k_{m+1,n-1}$$

$$+ k_{m,n+1} = 2k_{m,n} + k_{m,n-1}) .$$

The equations (15) include several nonlinear terms such as

$$u\frac{\partial u}{\partial x} .$$

These nonlinear terms are simplified by Newton's approximation, for example,

$$u_{m+1/2,n}\left(\frac{\partial u}{\partial x}\right)_{m+1/2,n} = \frac{u_{m+1,n}}{\Delta x}(u_{m+1,n}) \tag{23}$$

$$- \frac{u^2_{m+1,m}}{2\Delta x} - \frac{u^2_{m,n}}{2\Delta x}$$

In the above equation, the value in ( ) on the right hand side is an unknown variable while other terms without ( ) have known values which are obtained from the previous iteration of the computation. Rewriting the differential equations (15) by using the difference forms such as (22) and (23), the following simultaneous equations for k and u and the following algebraic equations for P and h are obtained.

$$a_n k_{m+1,n+1} + b_n k_{m+1,n} + c_n k_{m+1,n-1} = d_n$$

$$(n=1,2,3,\ldots\ldots,N-1) \qquad (24a)$$

$$a_n = \frac{h_{m+1/2,n}}{4\Delta\zeta} - \frac{n(\lambda_{m+1} - \lambda_m)}{4\Delta x(\lambda_{m+1} + \lambda_m)}(u_{m+1,n} + u_{m,n}) + \frac{1 - 2n}{n\Delta\zeta^2(\lambda_{m+1} + \lambda_m)^2}$$

$$b_n = \frac{1}{2\Delta x}(u_{m+1,n} + u_{m,n}) + \frac{4}{\Delta\zeta^2(\lambda_{m+1} + \lambda_m)^2}$$

$$c_n = -a_n - \frac{4}{\Delta\zeta^2(\lambda_{m+1}+\lambda_m)^2}$$

$$d_m = \frac{k_{m,n}}{2\Delta x}(u_{m+1,n}+u_{m,n}) + \frac{2}{\Delta\zeta^2(\lambda_{m+1}+\lambda_m)^2}$$

$$\times (k_{m,n+1} - 2k_{m,n} + k_{m,n-1})$$

$$-\left(a_n + \frac{2}{\Delta\zeta^2(\lambda_{m+1}+\lambda_m)^2}\right)(k_{m,n+1} - k_{m,n-1})$$

$$a_n^* u_{m+1,n+1} + b_n^* u_{m+1,n} + c_n^* u_{m+1,n-1} = d_n^*$$

$$(n=0,1,2,\ldots\ldots,N-1) \qquad (24b)$$

$$a_n^* = \frac{h_{m+1/2,n}}{4} - \frac{n(\lambda_{m+1}-\lambda_m)}{4\Delta x(\lambda_{m+1}+\lambda_m)}(u_{m+1,n}+u_{m,n})$$

$$-\frac{1+2n}{n\Delta\zeta^2(\lambda_{m+1}+\lambda_m)^2}$$

$$b_n^* = \frac{u_{m+1,n}}{\Delta x} + \frac{4}{\Delta\zeta^2(\lambda_{m+1}+\lambda_m)^2} - \frac{n(\lambda_{m+1}-\lambda_m)}{4\Delta x(\lambda_{m+1}+\lambda_m)}$$

$$\times (u_{m+1,n+1} - u_{m+1,n-1} + u_{m,n+1} - u_{m,n-1})$$

$$c_n^* = -a_n^* - \frac{4}{\Delta\zeta^2(\lambda_{m+1} + \lambda_m)^2}$$

$$d_n^* = \frac{1}{2\Delta x}(u^2_{m+1,n} + u^2_{m,n}) - \frac{4(u_{m,n} - u_{m,n-1})}{\Delta\zeta^2(\lambda_{m+1} + \lambda_m)^2}$$

$$- a_n^*(u_{m,n+1} - u_{m,n-1}) - \frac{\nu(\lambda_{m+1} - \lambda_m)}{4\Delta x(\lambda_{m+1} + \lambda_m)}$$

$$x\,(u_{m+1,n+1} - u_{m+1,n-1} + u_{m,n+1} - u_{m,n-1})\,u_{m+1,n}$$

$$- \frac{1}{\Delta x}(P_{m+1,n} - P_{m,n})$$

$$P_{m+1,n} = P_{m+1,n+1} - \frac{(k_{m+1,n+1} + k_{m+1,n})^2}{4(n+1/2)^3 \Delta\zeta^2 \lambda_{m+1}^2} \qquad (24c)$$

$$h_{m+1/2,n} = (1-1/n)\, h_{m+1/2,n-1} - \frac{(1-1/2n)}{2\Delta x} \Delta\ell$$

$$x\ (u_{m+1,n} - u_{m,n} + u_{m+1,n-1} - u_{m,n-1})$$

$$+ \frac{(n-1/2)^2}{n} \frac{\Delta\zeta(\lambda_{m+1} - \lambda_m)}{\Delta x(\lambda_{m+1} + \lambda_m)}$$

$$x\ (u_{m+1,n} - u_{m+1,n-1} + u_{m,n} - u_{m,n-1}) \qquad (24d)$$

The equation (24b) is meaningless on the central axis where $\zeta = 0$ and a special form is necessary for handling the boundary condition (17) on the central axis. Thus, the coefficients in equation (24) must have special forms such as,

$$a_0^* = -\frac{8}{\Delta\zeta^2(\lambda_{m+1} + \lambda_m)^2}$$

$$b_0^* = \frac{u_{m+1,0}}{\Delta x} - a_0^*$$

$$c_0^* = 0 \qquad (25)$$

$$d_0^* = \frac{1}{2\Delta x}(u^2_{m+1,0} + u^2_{m,0}) - a_0^*(u_{m,1} - u_{m,0})$$

$$- \frac{1}{\Delta x}(P_{m+1,0} - P_{m,0})$$

The equation (24a) gives an (N-1)-variable simultaneous equation while equ. (24b) gives an N-variable simultaneous equation. In each case, the coefficient matrix is a triple diagonal matrix which has a non-zero element only at each diagonal position and its adjacent positions, and, hence, the two systems of equations can be solved without any difficulty.

A flow chart showing a computation program for solving this problem is shown in Fig. 37.

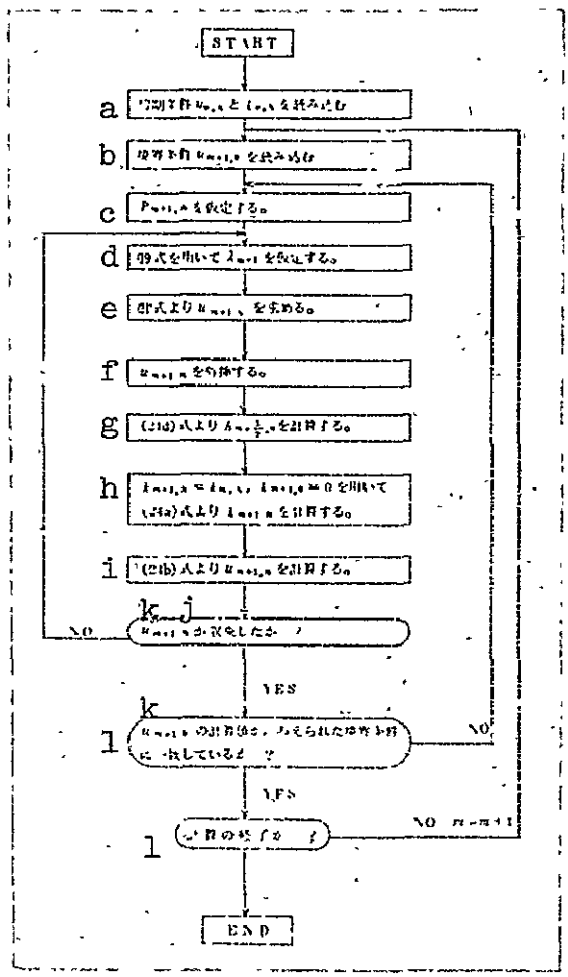

Fig. 37. Flow Chart of Computation Program.

Key: a: Read the initial condition, $u_{o,n}$ and $k_{o,n}$.

b: Read the boundary condition, $u_{m+1,o}$.

c: Assume $P_{m+1,\ n}$.

d: Assume λ_{m+1} using (19).

e: Determine $u_{m+1,n}$ by (21).

f: Extrapolate $u_{m+1,n}$.

g: Compute $h_{m+\frac{1}{2},n}$ by (24d).

h: Compute $k_{m+1,n}$ by (24a).
with $k_{m+1,N} = k_{m,N}$ and $k_{m+1,O} = 0$.

i: Compute $u_{m+1,n}$ by (24b).

j: Does $u_{m+1,n}$ converge?

k: Is the computed value of $u_{m+1,O}$ consistent with the given boundary condition?

l: Is the computation finished?

First, the distribution $u_{O,n}$ and $k_{O,n}$ is given as the initial condition. Next, the boundary condition $u_{m+1,O}$ on the central axis in the next cross-section is read in. Then, assuming the values of $P_{m+1,N}$ and λ_{m+1}, $u_{m+1,N}$ can be determined according to equ. (21). By obtaining the axial velocity distribution $u_{m+1,n}$ by extrapolation, $h_{m+\frac{1}{2},n}$ can be determined according to equ. (24d) and every coefficient in equ. (24a) is thus determined. Then, $k_{m+1,n}$ may be obtained by solving the (N-1)-variable simultaneous equations with the boundary condition, $k_{m+1,N} = k_{m,N}$ and $k_{m+1,O} = 0$. Since the value of $u_{m+1,N}$ has already been determined and every coefficient in equ. (24b) is hence given, the axial velocity distribution $u_{m+1,n}$ may be obtained by solving the N-variable simultaneous equations. If all the values of $u_{m+1,n}$ do not converge, assume another value of λ_{m+1} and repeat the same procedure. When $u_{m+1,n}$ converges within a permissible range, the computed value of $u_{m+1,O}$ is compared with the $u_{m+1,O}$ value which has been given as the boundary condition. If they do not coincide with each other, correct the value of $P_{m+1,N}$ and repeat the computation until consistency

is obtained. When the computation at this stage is finished, the same process moves to the next cross-section m+2. Thus, the computation procedure is continued by a step-by-step method for each cross-section while moving in the x-direction until the whole flow-field is computed. /34

4. Comparison of Experimental and Computational Results

As actual numerical computation was done with the data of the experiment using a 65°-apex angle model fixed at a 17°-attack angle, in which the total pressure on the central axis was measured. This case was selected based on the volume and the accuracy of the data. Since the velocity distribution was not measured at the location where the velocity on the central axis is maximum, the cross-section position selected for the computation was at the location S/L = 0.55, which is slightly on the downstream of the location where the velocity on the central axis attains its maximum. Fig. 38 shows the velocity in the vortex center used as the boundary condition, while Fig. 39 shows the velocity distribution used as the initial condition.

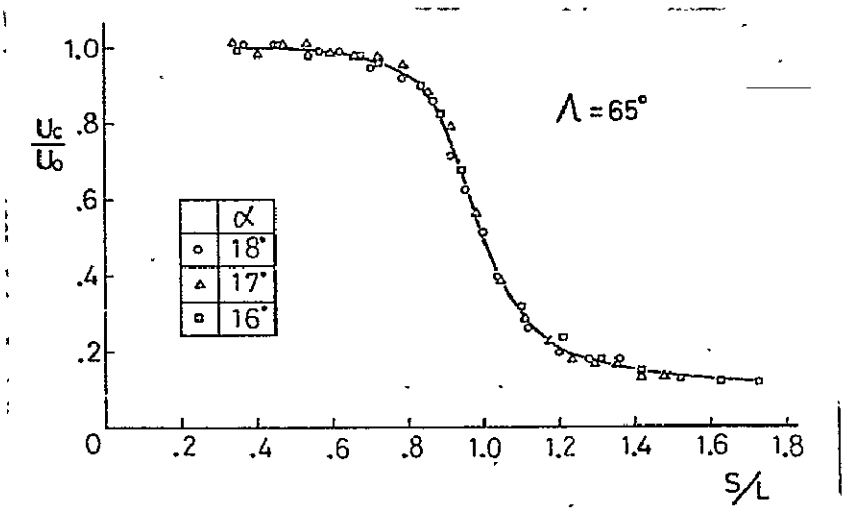

Fig. 38. Vortex Center Velocity Used as Boundary Condition.

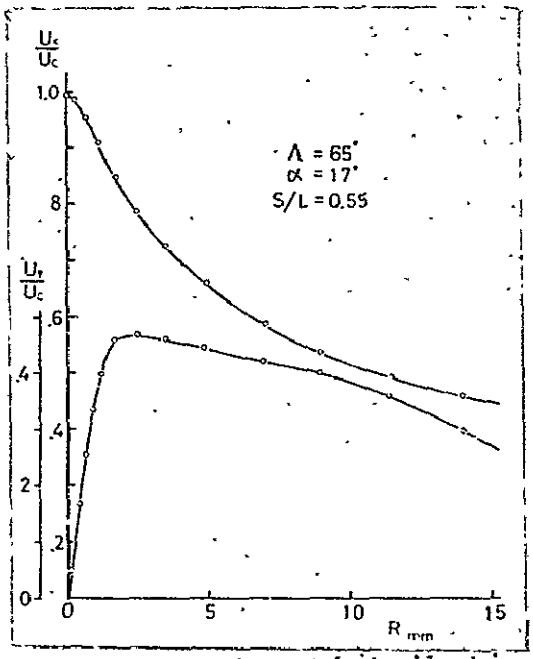

Fig. 39. Velocity Distribution Used as Initial Condition.

When a difference approximation is used to solve a differential equation and the computational region is divided in a lattice; the size of the lattice has a large influence on computational stability and accuracy. Figs. 40 and 41 show the influence of the size Δx of the x-direction division and the size $\Delta \zeta$ of the ζ-direction division to the velocity distribution. Both figures show the computed values of the axial velocity component U_x and the circumferential velocity component U_φ, both corresponding to the development of the vortex.

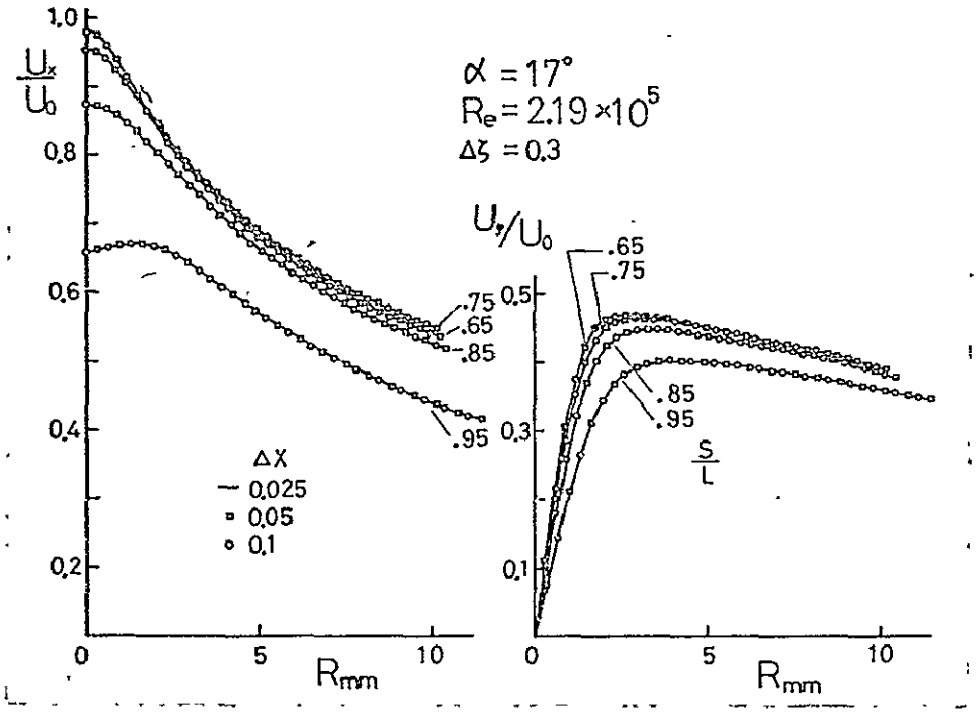

Fig. 40. Influence of x-Direction Division Size

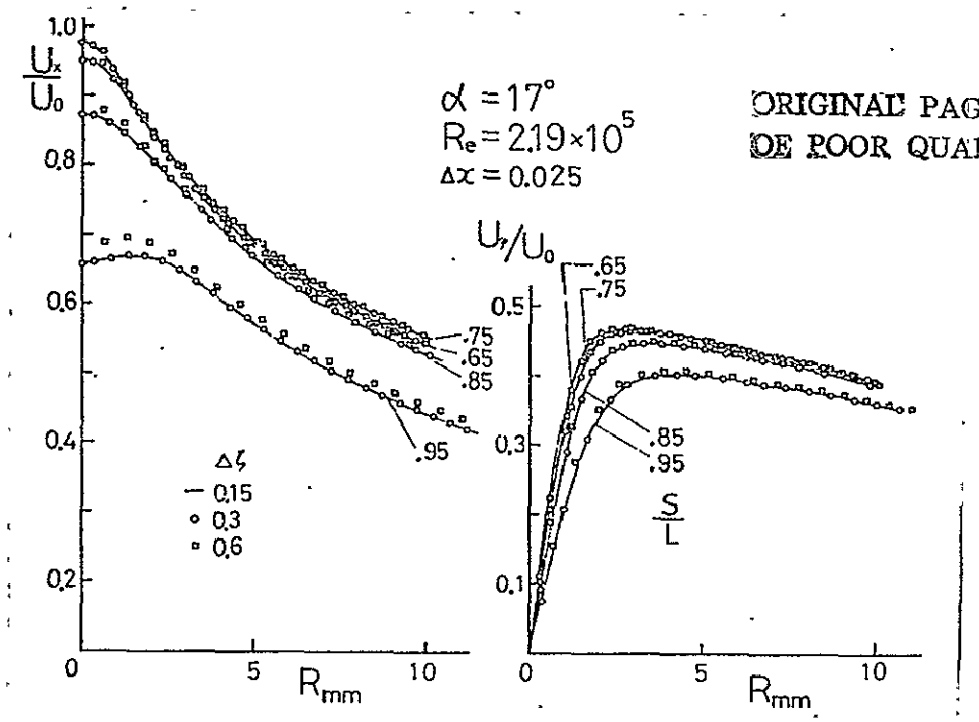

ORIGINAL PAGE IS OF POOR QUALITY

Fig. 41. Influence of ζ-Direction Division Size

In the computation, the Reynolds number $R_e = 2.19 \times 10^5$ was used. This was given by calculating the vortex viscosity coefficient according to $\varepsilon = 4\nu$, where ν is the dynamic viscosity coefficient under the experiment's condition. Fig. 40 indicates that, when $\Delta\zeta = 0.3$ is held constant and Δx is varied from 0.025 to 0.1, no significant influence on the computation of the velocity distribution can be observed. However, when $\Delta x = 0.025$ is held constant and $\Delta\zeta$ is varied from 0.15 to 0.6, a significant influence by the division on the computation can be observed. Only when $\Delta\zeta$ is less than or equal to 0.3, is the influence not observable. This fact indicates that the vortex of a delta wing has a greater change in the radial direction /36 than that in the axial direction. The computational time was about 6 minutes with FACOM 230-60 when 19 steps are used in the x-direction with $\Delta x = 0.025$, and 36 points are used in the ζ-direction with $\Delta\zeta = 0.3$. After realizing that the division of $\Delta x = 0.025$ and $\Delta\zeta = 0.3$ is sufficient, all the computations were done with this condition.

In the numerical computation, a potential flow is approximately assumed outside the external boundary of the vortex since there is little influence by viscosity or other factors. However, due to this assumption, it is conceivable that the way of defining the ζ-direction boundary may affect the computational result to a large extent. Fig. 42 shows the computational results of the velocity distribution on the downstream of the location, S/L = 0.55, where the initial condition is given (see Fig. 39), with the vortex radius R_{ei} being 10.5 mm or 13.5 mm. As seen in Fig. 42, the computational results in both cases are consistent with each other, indicating that the non-diffusion condition can be approximately assumed outside the external boundary if R_{ei} is 10.5 mm or greater. If R_{ei} is greater than 13.5 mm, the computational results are deteriorated since the axial symmetry of the velocity distribution Ux or $U\varphi$ as the initial condition at S/L = 0.55 includes the region where the counter-flow is wound up. Hence, R_{ei} cannot be too large. Thus,

the following computations use the computational region determined by R_{ei} = 10.5 mm.

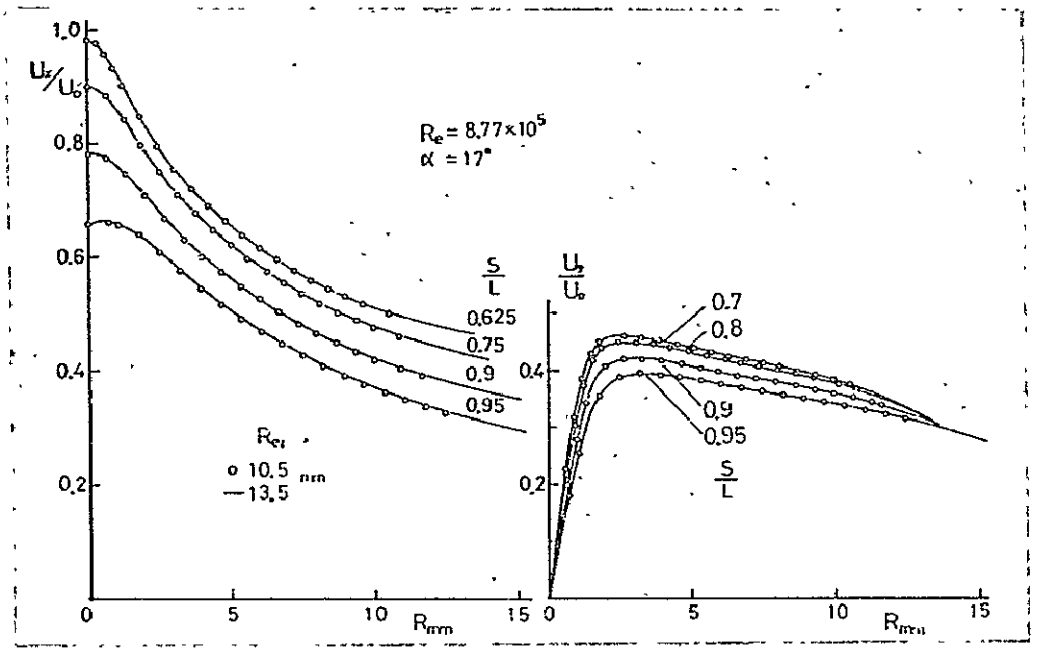

Fig. 42. Influence of Vortex External Boundary to Velocity Distribution.

Fig. 43 shows the breakdown position $(S/L)_B$ which is determined by the criterion $dH_c/dx = 0$ mentioned in Section 2.4.2 and based on the numerical calculation with the 17°-attack angle and the initial condition at S/L = 0.55, with the Reynolds number being given as a parameter. Although the available data are less, in order to investigate the influence of the attack angle, i.e., the initial condition, a computation was done with the attack angle of 18° and the initial condition at S/L = 0.675. Since the boundary condition is the velocity change (see Fig. 38) on the central axis, it remains the same despite the change of the attack angle. Hence, when the attack angle α is varied from 17° to 18°, the difference in the numerical computation is made only by the initial condition. The Reynolds number experimentally determined from the dynamic viscosity coefficient is 8.77×10^5 at $\alpha = 17°$ and 7.78×10^5 at $\alpha = 18°$. The breakdown

position $(S/L)_B$ obtained by the numerical computation is 0.893 and 0.878 with $\alpha = 17^\circ$ and 18°, respectively. When the Reynolds number is 10^5 or greater, the breakdown position does not change much and $(S/L)_B = 0.9$ with $\alpha = 17^\circ$. As the Reynolds number becomes small, $(S/L)_B$ also becomes small. For example, when $\alpha = 17^\circ$, the breakdown position with the experimental Reynolds number being 8.77×10^5 is different from that with the one-tenth Reynolds number 8.77×10^4 by 27 mm which is about 7% of the central chord length of the model, when L is assumed to remain the same. As mentioned in Section 2.2.4, the value of L does not change much in response to the Reynolds number, as shown by the experiments with two different Reynolds numbers. When the Reynolds number is defined as $U_o L/\varepsilon$, the Reynolds numbers in those experiments are 1.3×10^5 and 3.2×10^5 which are in the region of Fig. 43 where $(S/L)_B$ changes. Taking into account these experimental results, the change in which ε becomes larger so that the Reynolds number and $(S/L)_B$ becomes less, means the change in which the value of S becomes smaller since L is almost constant, indicating that the breakdown position moves forward with such a change.

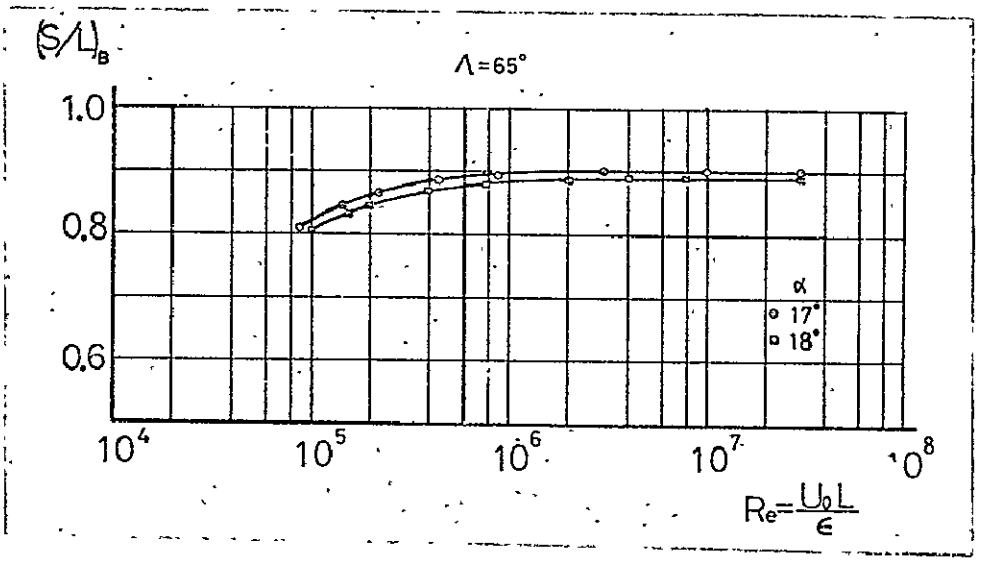

Fig. 43. Breakdown Position Determined by the criterion dHc/dx = 0.

Taking into account the experimental results shown in Fig. 16, it may be said that the numerical computation indicates the change of the breakdown position in response to the vortex viscosity coefficiency ε. The breakdown position moves forward as the vortex viscosity coefficient ε becomes larger. It should be pointed out that the change of the breakdown position in response to ε, i.e., to the Reynolds number, is opposite to that in the case of a swirl flow in a cylinder. In the case of the swirl flow, the breakdown position moves upstream when the Reynolds number becomes larger. The swirl flow has a specific relationship with the boundary layer developed on the wall surface, and the effective radius of the cross-section changes, thereby causing the change in the pressure gradient in the axial direction. /38

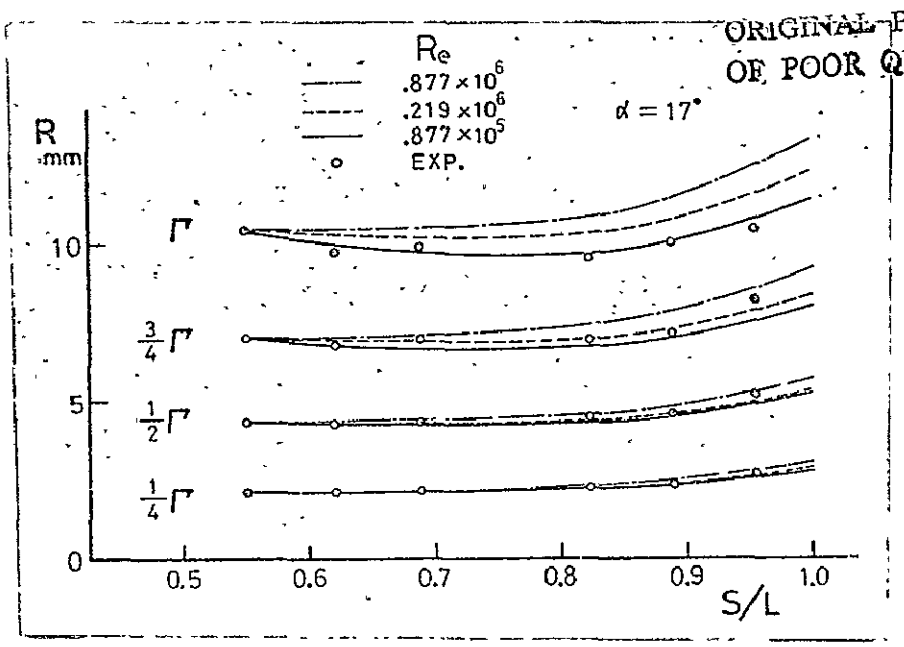

Fig. 44. Divergence of Swirl

Fig. 44 shows the change of the flow direction of the vortex tube radius. The figure shows a curve tracing the radius R which gives the same circulation Γ at each cross-section, 3/4 Γ, 1/2 Γ and 1/4 Γ, where Γ denotes the constant circulation at the end of the vortex. Although several computations were done with different Reynolds numbers, the figure shows only three

representative results. Since the flow is not a potential flow, the change of R is not equal to that of the flow tube in a strict sense. However, since they are approximately identical to each other in our case, it may be said that Fig. 44 shows the change of the flow direction of the flow tube radius. The curve at 1/4 Γ near the central axis increases monotomically while moving downstream. However, the curve at Γ which is the end of the vortex decreases initially and increases afterward while moving downstream. Such a divergence of the vortex tube was observed clearly in the experimental results. The computational and experimental values of the 1/2 Γ - and 1/4 Γ - curves are most consistent to each other when the Reynolds number is 2.19×10^5. However, they are most consistent when the Reynolds number is 8.77×10^4 in the case of the Γ-curve. This indicates that the effect of the turbulence in the vortex center is different from that outside the vortex. Furthermore, it is observed that the experimental data agreed with the computational data, when the Reynolds number is large in the region near the central axis and the Reynolds number is small outside that region. This indicates that the spiral transformation after the breakdown causes an intense turbulence mixture in outside regions, and the vortex viscosity coefficient is high there. In addition, the fact that the experimental and computational results are not consistent in the region near the vortex center or near the vortex end unless the Reynolds number is changed may be explained as follows: In the computations, the turbulence effect is represented by the vortex viscosity coefficient and is assumed to be a constant scalor in the flow-field. The difference may be due to the violation of this assumption. However, the experimental and computational results exhibit consistency within a range of about 3/4 of the vortex radius up to the location slightly downstream of the breakdown, if the vortex viscosity coefficient is about four times as great as the dynamic viscosity coefficient.

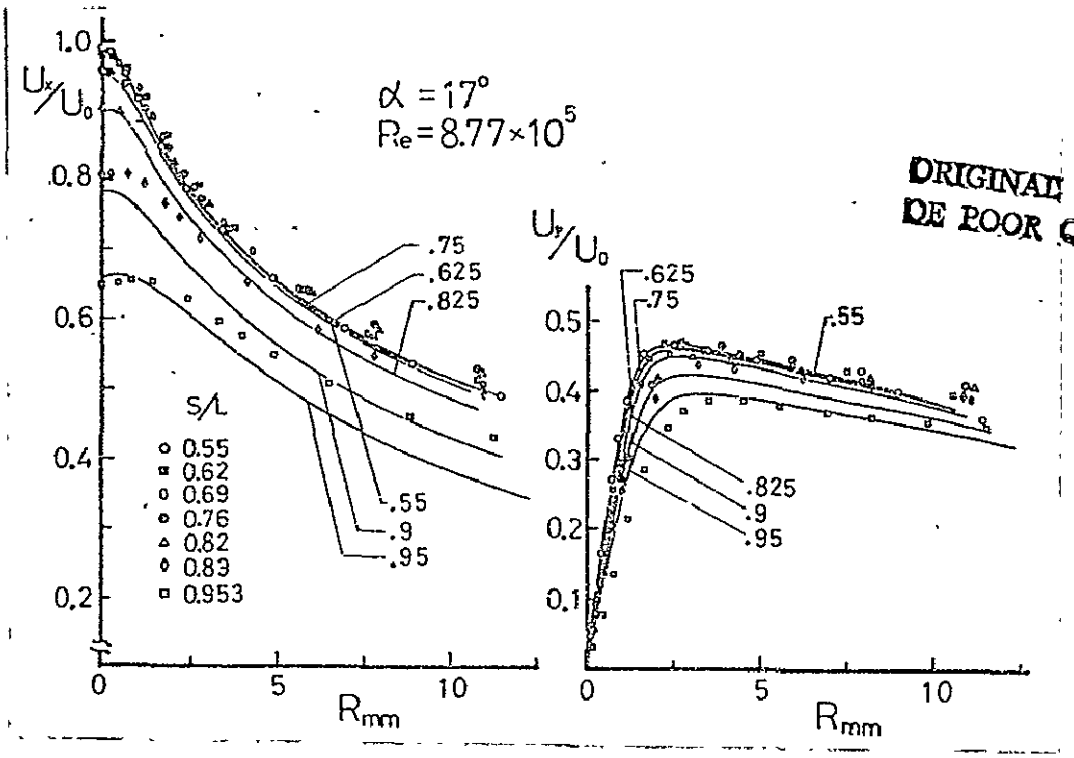

Fig. 45. Velocity Distribution
($\varepsilon = \nu$)

Fig. 45 shows a comparison of the computational and the experimental values of the axial and the circumferential velocity distributions. The computations were done with the Reynolds number, 8.77×10^5, which had been experimentally determined by the dynamic viscosity coefficient. The experimental values are given for seven cross-sections, i.e., for seven different values of S/L. Although the values of S/L for the experiments data are different from those for the computed data, two kinds of data can be compared if the computational data are extrapolated. As for the axial velocity component, the computed values are generally smaller and the consistency deteriorates more in the outside region where R is large, or while moving downstream where S/L is large. The same tendency is observed in the circumferential velocity distribution. This indicates that the structure of the turbulence has a large influence on the velocity distribution. /39

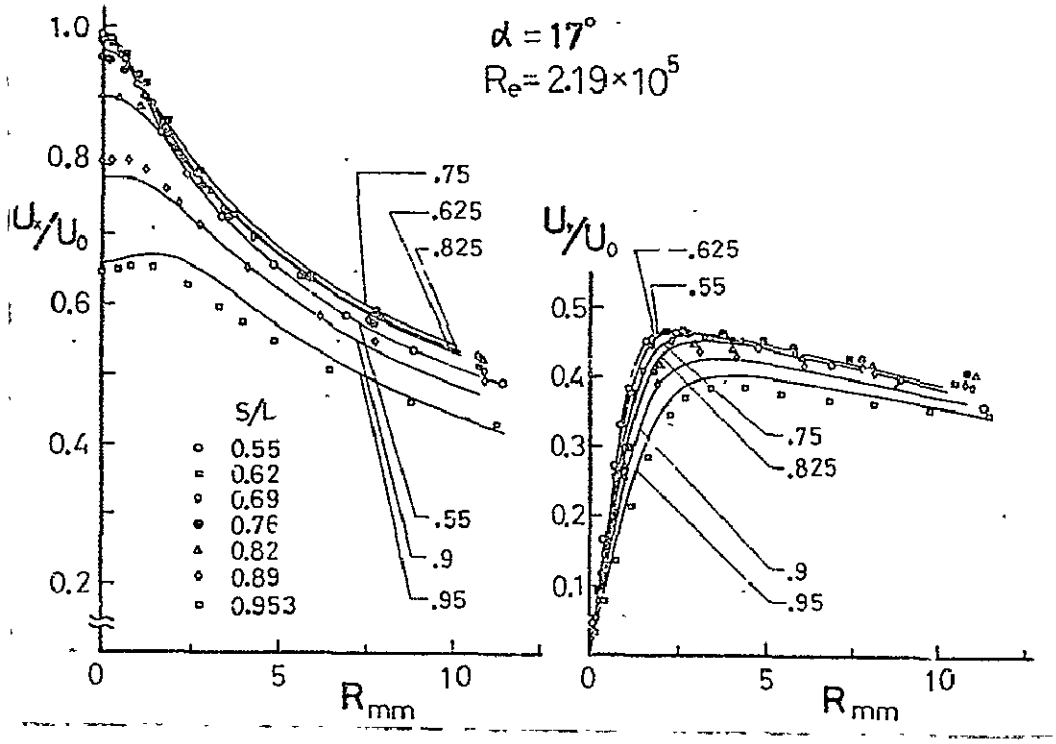

Fig. 46. Velocity Distribution
($\varepsilon = 4\nu$)

Fig. 46 shows the computational result with the Reynolds number, 2.19×10^3, which gives the greatest consistency of experimental and computational data appearing in Fig. 44, which shows the divergence of the vortex. The consistency is much greater than in the case where the Reynolds number is 8.77×10^5. Particularly, excellent consistency can be observed on the upstream of the breakdown, where S/L is 0.82 or less. Although the data are not shown in the figure due to the lack of the data number, in the case of $\alpha = 18^\circ$, the computational results are most consistent with the experimental results when the vortex viscosity coefficient is 5 times as great as the dynamic viscosity coefficient. Owen [30] reported that he had evaluated the vortex viscosity coefficient based on the velocity distribution measurement results of the leading-edge vortex of a delta wing before the breakdown, provided by Earnshaw, and that he obtained the vortex viscosity coefficient which was about five times as

great as the dynamic viscosity coefficient. Our computational results for the region near the breakdown give almost the same value to the vortex viscosity coefficient. The reason that the experimental and the computational data of the velocity distribution are not very consistent at the location after the breakdown may be explained as follows: First, the quasi 2-dimensional assumption which is essential to the computation cannot be well preserved at that region. Secondly, the spiral transformation after the breakdown causes an intense velocity fluctuation and creates a turbulence structure which is different from the initial one. Consequently, the spiral transformation creates a non-stationary flow-field and its effect cannot be represented by a simple eddy (vortex) viscosity any longer. Figs. 45 and 46 indicate that, even if a viscosity model is employed, the vortex (eddy) viscosity ε must be varied spacially and must have a greater value outside the vortex. Thus, a vortex viscosity model cannot provide great accuracy if the turbulence term is given by a simple scalor value. However, in a wake flow-field, the vortex viscosity coefficient is $10 \sim 100$ times as great as that of the flow-field of the leading-edge vortex of a delta wing and about 100 times as great as that of jets. The majority of the phenomena in the flow-field created by a delta-wing leading-edge vortex is dominated by potential-flow effects, i.e., the pressure gradient. Furthermore, our model is sufficient for the purpose of determining the breakdown position.

Fig. 47 shows a comparison of the experimental and the computational results of the total pressure. The figure shows the numerical computation using the Reynolds number, 2.19×10^5, which gives the greatest consistency of the experimental and the computational results. It is readily understood that the numerically computed breakdown position is very close to the experimentally determined breakdown point, i.e., the location where $S/L = 0.864$ and the criterion $dH_c/dx = 0$ holds.

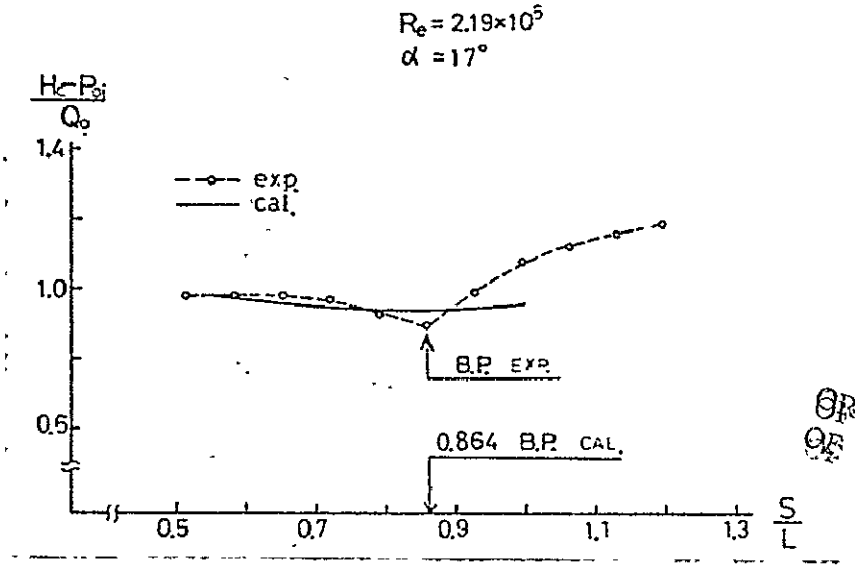

Fig. 47. Total Pressure in Vortex Center

However, a significant difference between the computational and the experimental values of the total pressure itself is observable. The experimental data exhibit a discontinuous change of the total pressure and an upward convex change in the neighborhood of the breakdown point. However, the computational result shows a continuous change and the shape is always convex downward. First, such inconsistency may be explained by the problems involved in the experiment, as mentioned in Sec. 2.2.3. Namely, since the keel tube diameter is large compared with the vortex diameter on the upstream where the vortex diameter is relatively small, the measured total pressure indicates the average value near the center, giving higher measurement values. Furthermore, after the breakdown, the spiral transformation of the vortex causes the axial direction of the measurement probe to be different from the instantaneous direction of the flow, also giving higher measurement values. Secondly, the computational results of the circumferential velocity distribution are higher than the corresponding experimental results. As seen from the third equation of (13), the static pressure P is determined only by the

distribution of the circumferential velocity V. Thus, in the computational procedure, the velocity on the vortex central axis is first given and the static pressure at the outer end of the vortex is determined accordingly. Therefore, P is substantially given as an external condition and the static pressure on the central axis is determined only by the radial distribution of V. It will be understood even by a simple calculation that the static pressure on the central axis decreases as the radial change of the circumferential velocity in the neighborhood of the vortex center increases. Since the dynamic pressure on the central axis is given, the computational values of the total pressure are particularly less after the breakdown point. Third, the change in the computational results of the axial velocity distribution near the central axis after the breakdown is much more moderate than the change in the corresponding experimental results. As seen from the equ. (9), dH_c/dx is equal to the 2nd order derivative of the axial velocity in the center. The drop in the increasing rate of the total pressure after the breakdown is caused by the fact that the computed axial velocity distribution has less change in the radial direction and by the fact that the computed value of $\partial^2 U_x / \partial R^2$ is too small. Fourth, after the breakdown, the spiral transformation causes an intense turbulence mixture and the turbulence structure becomes very different from that before the breakdown, as was shown in Fig. 26. In particular, in the neighborhood of a point through which the spiral passes, a non-stationary flow from outside toward the vortex center is induced and the turbulence mixture becomes very intense. These effects cannot be represented by a scalar vortex viscosity model. Fifth, the velocity or the pressure varied rapidly after the breakdown and the quasi 2-dimensional assumption essential to the numerical computation cannot be preserved very well. However, as seen in Fig. 38, immediately after the breakdown, the change in the axial velocity direction is not very large and the quasi 2-dimensional assumption may be thought to be well preserved. Further downstream, however, this

assumption cannot be assured anymore, thus causing the radial change of the circumferential velocity to be computed as having excessively high values.

Therefore, when the experimental and the computed results are compared in Fig. 47, the comparison should be concentrated in a narrow region near the breakdown, taking into account the above facts. Furthermore, the above arguments suggest that, if the turbulence structure is taken into account more thoroughly /41
in the computation procedure and if the experimental method is improved, both experimental and computed data of the total pressure may exhibit an improved consistency. In any case, the location at which the total pressure on the central axis attains its minimum will not be greatly affected. Thus, whenever the initial and the boundary condition can be given, the numerical computation described in Sec. 3.2 can give the predicted breakdown point as a location where the condition $dH_c/dx=0$ is satisfied.

Fig. 48 shows the breakdown points which are determined by another criterion, i.e., $(\partial^2 U_x/\partial R^2)_{R=0}=0$. In the figure, the abscissa R_{max} denotes the radius R at which the axial velocity distribution at a given cross-section attains the maximum value. Before the breakdown, the maximum point is always on the central axis, i.e., $R_{max}=0$. However, after the breakdown, the maximal point moves outside of the central axis and R_{max} increases moving downstream. The O in the figure denotes R_{max} which is determined by the experimental data. The solid line curves in the figure denote the results of the numerical computation with three different Reynolds numbers. When the Reynolds number is 8.77×10^5 which is calculated by setting $\varepsilon = \nu$, the computed breakdown point is too far behind. When the Reynolds number is determined by $\varepsilon = 4\nu$ and is 2.19×10^5, the computed result is consistent with the experimental one. Thus, it has been shown that the breakdown point can be

determined by numerical computation as the point where the condition $(\partial^2 U_x / \partial R^2)_{R=0}=0$ holds.

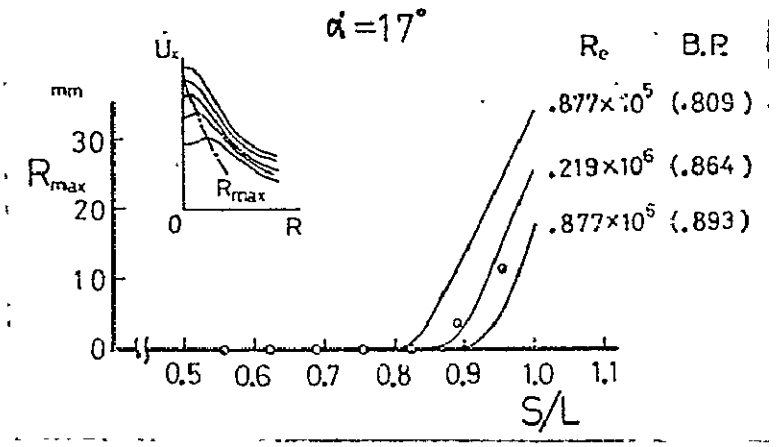

Fig. 48. Breakdown Point Determined by $(\partial^2 U_x / \partial R^2)_{R=0}=0$.

As indicated by the above computational results, the breakdown point can be predicted by the numerical computation method described in Sec. 3.2 if the initial and the boundary conditions are given.

Fig. 49 shows the computational results of the flow-directional changes of the velocity components on the central axis and the end of the vortex and of the static and the total pressure. The total pressure H_e at the end of the vortex is constant since the viscous diffusion can be ignored there, while the total pressure H_c on the central axis exhibits a change. Although the change of H_c is small, it is a very important quantity since the location at which the minimum value is attained indicates the breakdown point. The vortex diameter decreases initially slightly but it increases rapidly after the breakdown. Since the circulation quantity is assumed to be constant, when the vortex radius R_e decreases, the circumferential velocity $U_{\varphi e}$ increases, and when R_e increases, $U_{\varphi e}$ decreases. The velocity

U_c/U_o on the central axis is given as the boundary condition. The axial velocity U_{xe} at the end of the vortex exhibits a change which is similar to that of the circumferential velocity $U_{\varphi e}$, but it does not change so rapidly as the velocity on the central axis. The static pressure P_e at the end of the vortex decreases slightly initially but increases afterward. The static pressure P_c on the central axis increases at a rate which is much greater than that of the static pressure P_e at the vortex end. In order to facilitate the comparison with the experimental data, the velocity U_c on the central axis is given as the boundary condition in the presently proposed numerical computation. As a result, the procedure is equivalent to the calculation of the flow-field when a vortex with a certain initial condition is placed a potential flow with a pressure gradient of P_e. This indicates the mechanism in which, despite the slight increase of the pressure outside the vortex, a sharp pressure gradient is created in the vortex central axis, and the axial velocity near the central axis consequently decreases more rapidly than the axial velocity of the outside, thereby creating an axial velocity distribution which is convex downward in the neighborhood of the central axis.

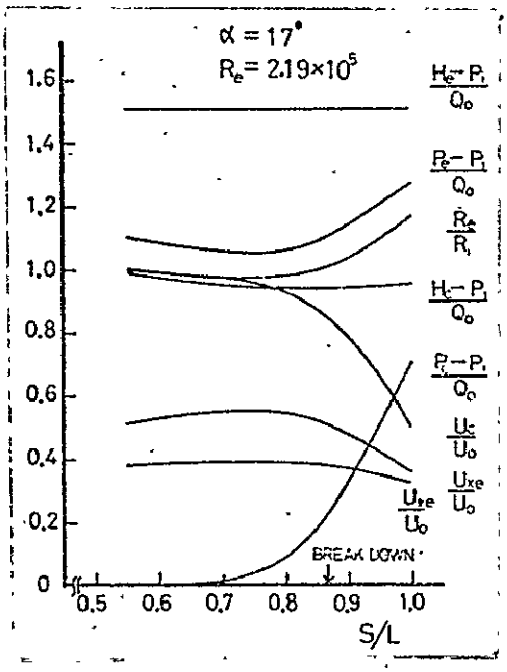

Fig. 49. Physical Quantities on the Boundaries.

Fig. 50 shows a computed radial velocity distribution. The flow is always directed outward near the central axis. Near the end of the vortex, however, the flow is directed inward on the upstream while it is directed outward on the downstream. It should be noted in particular that the gradient of the radial velocity is large near the central axis. This indicates that the vortex is more expanded near the central axis than it is around the end of the vortex and that the decay of the vortex begins in its inside due to the external pressure gradient. /42

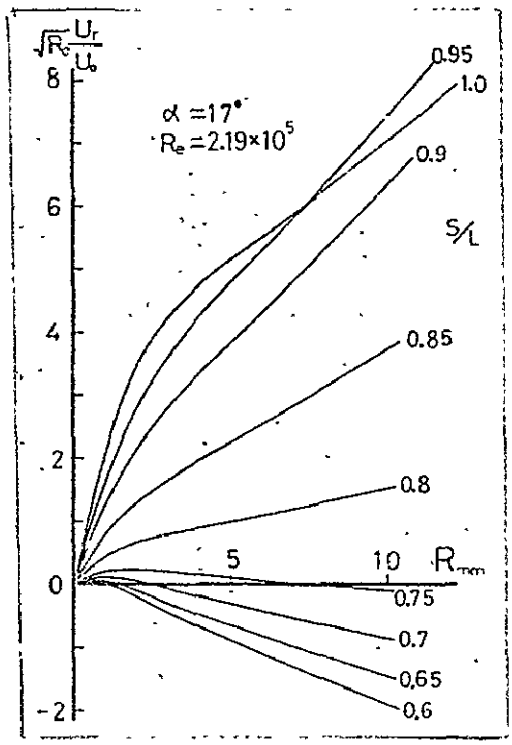

Fig. 50. Distribution of Radial Velocity Component.

Fig. 51 shows a computed distribution of the total pressure. The total pressure has a considerably low value on the central axis. Although the total pressure on the central axis increases after the breakdown, the total amount of the total pressure, integrated over the entire range of the vortex, decreases monotonically while moving downstream.

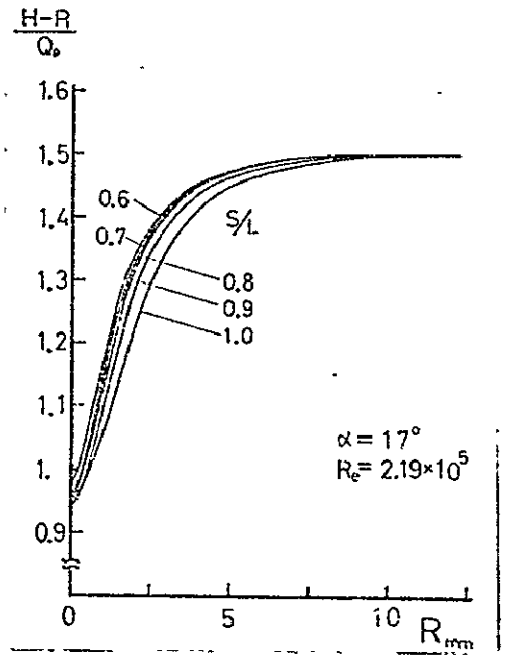

Fig. 51. Distribution of Total Pressure.

Fig. 52 shows a computed distribution of the static pressure. It has a low value on the central axis and increases while moving downstream, just like the total pressure. The figure shows further that the increase rate near the central axis is greater than that around the end of the vortex.

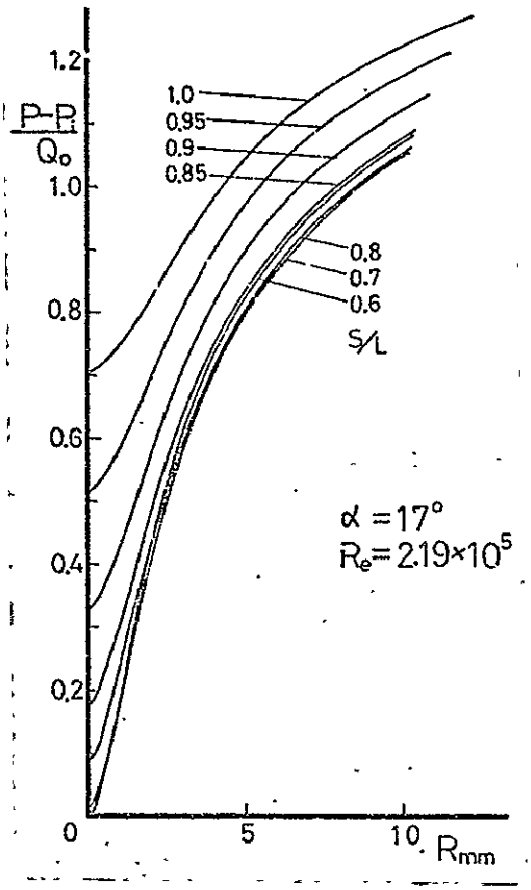

Fig. 52. Distribution of Static Pressure.

5. Conclusion

In the process where the flow is separated at the leading edge of a delta wing, an intense vortex is formed and developed downstream, and a breakdown of the vortex occurs, followed by a turbulent flow; the total pressure (head) and the velocity on the vortex central axis were measured together with the distribution of the average velocity vector. The experimental results were followed by a conclusion that the breakdown point can be determined by the criterion $dH_c/dx=0$ or $(\partial^2 U_x/\partial R^2)_{R=0}=0$. We have also shown that, if the initial and the boundary conditions are given, the breakdown point can be theoretically determined by representing the turbulence effect by a scalar vortex (eddy) viscosity coefficient and by numerically computing /43

difference equations under the quasi 2-dimensional assumption. Unlike the conditions considered by other researchers, such as the condition in which there exists a stagnation in the flow or that in which a finite transition occurs between two conjugate states, the conditions considered by us can be said to be much more appropriate for application to an acute vortex with a small core and an axial velocity on its central axis which is much greater than that on its periphery, such as the vortex generated at the leading edge of a delta wing.

We have also shown that, in the numerical computation, the computed velocity distribution is most consistent with the experimental results when the vortex viscosity coefficient ε is 4 to 5 times as great as the dynamic viscosity coefficient. However, it was also pointed out that, in order to obtain the velocity distribution of the flow-field within the vortex with more accuracy, the computational procedure must include evaluation of the turbulence structure, i.e., each Reynolds stress component, rather than simply using a viscosity model with a simple scalar vortex viscosity coefficient. In particular, in the flow-field after the breakdown, the occurrence of the spiral transformation causes a turbulence structure which is completely different from that before the breakdown. Thus, a model representing the turbulence structure of the flow-field with more accuracy is essential for the exact numerical calculation of the flow-field after the breakdown.

Our computational results show that the breakdown point does not change in response to ε within the range $R_e \geq 10^6$ but it is influenced by ε and moves upstream as ε increases if it is in the range $R_e < 10^6$. This result is different from a common conclusion that the breakdown point is not largely influenced by the turbulence. Similarly, our conclusion is also different from the result which says that the breakdown point moves upstream as the Reynolds number increases.

In the case of the delta-wing leading-edge vortex, even if the Reynolds number is sufficiently high, the breakdown is followed by a spiral transformation which Lambourne et al showed. The occurrence of the spiral transformation gave sufficient explanations to our experimental results: The axial velocity distribution changes its shape, at the breakdown position, from "upward convex" to "downward convex". The total pressure on the central axis increases rapidly at the breakdown point. These results are well understood when considering the following explanations: The reverse-directional spiral transformation of the vortex center induces a velocity directed toward the central axis. At the same time, the outside flow with a high total pressure flows into the region around the central axis in a non-stationary mode. (This process is modelled by the term of the turbulence mixture in the equation representing the time-average behavior.)

We have given our explanation to the following behaviors: The rotational direction of the spiral which appears behind the breakdown is different from that of the vortex core. The fluid of the vortex center does not move along the spiral but moves along the generatrices of a cone-like surface. Our explanation, using an analogy of rigid-body precession motion, is as follows: The vortex core cross-section exhibits a precession motion at the breakdown point as if it were a rigid body, due to the reverse pressure gradient in the axial direction. We also showed that the period of this precession motion is the same as that of the velocity fluctuation in the flow which appears behind the breakdown, and the corresponding frequency is proportional to U_o/L. There is a commercially produced flow meter utilizing the vortex breakdown. This flow meter measures the flow passing through a tube by creating a concentrated vortex in the tube and by measuring the frequency of the velocity fluctuation which appears after the breakdown. This device utilizes the fact that the frequency of the velocity fluctuation appearing after the

breakdown is proportional to the flow velocity U. Thus, there seems to exist sufficient support for our conclusion that the non-stationary phenomena appearing behind the breakdown may be well explained by using an analogy to the rigid-body precession motion. /44

In our experiments, the velocity, the total pressure and the turbulence were measured with three different models and different attack angles in order to investigate the structure of the delta-wing leading-edge vortex and the breakdown phenomenon. We have shown that, by the non-dimensionalization in terms of the reference velocity U_o and the reference distance L, the flow-field may be treated integrally and similarly, even when the attack angle changes, if the same model is used.

The main objective of this study is to establish a criterion for determining the breakdown point when the Reynolds number is relatively high, and to prove its validity by experiments. We have established the two criteria by which the numerical computation can predict the breakdown point. Another objective is to give an explanation, even a qualitative one, to the structure of the flow-field behind the breakdown. Our experimental results and those of the numerical analysis prove that the above objectives have been accomplished.

The authors gratefully acknowledge Mr. Shigemi, division director, and Mr. Endo, laboratory chief, who gave us much useful advice in the course of this study.

REFERENCES

[1] Spence, A. and D. Lean, "Some low speed problems of high speed aircraft," J. Roy. A. Soc., Vol. 66, (1962).

[2] Collar, A.R. , "Some aspects of Aeronautical Research in the United Kingdom," R. Ae. S. Paper, No. 4.

[3] Jones, R.T., "Properties of low-aspect-ratio pointed wings at speeds below and above the speed of sound," NACA Report, No. 835.

[4] Brown, C.E. and W.H. Michael, "Effect of leading-edge separation on the lift of a delta wing," J. Aero Sci., 10,(1954).

[5] Mangler, K.W. and J.H.B. Smith, "A theory of the flow past a slender delta wings with leading edge separation," Proc. Roy. Sci., A., 251, (1959).

[6] Smith, J.H.B., "Improved calculations of leading-edge separation from slender delta wings," REA Tech. Rep., 66070, (1966).

[7] Levinsky, E.S. and M.H.Y. Wei, "Nonlinear lift and pressure distribution of slender conical bodies with strakes at low speeds," NASA CR 1202, (1968).

[8] Polhamus, E.C., "Application of the leading-edge-suction analogy of vortex lift to the drag due to lift of sharp-edge delta wings," NASA TN, D-4739, (1968).

[9] Polhamus, E.C., "A concept of the vortex lift of sharp-edge delta wings based on a leading-edge-suction analogy," NASA TN., D-3767, (1966).

[10] Hedman, S.G., "Vortex lattice method for calculation of Quasi-steady loading on thin elastic wing in supersonic flow," FFA Rep., 105, (1965).

[11] Ohmura, M. and C. Takaoka, "Estimation of wing characteristics when accompanied by leading-edge vorteces - an application of the lift surface theory," Transaction of the Japan Aeronautic and Space Society, Vol. 20, No. 226, (1972).

[12] Kuchemann, D., "Types of flow on swept wings," J. Roy, A. Soc., Vol. 57, (1953).

[13] Hummel, D., "Untersuchungen uber das Aufplatzen der Wirbel

an Schlanken Delta flugeln," Z. Flugwiss, 13, Heft 5, (1965).

[14] Owen, T.B., "Low-speed wind-tunnel measurements of oscillatory rolling derivatives on a sharp-edged slender wing - Effects of frequency parameter and of ground," A.R.C. R & M., No. 3671, (1968).

[15] Fink, P.T. and J. Taylor, "Some early experiments on vortex separation," A.R.C. R & M., No. 3489, (1967).

[16] Moss, G.F., "Low-speed wind-tunnel measurements of longitudinal oscillatory derivatives on three wing plan-forms, A.R.C. R & M., No. 3009, (1957).

[17] Lowson, M.V., "Some experiments with vortex breakdown," J. Roy. A. Soc., Vol. 68, (1964).

[18] Morgan, S.M., "A new shape in the sky," Aero. J., (1972).

[19] Werle, H., "Turbillions d'ailes minces très elancees," La Racherche Aeronautique, No. 109, (1965).

[20] Elle, B.J., "On the breakdown at high incidences of the leading edge vortices on delta wings," J. Roy. A. Soc., Vol. 64, (1960).

[21] Lambourne, N.C. and D.W. Bryer,"The bursting of leading edge vortices - Some observation and discussion of the phenomenon," A.R.C. R & M., No. 3282, (1962).

[22] Lambourne, N.C., "The breakdown of certain types of vortex," A.R.C. R & M., No. 3282, (1962).

[23] Earnshaw, P.B., "An experimental investigation of the structure of a leading edge vortex," A.R.C. R & M., No. 3281, (1962).

[24] Harvey, J.K., "Some observations of the vortex breakdown phenomenon," J.F. Mech., 14, (1962). /45

[25] Cassidy, J.J. and H.T. Falvey, "Observation of unsteady flow arising after vortex breakdown," J.F. Mech., 41, (1970).

[26] Sarpkaya, T., "On stationary and travelling vortex breakdowns," J.F. Mech., Vol 45, (1971).

[27] Sarpkaya, T., "Effect of the adverse pressure gradient on vortex breakdown," A.I.A.A. J., May, (1974).

[28] Sarpkaya, T., "Vortex breakdown in swirling conical flows," AIAA J., Vol. 9, No. 9, (1971).

[29] Hall, M.G., "A numerical method for solving the equations for a vortex core," A.R.C. R & M., No. 3467, (1965).

[30] "Progress in aeronautical sciences," Vol. 7, Pergamon Press, (1966), pp 1-110.

[31] Stewartson, K. and M.G. Hall, "The inner Viscous solution for the core of a leading-edge vortex," J.F. Mech., 15, (1963).

[32] Brown, S.N., "The compressible invicid leading-edge vortex," J.F. Mech., 15, (1963).

[33] Hall, M.G., "Vortex Breakdown," Annual Review of Fluid Mechanics, Vol. 4, (1972), p. 195.

[34] Bossel, H.H., "Vortex breakdown flowfield," The Physics of Fluids, Vol. 12, No. 3, (1969).

[35] Ludwieg, H., "Stabilität der Strömung in einem Zylindrischen Ringraum," Z. Flugwiss, Heft 11, (1961).

[36] Ludwieg, H., "Experimentelle Nachprüfung der Stabilitäts-theorien für reibungsfreie Strömungen mit schraubenlinien-förmingen Stromlinien," Z. Flugwiss, 12, (1964).

[37] Ludwieg, H., "Erklärung des Wirbelaufplatzens mit Hilfe der Stabilitästheorie für Strömungen mit schraubenlinien-förmigen Stromlinien," Z. Flugwiss, 12, (1965).

[38] Benjamin, T.B., "Theory of the vortex breakdown phenomenon," J.F. Mech., 14, (1962).

[39] Fraenkel, L.E., "On Benjamin's theory of conjugate vortex flows," J.F. Mech., Vol. 28, (1967).

[40] Sheer, A.F., "On the nature of conjugate vortex flows," J.F. Mech., Vol. 33, (1968).

[41] Leibovich, S., "Weakly non-linear waves in rotating fluids," J.F. Mech., Vol. 42, (1970).

[42] Leibovich, S. and J.D. Randall, "Dissipative Effects on nonlinear waves in rotating fluids," The Physics of Fluids, Vol. 14, No. 12, (1971).

[43] Randall, J. D. and S. Leibovich, "The critical state: A trapped wave model of vortex breakdown," J.F. Mech, Vol. 58,

(1973).

[44] Leibovich, S. and J.D. Randall, "Amplification and decay of long nonlinear waves," J.F. Mech., Vol. 58, (1973).

[45] Mager, A., "Imcompressible, viscous, swirling flow through a nozzle," AIAA J., Vol. 9, No. 4, (1971).

[46] Mager, A., "Dissipation and breakdown of a wing-tip vortex," J.F. Mech., Vol. 55, (1972).

[47] Petersohn, E., "The stability criterion for vortices by Ludwieg and its application to some experimental results," FFA Rep. 119.

[48] Hayashi, "Problems in aerodynamics: On delta-wing leading-edge vortex," National Aeronautic Laboratory, N-16, (1973), (in Japanese).

[49] Kirkpatrick, D.L.I., "Experimental investigation of the breakdown of a vortex in a tube," A.R.C.C.P. No. 821, (1965).

[50] Kawabata and Nakatani, "Air direction-speed meter with automatic tracking device," National Aeronautic Laboratory Report, TM-172, (1970), (in Japanese).

[51] Hayashi and Nakatani, "Measurement of three-dimensional average velocity vector and Reynolds stress using hot wire," National Aeronautic Laboratory Report, TR-242, (1971), (in Japanese).

[52] South, P., "A simple theory of vortex bursting," N.R.C. of Canada Aero. Report, LR-414, (1964).

[53] Usui, "On breakdowns of vortices generated in cilinders," Journal of the Japan Aeronautic and Space Society, Vol. 20, No. 226, (1972), (in Japanese).

[54] Hayashi and Nakatani, "Delta-wing leading-edge vortex and breakdown," Journal of the Japan Aeronautic and Space Society, Vol. 20, No. 226, (1972).

[55] Jones, W.P. "Research on unsteady flow," J. Aero. Sci., Vol. 29, No. 3, (1962).

[56] Das, A., "Zum Anschwellen Aufgerollter Wirbeltlachen und aufplatzen des Wirbelkerns bei Schlanken Tragflugeln," Z. Flugwiss, 15, (1967).

[57] Hinze, J.O., Turbulence, McGraw Hill, (1959).

[58] Hall, M.G., "A theory for the core of a leading-edge vortex," J.F. Mech., 11, 209, (1961).